Title: Golgi-Resident Gαo Promotes Protrusive Membrane Dynamics.

Authors: Solis GP, Bilousov O, Koval A, Lüchtenborg AM, Lin C, Katanaev VL

Journal: Cell

Year: 2017 Aug 24

Issue: 170

Volume: 5

Pages: 939-955.e24

DOI: 10.1016/j.cell.2017.07.015

Cell

Golgi-resident Gαo promotes protrusive membrane dynamics

--Manuscript Draft--

Manuscript Number:	CELL-D-17-01257R1
Full Title:	Golgi-resident Gαo promotes protrusive membrane dynamics
Article Type:	Research Article
Keywords:	heterotrimeric G proteins; interactome; signaling; vesicular trafficking; Golgi; neurite formation; protrusions; exocytosis; KDELR; Rab1; Rab3; Drosophila; G protein-coupled receptors
Corresponding Author:	Vladimir L. Katanaev, Prof. University of Lausanne Lausanne, SWITZERLAND
First Author:	Gonzalo P. Solis
Order of Authors:	Gonzalo P. Solis
	Oleksii Bilousov
	Alexey Koval
	Anne-Marie Lüchtenborg
	Chen Lin
	Vladimir L. Katanaev, Prof.
Abstract:	To form protrusions like neurites, cells must coordinate their induction and growth. The first requires cytoskeletal rearrangements at the plasma membrane (PM), the second - directed material delivery from cell's insides. We find that the Gαo-subunit of heterotrimeric G-proteins localizes dually to PM and Golgi across phyla and cell types. The PM pool of Gαo induces, and the Golgi pool feeds the growing protrusions by stimulated trafficking. Golgi-residing KDELR binds and activates monomeric Gαo, atypically for G protein-coupled receptors which normally act on heterotrimeric G-proteins. Through multidimensional screenings identifying >250 Gαo interactors, we pinpoint several basic cellular activities, including vesicular trafficking, as being regulated by Gαo. We further find small Golgi-residing GTPases Rab1 and Rab3 as direct effectors of Gαo. This KDELR→Gαo→Rab1/3 signaling axis is conserved from insects to mammals and controls material delivery from Golgi to PM in various cells and tissues.
Opposed Reviewers:	
Suggested Reviewers:	

Golgi-resident Gαo promotes protrusive membrane dynamics

Gonzalo P. Solis,[1,3,*] Oleksii Bilousov,[1,3] Alexey Koval,[1] Anne-Marie Lüchtenborg,[1] Chen Lin,[1] and Vladimir L. Katanaev[1,2,4,*]

[1]Department of Pharmacology and Toxicology, University of Lausanne, CH-1011 Lausanne, Switzerland

[2]School of Biomedicine, Far Eastern Federal University, Vladivostok 690950, Russian Federation

[3]These authors contributed equally

[4]Lead Contact

*Correspondence: gonzalo.solis@unil.ch (G.P.S.), vladimir.katanaev@unil.ch (V.L.K.)

SUMMARY

To form protrusions like neurites, cells must coordinate their induction and growth. The first requires cytoskeletal rearrangements at the plasma membrane (PM), the second – directed material delivery from cell's insides. We find that the Gαo-subunit of heterotrimeric G-proteins localizes dually to PM and Golgi across phyla and cell types. The PM pool of Gαo induces, and the Golgi pool feeds the growing protrusions by stimulated trafficking. Golgi-residing KDELR binds and activates monomeric Gαo, atypically for G protein-coupled receptors which normally act on heterotrimeric G-proteins. Through multidimensional screenings identifying >250 Gαo interactors, we pinpoint several basic cellular activities, including vesicular trafficking, as being regulated by Gαo. We further find small Golgi-residing GTPases Rab1 and Rab3 as direct effectors of Gαo. This KDELR→Gαo→Rab1/3 signaling axis is conserved from insects to mammals and controls material delivery from Golgi to PM in various cells and tissues.

INTRODUCTION

G protein-coupled receptors (GPCRs) form the biggest receptor family in animals. Main intracellular GPCR effectors are heterotrimeric G proteins composed of α, β, and γ subunits, of which the α-subunit binds guanine nucleotides. Four main subgroups of Gα-subunits exist: Gαs, Gαq, Gαi/o, and Gα12/13 (Milligan and Kostenis, 2006). When bound to GDP, heterotrimeric G protein is competent to interact with the cognate GPCR. The activated receptor acts as a guanine nucleotide exchange factor (GEF), catalyzing exchange of GDP for GTP on the Gα. This triggers dissociation of the G protein into Gα-GTP and the βγ-heterodimer, which can bind and activate downstream transducer proteins. When GTP on Gα is hydrolyzed, the inactive Gαβγ heterotrimer re-associates for a new cycle of activation. Alternatively, the Gα-subunit can be reloaded with GTP and continue its signaling activity (Lin et al., 2014).

As Gα-subunits provide the main specificity in GPCR-initiated signaling cascades (Milligan and Kostenis, 2006), identification of the Gα targets is crucial to understand this type of signaling. Gαo was among the first α-subunits discovered, and is the major Gα-subunit of the nervous system across the animal kingdom (Sternweis and Robishaw, 1984; Wolfgang et al., 1990), controlling both development and adult physiology of the brain (Bromberg et al., 2008). Gαo is also expressed in other tissues and is a transducer of the developmentally and medically important Wnt signaling pathway (Egger-Adam and Katanaev, 2008; Koval et al., 2011).

Despite this importance, the list of known molecular targets of Gαo has been remarkably short. To uncover Gαo interactors, we performed several whole genome/proteome screenings resulting in >250 candidate targets, most of which not previously known to be regulated by Gα proteins. These Gαo targets can be clustered into functional modules, identifying several basic cellular activities, conserved from insects to humans, as being under regulation of Gαo-mediated GPCR signaling. We focus on vesicular trafficking as one of these functional modules and show that Gαo controls multiple steps within it. From *Drosophila* epithelia to mammalian neuronal cells, Gαo controls outgrowth formation through coordinated activities from the plasma membrane (PM) and the Golgi apparatus, the latter involving the KDEL receptor and small GTPases Rab1 and Rab3.

RESULTS

Massive screenings identify numerous Gαo partners

With only a few Gαo effectors previously known, we performed several screenings to massively identify Gαo partners. Our primary screenings were: yeast two-hybrid (i), proteomic (ii), and genetic suppressor-enhancer screens in *Drosophila* using *Gαo* overexpression (iii) and RNAi-mediated downregulation (iv). We expected to approach covering with them, in a complementary manner, the whole Gαo interactome. We then complemented these screens with an extensive scrutiny of the literature data (v), and bioinformatics analysis of the resulting network and translation of this network into proteins orthologous between *Drosophila* and humans. This type of interactome identification has not been performed for any Gα protein and produced an impressive list of 254 proteins being candidate Gαo partners (Table S1 and STAR Methods).

Next, we aimed at functional clusterization of the Gαo targets, performing the gene ontology enrichment analysis of the Gαo interactome. This analysis identifies several functional modules, such as cytoskeleton organization, cell division, cell adhesion, etc., within the Gαo interaction network (Figures 1A and S1A, and Table S2). These modules may represent key cellular activities being directly controlled by Gαo-mediated GPCR signaling. As opposed to analysis of isolated individual targets, we decided to select a functional module from this network and to holistically investigate the role of Gαo in the regulation of this module. For this purpose, we selected the vesicular trafficking group of Gαo targets.

Gαo induces outgrowth formation in different cellular systems

Previously, we showed that *Drosophila* Gαo (dGαo) directly interacts with Rab5 to regulate the Wnt/Frizzled (Fz) signaling (Purvanov et al., 2010). The screenings now identified components of the vesicular trafficking machinery as partners of Gαo (Figures 1B and 1C, and Table S2), suggesting that Gαo may function as a master regulator in vesicular trafficking.

To experimentally validate our hypothesis, we looked for a Gαo-mediated cellular program that may require vesicle-mediated transport. We chose the process of neurite formation, and more broadly – outgrowth formation, for this purpose. Indeed, Gαo expression in neuronal cells

coincides with, and Gαo activity is required for, neuritogenesis (Fremion et al., 1999; Lee et al., 2006; Strittmatter et al., 1994; Wolfgang et al., 1990). The need for vesicle-mediated delivery of material to growing neurites is well-known, although Gαo has not previously been implicated in this vesicle delivery. Gαo is also required for the patterning and formation of *Drosophila* wing hairs – stable actin-rich outgrowths of wing epithelial cells (Katanaev et al., 2005).

Mouse neuroblastoma N2a cells rarely produce spontaneous neurites, which correlates with their low endogenous levels of Gαo (Figure S1B). As previously shown (Bromberg et al., 2008; Luchtenborg et al., 2014), expression of Gαo in these cells induces a massive neurite outgrowth (Figures S1C and S1D) providing us with a necessary readout system.

We additionally used *Drosophila* S2 cells, which also have low endogenous Gαo levels (http://flybase.org/reports/FBgn0001122.html). Remarkably, we observed that dGαo expression induced long protrusions, not typical for these cells (Figures 1D-1G). These protrusions are initially F-actin-positive, but with time become wider and additionally filled with microtubules (Figure 1D). Live imaging reveals the dynamic nature of these structures (Movie S1). Gαo-induced formation of protrusions in S2 cells served as another, evolutionary distant, readout for the role of Gαo in trafficking.

Gαo shows dual plasma membrane and Golgi localization

Before going further, we checked the subcellular localization of Gαo in our systems. In N2a cells transfected with human Gαo, immunostainings showed expected PM localization, and a strong perinuclear accumulation co-staining with the *trans*-Golgi marker GalT-GFP (Figure S1E). A functional C-terminal GFP-fusion of Gαo (Gαo-GFP, Figures S1C and S1D) also stained PM and Golgi, the latter recognized by the *cis*-Golgi marker GM130 and a broader Golgi marker MannII-BFP (Figure 2A). Golgi localization of Gαo was not affected by cycloheximide (up to 6h, not shown), and live imaging of Gαo-GFP revealed a rather static Golgi localization (Movie S2) as opposed to the more dynamic GalT-GFP marker (Movie S3), suggesting that Gαo does not merely stain Golgi on its way to PM after synthesis. Endogenous Gαo was also found dually at PM and Golgi in human neuroblastoma BE(2)C cells (Figure 2B) and in primary mouse cortical neurons (Figure S1F).

A Golgi localization of mammalian Gαo, with unclear biological relevance, has been seen previously (Akgoz et al., 2004), while such localization has not been described for dGαo or any insect Gα-subunit. In *Drosophila*, Golgi stacks spread all over cytoplasm (Kondylis and Rabouille, 2009), and dGαo-GFP in S2 cells localized at PM and at *cis*- and *trans*-Golgi stacks, identified, respectively, with the GMAP-210 and GalT-mRFP (Figure 2C). Upon heterologous expression in N2a cells, dGαo-GFP also localized at PM and Golgi (Figure S1G).

As a *Drosophila* tissue with endogenous dGαo, pupal wings expressing dArf79F-GFP as a *cis*-Golgi marker (Shao et al., 2010) revealed dGαo localized at PM and at compartments overlapping with this marker (Figure 2D). Some dArf79F-negative dGαo clusters may represent *medial*- and *trans*-Golgi stacks, although we cannot exclude additional intracellular compartments. The immunostaining specificity was confirmed by RNAi knockdown (k/d) of dGαo in pupal wings (Figure S1H).

Cumulatively, our findings in different cellular and organism readouts show a dual localization of Gαo – to the PM and Golgi compartments.

Gαo regulates vesicular trafficking at Golgi

To test for the role of the Golgi-localizing Gαo, we first roughly approached the function of the Golgi apparatus in Gαo-induced neuritogenesis using brefeldin A (BFA). As expected (Nakamura et al., 1995), BFA induced diffuse GM130 staining in Gαo-transfected N2a cells; loss of Gαo-GFP from the perinuclear region was also seen leaving the PM pool intact (Figure S1I), while total Gαo levels did not change (Figure S1J). We found that BFA-treated Gαo-expressing cells still formed neurites, with the percentage of cells with neurites and neurite number not significantly affected (Figures 2E-2G). However, these neurites were much shorter and thinner than in the control cells (Figures 2E and 2H).

Similarly, BFA treatment in *Drosophila* S2 cells had no effect on dGαo protein levels (Figure S1K), but significantly reduced the length of protrusions (Figures 2I and 2L), confirming that Golgi functions are also required for protrusion elongation in S2 cells. However, BFA additionally

reduced the average number of protrusions per cell (Figures 2I-2K), which may be due to instability of these structures.

These results indicate that Golgi is required for membrane trafficking needed during elongation of Gαo-induced protrusions. To test this directly, we quantified the PM-directed transport using GFP-fusion of the thermosensitive vesicular stomatitis virus glycoprotein ($VSVG^{ts045}$-GFP). This construct is retained in ER at 42°C, being released at 32°C for its transport to PM through Golgi (Presley et al., 1997). Analyzing kinetics of surface accumulation of this construct at 32°C, we found strong acceleration of PM delivery of $VSVG^{ts045}$-GFP upon co-expression of Gαo (Figures 2M and 2N).

To provide an independent meter of the effect of Gαo on the Golgi-emanating trafficking, we employed the reverse dimerization (RD) system, whereby the GFP-FM4-hGH fusion protein aggregates in ER until addition of the D/D solubilizer drug, permitting then the secretory trafficking (Gordon et al., 2010). We found that expression of Gαo in N2a cells strongly speeds up secretory protein trafficking of this construct (Figures 2O and 2P). Further, we show with two independent shRNAs (Figures S2A and S2B) that k/d of endogenous Gαo from BE(2)C cells significantly slows down the secretory trafficking – effect rescued by re-expression of Gαo (Figures 2Q and 2R). It can be seen from Figures 2M-R that the speed of secretory trafficking is reduced roughly 2-fold upon k/d of Gαo in BE(2)C cells, and increased >2-fold upon expression of Gαo in N2a cells.

Collectively, these data suggest that Golgi Gαo regulates the PM-directed transport. Our data also indicate that the two pools of Gαo may function cooperatively in the outgrowths: the PM pool of Gαo providing the initial inductor signal for the outgrowth formation, and the Golgi pool maintaining and elongating the outgrowth through stimulating material delivery. In order to separate the PM and Golgi functions of Gαo, we generated a Golgi-only form, goGαo (STAR Methods). In N2a cells, goGαo shows a prominent Golgi but essentially no PM localization (Figure 3A), and robust interaction with Golgi partners of Gαo (Figure S2C, see below). Fully supporting our expectations, goGαo fails to induce any neurite outgrowths (Figures S1C and S1D). At the same time, goGαo parallels wild-type (WT) Gαo in the speeding up of material delivery from Golgi in the RD assay (Figures 3B and 3C).

Gαo physically and functionally interacts with small GTPases at mammalian Golgi

How does the Golgi pool of Gαo activate cargo delivery to PM? We hypothesized that this is achieved through direct interaction with Gαo targets of the vesicular trafficking module (Figure 1C and Table S2). The following mammalian orthologues of the dGαo targets were chosen for physical interaction analysis: small GTPases of the Rab (Rab1a, 3a, 4a, 5a, 7a and 11a) and Arf (Arf1-6) families, dynamin-1 and -2, and clathrin, all crucial components of the secretory and/or endocytic pathways. GFP-fusions of these proteins were expressed in N2a cells together with Gαo-GST (which displayed correct dual localization (Figure S2D)) for the pull-down analysis; empty plasmid or GST-fusion of the Golgi-resident KDEL receptor (KDELR, Figure S2D) (Townsley et al., 1993) were used as controls. Pull-downs showed robust binding of Gαo-GST to Rab1a, 3a, 4a and 5a; Rab7a and 11a where only weakly co-precipitated (Figures 3D, S2E and S2F). From the Arf family, Gαo-GST strongly interacted with all Golgi-associated Arfs (Arf1-5) but not with the endocytic Arf6 (Figures 3D, S2E and S2G). In contrast, no direct interactions were detected in this system for clathrin and dynamins (Figure S2H).

We next analyzed co-localization, expressing Gαo-mRFP with the GFP-fusions of the target proteins. Perinuclear Gαo strongly co-localized with the Golgi-associated Rab1a and Arf1-5, and to a lesser extent with Rab3a (Figures 3E and S3A). A limited co-localization was observed between perinuclear Gαo and Rab11a, clathrin and dynamins, and even less with the endocytic Rab4a, 5a and 7a (Figures S3B and S3C). Together, these results identify the small GTPases Rab1a, Rab3a, and Arf1-5 as potential players in the Gαo functions at Golgi.

Next, we analyzed cooperation of Gαo with these partners in neurite outgrowth, using WT and dominant-negative (DN) versions of Rab1a, Rab3a and Arf1. While Rab1a, Rab3a or Arf1 alone did not induce any neurite formation nor affected the length of the few spontaneous N2a cell neurites (Figures S3D-S3F), WT versions of Rab1a and Rab3a strongly potentiated, and their DN forms strongly suppressed, the length of Gαo-induced neurites in N2a cells (Figures 3F and 3I). At the same time, the proportion of neurite-forming cells and the neurites-per-cell numbers were not influenced by WT and DN forms of Rab3a, and modestly affected by the forms of Rab1a (Figures 3F-3H), confirming that the interaction between Gαo and these GTPases is important for

elongation but not induction of protrusions. In contrast to Rabs, Arf1 WT showed no functional interaction with Gαo, while Arf1DN reduced all Gαo-dependent responses (Figures 3F-3I) through a yet unclarified reduction of Gαo protein levels not seen in other co-transfections (Figures S3G-S3I). Arf1DN also induced a predicted BFA-like phenotype (Dascher and Balch, 1994): loss of the Golgi marker GM130 and of the perinuclear Gαo, while DN versions of Rab1a and Rab3a had no obvious effect on Gαo localization (Figures S4A and S4B).

Together, these data show that physical and functional interactions of Gαo with Rab1a and Rab3a at Golgi are required for neurite elongation in N2a cells.

Gαo functionally interacts with small GTPases at *Drosophila* Golgi

To support the above conclusion in an independent setting, we performed a similar set of experiments in *Drosophila* S2 cells. Upon co-transfection of mRFP-fusion constructs of dRab1, dRab3, and dArf79F with dGαo-GFP, all three small GTPases co-localized with dGαo at Golgi stacks stained by anti-GMAP-210 (Figures S4C and S4D). While expression of the GTPases alone did not induce protrusions (Figures S4E and S4F), dRab1 and dRab3 potentiated the number and length of dGαo-induced outgrowths (Figures 4A-4D) without changing the dGαo-GFP expression levels (Figures S4G and S4H). In contrast, dRab1DN and dRab3DN suppressed dGαo-induced protrusions (Figures 4A-4D). To continue the similarity with the mammalian system, the dArf79FDN mutant caused a ~50% drop in dGαo protein levels (Figures S4G and S4H), resulting in reduction in all parameters related to the formation of protrusions (Figures 4A-4D); it also was unique in disassembling Golgi stacks (Figure S5A).

Using live imaging, we found that the dynamics of dGαo-induced protrusions in S2 cells was strongly suppressed by dRab1DN, and strongly enhanced by dRab1WT (Movies S1, S4 and S5). These data show that the function of Gαo as a key player in the Golgi-controlled elongation of outgrowths is conserved from insects to mammals.

Gαo genetically interacts with small GTPases in developing *Drosophila* tissues

We next aimed at testing the role of Gαo in regulation of vesicular trafficking through Golgi-residing small GTPases *in vivo*, using two well-characterized phenotypes induced by *dGαo*: planar cell polarity (PCP) and wing hair formation defects in developing insect's wings (Katanaev et al., 2005) and neuromuscular junction (NMJ) phenotypes in larvae (Luchtenborg et al., 2014). Both phenotypes are linked to aberrant signaling by Fz receptors, which are GPCRs largely dependent upon Gαo for proper signal transduction (Egger-Adam and Katanaev, 2008; Koval et al., 2011). We hypothesized that these developmental processes may require not only the PM-associated activity of Gαo as a GPCR transducer, but also its Golgi function as a regulator of vesicular trafficking.

In pupal wings, each epithelial cell produces a stable outgrowth called trichome or hair. Aberrant Fz and dGαo activity results in the multiple wing hair (mwh) phenotype, when some cells form two or more hairs instead of one (Katanaev et al., 2005). Remarkably, co-overexpression of dGαo with dRab3 and especially dRab1 produced a marked, up to 15-fold, enhancement of the dGαo-induced mwh phenotype, whereas co-expression of dArf79F showed no enhancement (Figures 4E and 4F). Since the sole overexpression of each dRab produced no effect (Figures 4E and 4F), this result illustrates that dGαo synergistically interacts with dRab1 and dRab3 in this *in vivo* setting.

Drosophila NMJ is a glutamatergic synapse made by several distinct circular structures – the synaptic boutons – at the axon terminus. Boutons can be visualized with the postsynaptic CD8-GFP-Sh and the presynaptic anti-HRP staining. In larval NMJs, loss or RNAi-mediated k/d of dGαo leads to strong reduction in the number of boutons and to morphological abnormalities seen as elongated structures with defective overlap of pre- and postsynaptic markers (Figures 4G and 4H) (Luchtenborg et al., 2014). We speculated that motoneuron-specific overexpression of dRab1 or dRab3 may revert this phenotype, provided that these Rabs act downstream from dGαo in NMJ formation. Indeed, we found that the *dGαo* k/d phenotype (both the number of boutons and the NMJ morphology) was fully rescued by overexpression of dRab1 or dRab3, while these overexpressions on the wild-type background produced no effects (Figures 4G and 4H). As the k/d effect of the *dGαo*-targeting RNAi cannot be down-titrated by overexpression of an unrelated protein (Luchtenborg et al., 2014), these data demonstrate the *in vivo* functional interaction of dGαo with dRab1 and dRab3 during NMJ development.

The findings in this section provide evidence for the genetic interactions of Gαo with Rab1 and Rab3 *in vivo*, in two different tissues, supporting our cellular observations.

Gαo activates small GTPases at Golgi

Experiments described above show that Gαo physically and functionally interacts with Golgi-residing small GTPases. Next, we bacterially produced GST-tagged Rab1a, Rab3a and Arf1, as well as previously characterized His_6-tagged Gαo (Lin et al., 2014) and preloaded these G proteins with GDP or GTPγS mimicking their inactive and active conformations. Subsequent pull-downs confirmed that Gαo interactions with Rab1a, Rab3a, and Arf1 are direct (Figure 5A). Importantly, while the nucleotide state of the small GTPases did not affect the interaction with Gαo, Gαo-GTPγS bound Rab1a and Rab3a by folds more efficiently than Gαo-GDP did (Figures 5A and 5B). In contrast, binding to Arf1 was not influenced by the nucleotide state of Gαo (Figures 5A and 5B). These data might suggest that Rab1a and Rab3a are effectors of activated Gαo at the Golgi apparatus.

We thus analyzed if Gαo regulates Rab1a and Rab3a activities. Morphologically, co-expression of Gαo-mRFP and GFP-Rab1a in N2a cells induced a striking enlargement of the perinuclear region positive for both proteins – the phenotype not seen for Gαo co-expressions with other targets (Figure 3F). Similarly, in *Drosophila* S2 cells, co-expression of dGαo-GFP with mRFP-dRab1 induced clustering and tubulation of the Golgi stacks, also not seen in other experimental conditions (Figures S4C and S4D). As Rab1 has been previously associated with Golgi enlargement (Romero et al., 2013), we hypothesized that co-expression of Gαo stimulates Rab1a which in turn increases the Golgi size, in a manner conserved from insect to mammalian cells.

To address this, we measured the Golgi area marked by GM130 in N2a cells co-expressing non-tagged Gαo and GFP-Rab1a. While overexpression of Gαo or Rab1a alone had no effect, their co-expression significantly increased the Golgi size (Figures 5C and 5E). Proving that Rab1a activation is the cause, we found a similar enlargement of the Golgi area induced by the constitutive active Q70L mutant of Rab1a (Figures 5D and 5E), but not by other mutant forms of Rab1a or Gαo (Figure S5B). Co-expression with Rab1b also enlarged Golgi (Figure S5C), suggesting that Gαo activation of Rab1 is not isoform specific.

To further assess activation of Rab1 by Gαo, we used a FAPP1-PH-GFP construct, commonly served to evaluate phosphatidylinositol 4-phosphate (PI4P) levels in Golgi membranes (Balla et al., 2005). Since Rab1 activation increases PI4P production, FAPP1-PH-GFP recruitment to Golgi indirectly monitors the activity of endogenous Rab1 (Dumaresq-Doiron et al., 2010). Gαo overexpression in N2a cells significantly increased Golgi accumulation of FAPP1-PH-GFP (Figures 5F and 5G) without any changes in its protein levels (Figure 5H). As FAPP1-PH can also interact with Arf1-GTP (Balla et al., 2005), we separately employed a GST fusion of the Arf1 effector GGA3 (Dell'Angelica et al., 2000). Gαo overexpression did not increase the amount of Arf1-GTP pulled-down from N2a cell extracts by GST-GGA3 (Figures 5I and 5J). Thus, Gαo can activate endogenous Rab1 but not Arf1 at Golgi. Similarly, pull-down of Rab3a-GTP by its effector Rim2 was used as a probe to monitor Rab3 activation (Fukuda, 2004), revealing that Gαo overexpression increased 2-fold the amount of activated Rab3a (Figures 5I and 5J). We further found that Gαo overexpression increased Golgi accumulation (Figures S5D and S5E) but not protein levels of GFP-Rim2 (Figure S5F) in N2a cells. Since Rab3a also localizes to regions other than Golgi (Figure 3F), these data suggest that Gαo can activate endogenous Rab3 at Golgi, which results in recruitment of GFP-Rim2 to this compartment.

Overall, these results speak for Rab1 and Rab3 being direct binding partners of Gαo. Further, Gαo can activate these small GTPases *in vivo*, resulting in enhanced Golgi-derived vesicular transport, necessary for the stabilization and elongation of membrane protrusions.

Gαo interacts with the αGDI-complexed Rab1/3 at Golgi

We hypothesized that Gαo might act as a GDI displacement factor, 'handing over' Rabs from GDI to a *bona fide* GEF localized to the Golgi. To test this, we co-overexpressed Rab-αGDI – efficient GDI for both Rab1 and Rab3 (Yang et al., 1994) – together with Gαo and GFP-Rab1a/3a. Surprisingly, we found αGDI to promote Gαo-Rab1a/3a interactions (Figures 5K and 5L). Gαo also pulled down αGDI without co-expression of any Rab (Figures S5G); this interaction is likely mediated by endogenous Rabs as recombinant Gαo and αGDI did not directly interact (Figure 5M). In order to test if Gαo is able to directly interact with Rab/αGDI complexes, we purified Rab1a and Rab3a using the baculovirus expression system preserving post-translational

prenylation of Rabs, crucial for their interaction with GDIs (Maltese et al., 1996). As expected, prenylated Rab1a/3a were also able to interact with Gαo (Figure S5H) but are not activated by Gαo *in vitro* (Figures S5I and S5J). Notably, we also succeeded in reconstitution of the Gαo-Rab1/3-αGDI complexes *in vitro* (Figure 5M). Cumulatively, these data indicate that multimeric Gαo-Rab1/3-αGDI complexes may exist at Golgi.

Stimulation of KDELR activates βγ-free Gαo at Golgi

We next investigated how Gαo activation at Golgi is organized, considering two possibilities: translocation of active Gαo from PM to Golgi post-activation by GPCRs *vs.* the independent activation of Gαo at Golgi. It was suggested that Gβγ heterodimers, but not Gα-subunits, could translocate from PM to Golgi after GPCR activation (Akgoz et al., 2004). Despite poor expression (Figures S6A and S6B), the $G\alpha o^{Gly92}$-GFP construct used in those previous experiments revealed the dual PM and Golgi localization similar to our GFP-tagged Gαo construct (Figure S6C). We then applied 3 different means of Gαo activation at PM: co-transfection with muscarinic acetylcholine receptor 2 used in previous translocation studies (Akgoz et al., 2004) or with neuronal cannabinoid receptor type-1, followed by stimulation with acetylcholine or HU-210, respectively. Alternatively, we used the Gi/o-activating peptide mastoparan (Higashijima et al., 1988). In agreement with prior work (Akgoz et al., 2004), none of these treatments increased the perinuclear fluorescence of Gαo-GFP or $G\alpha o^{Gly92}$-GFP (Figures S6D-S6I), confirming that Gαo is not translocated from PM to Golgi upon activation.

Thus Gαo is a resident of Golgi and must be activated at this compartment. A GPCR-like activity of KDELR has been implicated in activation of the Golgi pool of Gαq and Gαs, which in turn regulate anterograde and retrograde trafficking, respectively (Cancino et al., 2014; Giannotta et al., 2012). KDELR is abundantly localized to Golgi, where it is constantly activated by the C-terminal KDEL sequence of chaperones delivering cargo from ER. A dominant-negative D193N mutant ($KDELR^{D/N}$) can bind the KDEL peptide but does not recycle to ER and cannot activate Gαq/Gαs (Cancino et al., 2014; Giannotta et al., 2012; Townsley et al., 1993).

We found that KDELR-GFP co-localized with Gαo-mRFP at Golgi (Figure 5N) and was efficiently pulled-down by Gαo-GST (Figure 5O) from N2a cells. Similarly, dGαo and dKDELR

co-localize at Golgi stacks in *Drosophila* S2 cells (Figure 6A). We generated a transgenic *Drosophila* line for *in vivo* overexpression of dKDELR (Figure S6J). Co-expression with dKDELR strongly enhanced the dGαo-induced mwh phenotype in *Drosophila* wings, while the single overexpression of dKDELR produced no PCP phenotype (Figures 6B and 6C), demonstrating that dGαo synergistically interacts with dKDELR *in vivo*. Together, these data show that Gαo and KDELR physically and functionally interact in an evolutionary conserved manner.

To test whether KDELR may possess a GEF activity towards Gαo, we employed the GTP-Eu loading assay in saponin-permeabilized HeLa cells (Koval and Katanaev, 2011). We found that expression of Gαo renders them responsive to the external stimulation with a KDEL-containing synthetic peptide (Figure 6D). Co-expression of the D/N but not WT KDELR blocked the KDEL-peptide-mediated activation of Gαo (Figure 6D).

We next tested where KDELR activates Gαo, using an antibody specific for the GTP-bound form of Gαo (Figures S6K and S6L). We generated a secretable BFP construct carrying a C-terminal KDEL signal (ssBFP^{KDEL}) that acts as a long-lasting KDELR ligand (Figures S6M-S6O) (Pulvirenti et al., 2008). N2a cells we co-transfected with Gαo-GFP and ssBFP^{KDEL} or a control (ssBFP). The anti-Gαo-GTP staining and GFP-fluorescence were used to estimate the GTP-loading of Gαo relative to its total protein level at PM *vs.* Golgi. We found that ssBFP^{KDEL} significantly increased the Gαo-GTP/Gαo-total ratio at Golgi but not PM without changing the Gαo Golgi/PM distribution (Figures 6E-6G), proving that stimulation of endogenous KDELR induced activation of Gαo at Golgi. Furthermore, KDELR overexpression (known to induce its self-stimulation (Hsu et al., 1992)) also activated the Golgi Gαo (Figures S7A and S7B).

Although GPCRs act on heterotrimeric Gαβγ proteins, we found no Golgi localization of the ubiquitous Gβ1-subunit (endogenous nor overexpressed) in Gαo-expressing N2a cells (Figure S7C). Even the triple co-expression of Gαo, Gβ1 and the neuronal Gγ3 (the complex previously reported to exist in Golgi (Ajith Karunarathne et al., 2012)) revealed essentially no localization of Gβγ to the Golgi enriched in Gαo in N2a cells (Figure 6H). We next performed pull-downs using GST-Gαo or GST-Gβ1 from cells expressing GFP-fusions of KDELR, Gγ3, and Gβ1 or Gαo. As expected, Gαo-GST efficiently precipitated not only KDELR-GFP but also GFP-Gβ1 and GFP-Gγ3 (Figure 6I). On the other hand, GST-Gβ1 effectively pulled-down Gαo and Gγ3 whereas binding with KDELR was totally absent (Figure 6I). Together, these experiments suggest that

uniquely for GPCRs, KDELR interacts with and activates βγ-free Gαo rather than a heterotrimeric Gαoβγ complex.

Next, we analyzed if the KDELR→Gαo activation influences neuritogenesis. We co-transfected N2a cells with both proteins and quantified the neurite outgrowth. We additionally used $KDELR^{D/N}$, which did not affect Gαo localization (Figure 5N) and interacted as efficiently as the WT with Gαo-GST (Figure 5O). The sole expression of KDELR did not induce neurite outgrowth, and co-expression of Gαo with the WT or D/N mutant of KDELR did not change the percentage of cells forming neurites (Figures 6J and 6K). Yet, co-expression of WT KDELR increased 3-fold the total neurite length accompanied by mild augmentation in neurite numbers (Figures 6J-6M) without varying Gαo protein levels (Figures S7D and S7E). Conversely, co-expression with $KDELR^{D/N}$ did not affect neurite number and length (Figures 6J-6M), implying that this mutant is unable to potentiate Gαo functions.

Similarly, dKDELR co-expression increased the length and number of dGαo-induced protrusions in *Drosophila* S2 cells (Figures 6N-6Q), whereas the sole expression of dKDELR had no effect (Figures S4E and S4F). On the other hand, $dKDELR^{D/N}$ reduced both the length and number of protrusions induced by dGαo (Figures 6N-6Q), without impact on dGαo localization and expression (Figures 6A, S4G and S4H). Regarding the $KDELR^{D/N}$ mutant, we provide evidence in three different cell types, in two of which it behaves dominant negatively (HeLa and S2, Figures 6D and 6N-Q) and in one – just negatively (N2a, Figures 6J-6M). We suspect that the negative activity of this form of KDELR becomes dominant depending on the cell type and/or relative expression levels.

Thus, KDELR emerges as an evolutionary conserved activator of the βγ-free Golgi pool of Gαo required for the elongation of cellular protrusions.

KDELR acts on a multiprotein complex containing Gαo and αGDI-Rab complexes

As Gαo interacts with the αGDI-Rab1a/3a pair, we wondered whether this pair might be present at the KDELR-Gαo complexes instead of Gβγ. Indeed, we found that the pull-down of αGDI (and by inference of αGDI-Rab complexes) is increased by several folds upon KDELR overexpression

(Figures 7A and 7B), although KDELR does not interact with αGDI (Figure S5G) nor Rabs (Figure S2E) in the absence of Gαo. Thus, we infer formation of multi-subunit assemblies containing KDELR, Gαo, αGDI, and Rabs at Golgi.

Next, we tested the reaction of these assemblies to KDELR activation. We showed above that it results in the nucleotide exchange on Gαo, as seen for other GPCRs. To continue this parallel, we find that KDELR activation with ssBFP^{KDEL} dissociates Gαo from the receptor (Figures 7C and 7D). In further resemblance to the heterotrimeric G protein activation by GPCRs whereas the Gβγ dissociates from Gα, we find that the interaction of Gαo with αGDI (Figure 7A and 7B) and Rab1a/3a (Figures 7E-7H) is strongly diminished upon KDELR activation.

Gαo does not act as a GEF for Rab1a/3a (Figures S5I and S5J). Further, nucleotide exchange on the small G proteins is not a prerequisite for the KDELR-induced dissociation of Rab1a/3a from Gαo, as the Rab1aDN and Rab3aDN mutant forms incapable of GTP-loading are also dissociated from Gαo upon KDELR activation (Figures 7E-7H). These findings imply an involvement of a *bona fide* Rab GEF localized to Golgi in the final step of Rab activation upon the release of Rabs from Gαo. The interaction between Gαo and Rabs, dissociated by KDELR activation, is a prerequisite for this final step.

To test if KDELR activation indeed results in Golgi Rab activation, we took the BE(2)C cells naturally expressing Gαo, stimulated endogenous KDELR by expression of ssBFP^{KDEL}, and monitored Rab1 activation by the Golgi enrichment of FAPP1-PH-GFP (Figures 5F-5H). We indeed found that KDELR stimulation leads to activation of Rab1 on Golgi (Figures 7I and 7J). This phenomenon is critically Gαo-dependent, as removal of Gαo by shRNA completely blocks activation of Rab1 by KDLER, and re-expression of Gαo rescues this block (Figures 7I and 7J).

Our work discovers a mechanism of KDELR-induced activation of Gαo and Rab GTPases at Golgi, needed to speed up material delivery to the growing cellular protrusions. The overall sequence of events starting from activation of KDELR by the arrival of the KDEL-containing chaperones accompanying the ER-delivered cargos and leading, in the Gαo-dependent manner, to activation of Rabs, is schematized in Figure 7K and is further detailed in the Discussion.

DISCUSSION

Intracellular signaling pathways currently emerge more as dynamic networks of protein interactions rather than linear cascades of activation/inactivation reactions. In this regard, thorough elucidation of the interaction targets of heterotrimeric G proteins – the immediate transducers of GPCRs – is of crucial importance to advance the understanding of this type of signal transduction. It is especially true for Gαo. Being the most abundant G protein in the nervous system and controlling multiple evolutionary conserved developmental, physiologic, and pathologic programs, it has been remarkably shy in revealing its signaling partners. Here, we disclose results of our multiple overlapping screens, identifying >250 interaction partners of Gαo. Each of the screens performed has its inherent advantages and limitations (Beltrao et al., 2012), and by complementation we expect to have reached a near complete coverage of the Gαo interactome – an endeavor rarely performed for a signaling protein. Cherry-picking of individual proteins from this network resulted in detailed descriptions of mechanisms of Gαo-controlled regulation of Wnt/Fz signaling, synapse formation, PCP, asymmetric cell divisions, endocytic regulation, *etc.* (Egger-Adam and Katanaev, 2010; Kopein and Katanaev, 2009; Lin and Katanaev, 2013; Lin et al., 2014; Luchtenborg et al., 2014; Purvanov et al., 2010), validating the interactome findings.

As opposed to characterizations of selected individual Gαo partners, we now aimed at identifying functional modules within the interactome. For this, we performed bioinformatics analysis clustering the individual components by their functions. This resulted in appearance of several major cellular activities, which now emerge to be regulated by Gαo-dependent GPCR signaling. We selected one of them, vesicular trafficking, for detailed investigation. Many important components of this cellular function, both endocytic and exocytic, are found among Gαo targets. We previously characterized interaction of Gαo and the endocytic master regulator Rab5, important for GPCR internalization and signaling (Purvanov et al., 2010). Now, we focus more on the exocytic function of Gαo. In various cell types (neuronal, epithelial, mesenchymal) of different animal groups (insect and mammalian) we now find a dual localization of Gαo to Golgi and PM, and the coordinated action of the two pools in exocytosis and formation of various types of cellular protrusions. We further uncover the evolutionary conserved KDELR→Gαo→Rab1/Rab3 pathway at Golgi, required for stimulated material delivery to PM and the growing protrusions.

KDELR is a Golgi-residing GPCR-like receptor, activated by the cargo delivery from ER and regulating both anterograde and retrograde trafficking from Golgi (Cancino et al., 2014; Giannotta et al., 2012; Townsley et al., 1993). Here we show that from *Drosophila* to mammals, KDELR binds Gαo and activates it, potentiating Gαo-induced cellular responses. Intriguingly, we show that it is the βγ-free form of Gαo, which is the binding and activation partner of KDELR – in a sharp contrast to the action of typical PM-localized GPCRs which act on heterotrimeric Gαβγ complexes. We further find that KDELR and Gαo form a multi-subunit complex, additionally containing Rab1/3 GTPses and αGDI. Activation of KDELR results in the nucleotide exchange on Gαo and its dissociation from KDELR. Although recombinant Rabs interact stronger with the GTP-loaded Gαo *in vitro* in absence of αGDI, in cells we find that activation of Gαo leads to dissociation of the Rab1/3-αGDI complexes, ultimately resulting in activation of the small GTPases and stimulated anterograde material delivery, necessary for the growth and stabilization of cellular protrusions. Activation of KDELR is known to induce formation of multicomponent aggregates recruiting a number of additional proteins (Majoul et al., 2001); recruitment of Rab-GEFs to these complexes to mediate ultimate activation of Rab1/3 is also conceivable but will require further investigation. Importantly, the Golgi pool of Gαo plays key roles in these processes, as the anterograde transport as well as KDELR-mediated Rab1 activation are inhibited upon depletion of Gαo.

Based on the data presented here, a model emerges whereas specific Gαo pools at PM and Golgi play different but cooperative roles during neuritogenesis and protrusion formation in general. At PM, Gαo initiates neurite formation regulating actin and microtubule cytoskeletons (Bromberg et al., 2008; Luchtenborg et al., 2014) in response to activation by specific GPCRs. At Golgi, the atypical GPCR KDELR induces activation of βγ-free Gαo, which subsequently activates Rab1 and Rab3, and the combined action of these proteins potentiates the PM-directed trafficking required for elongation and stability of membrane protrusions (Figure 7K). Being conserved from *Drosophila* to mammals, this molecular mechanism is of basic importance for the understanding of G protein functions in development, physiology, and disease.

AUTHOR CONTRIBUTIONS

GPS, OB, AML, CL, and AK performed experiments; GPS and VLK designed the work and wrote the paper.

ACKNOWLEDGEMENTS

We thank Alina Titova, Anke Ruedel, Birgit Gogol, Nadine Woessner and Diane Egger-Adam for technical help in genetic screens, Valerie Franzen – in cloning small GTPase mutants, Dmitry Ivankov and Natalya Bogatyreva for discussions on bioinformatics analysis, and Andrew Tomlinson for comments on the manuscript. This work was funded by Deutsche Forschungsgemeinschaft and Swiss National Science Foundation grants (SFB-TR11, 31003A_138350, and 31003A_156762/1) to VLK.

REFERENCES

Ajith Karunarathne, W.K., O'Neill, P.R., Martinez-Espinosa, P.L., Kalyanaraman, V., and Gautam, N. (2012). All G protein betagamma complexes are capable of translocation on receptor activation. Biochem Biophys Res Commun *421*, 605-611.

Akgoz, M., Kalyanaraman, V., and Gautam, N. (2004). Receptor-mediated reversible translocation of the G protein betagamma complex from the plasma membrane to the Golgi complex. J Biol Chem *279*, 51541-51544.

Balla, A., Tuymetova, G., Tsiomenko, A., Varnai, P., and Balla, T. (2005). A plasma membrane pool of phosphatidylinositol 4-phosphate is generated by phosphatidylinositol 4-kinase type-III alpha: studies with the PH domains of the oxysterol binding protein and FAPP1. Mol Biol Cell *16*, 1282-1295.

Beemiller, P., Hoppe, A.D., and Swanson, J.A. (2006). A phosphatidylinositol-3-kinase-dependent signal transition regulates ARF1 and ARF6 during Fcgamma receptor-mediated phagocytosis. PLoS Biol *4*, e162.

Beltrao, P., Ryan, C., and Krogan, N.J. (2012). Comparative interaction networks: bridging genotype to phenotype. Adv Exp Med Biol *751*, 139-156.

Bilousov, O., Koval, A., Keshelava, A., and Katanaev, V.L. (2014). Identification of novel elements of the Drosophila blisterome sheds light on potential pathological mechanisms of several human diseases. PLoS One *9*, e101133.

Bromberg, K.D., Iyengar, R., and He, J.C. (2008). Regulation of neurite outgrowth by G(i/o) signaling pathways. Front Biosci *13*, 4544-4557.

Cancino, J., Capalbo, A., Di Campli, A., Giannotta, M., Rizzo, R., Jung, J.E., Di Martino, R., Persico, M., Heinklein, P., Sallese, M.*, et al.* (2014). Control systems of membrane transport at the interface between the endoplasmic reticulum and the Golgi. Dev Cell *30*, 280-294.

Choudhury, A., Dominguez, M., Puri, V., Sharma, D.K., Narita, K., Wheatley, C.L., Marks, D.L., and Pagano, R.E. (2002). Rab proteins mediate Golgi transport of caveola-internalized glycosphingolipids and correct lipid trafficking in Niemann-Pick C cells. J Clin Invest *109*, 1541-1550.

Chun, J., Shapovalova, Z., Dejgaard, S.Y., Presley, J.F., and Melancon, P. (2008). Characterization of class I and II ADP-ribosylation factors (Arfs) in live cells: GDP-bound class II Arfs associate with the ER-Golgi intermediate compartment independently of GBF1. Mol Biol Cell *19*, 3488-3500.

Dascher, C., and Balch, W.E. (1994). Dominant inhibitory mutants of ARF1 block endoplasmic reticulum to Golgi transport and trigger disassembly of the Golgi apparatus. J Biol Chem *269*, 1437-1448.

Dell'Angelica, E.C., Puertollano, R., Mullins, C., Aguilar, R.C., Vargas, J.D., Hartnell, L.M., and Bonifacino, J.S. (2000). GGAs: a family of ADP ribosylation factor-binding proteins related to adaptors and associated with the Golgi complex. J Cell Biol *149*, 81-94.

Dumaresq-Doiron, K., Savard, M.F., Akam, S., Costantino, S., and Lefrancois, S. (2010). The phosphatidylinositol 4-kinase PI4KIIIalpha is required for the recruitment of GBF1 to Golgi membranes. J Cell Sci *123*, 2273-2280.

Dupre, D.J., Robitaille, M., Ethier, N., Villeneuve, L.R., Mamarbachi, A.M., and Hebert, T.E. (2006). Seven transmembrane receptor core signaling complexes are assembled prior to plasma membrane trafficking. J Biol Chem *281*, 34561-34573.

Egger-Adam, D., and Katanaev, V.L. (2008). Trimeric G protein-dependent signaling by Frizzled receptors in animal development. Front Biosci *13*, 4740-4755.

Egger-Adam, D., and Katanaev, V.L. (2010). The trimeric G protein Go inflicts a double impact on axin in the Wnt/frizzled signaling pathway. Dev Dyn *239*, 168-183.

Fremion, F., Astier, M., Zaffran, S., Guillen, A., Homburger, V., and Semeriva, M. (1999). The heterotrimeric protein Go is required for the formation of heart epithelium in Drosophila. J Cell Biol *145*, 1063-1076.

Fukuda, M. (2004). Alternative splicing in the first alpha-helical region of the Rab-binding domain of Rim regulates Rab3A binding activity: is Rim a Rab3 effector protein during evolution? Genes Cells *9*, 831-842.

Giannotta, M., Ruggiero, C., Grossi, M., Cancino, J., Capitani, M., Pulvirenti, T., Consoli, G.M., Geraci, C., Fanelli, F., Luini, A.*, et al.* (2012). The KDEL receptor couples to Galphaq/11 to activate Src kinases and regulate transport through the Golgi. EMBO J *31*, 2869-2881.

Goedhart, J., von Stetten, D., Noirclerc-Savoye, M., Lelimousin, M., Joosen, L., Hink, M.A., van Weeren, L., Gadella, T.W., Jr., and Royant, A. (2012). Structure-guided evolution of cyan fluorescent proteins towards a quantum yield of 93%. Nat Commun *3*, 751.

Gordon, D.E., Bond, L.M., Sahlender, D.A., and Peden, A.A. (2010). A targeted siRNA screen to identify SNAREs required for constitutive secretion in mammalian cells. Traffic *11*, 1191-1204.

Higashijima, T., Uzu, S., Nakajima, T., and Ross, E.M. (1988). Mastoparan, a peptide toxin from wasp venom, mimics receptors by activating GTP-binding regulatory proteins (G proteins). J Biol Chem *263*, 6491-6494.

Hsu, V.W., Shah, N., and Klausner, R.D. (1992). A brefeldin A-like phenotype is induced by the overexpression of a human ERD-2-like protein, ELP-1. Cell *69*, 625-635.

Katanaev, V.L., Ponzielli, R., Semeriva, M., and Tomlinson, A. (2005). Trimeric G protein-dependent frizzled signaling in Drosophila. Cell *120*, 111-122.

Kondylis, V., and Rabouille, C. (2009). The Golgi apparatus: lessons from Drosophila. FEBS Lett *583*, 3827-3838.

Kopein, D., and Katanaev, V.L. (2009). Drosophila GoLoco-protein Pins is a target of Galpha(o)-mediated G protein-coupled receptor signaling. Mol Biol Cell *20*, 3865-3877.

Koval, A., and Katanaev, V.L. (2011). Wnt3a stimulation elicits G-protein-coupled receptor properties of mammalian Frizzled proteins. Biochem J *433*, 435-440.

Koval, A., Purvanov, V., Egger-Adam, D., and Katanaev, V.L. (2011). Yellow submarine of the Wnt/Frizzled signaling: submerging from the G protein harbor to the targets. Biochem Pharmacol *82*, 1311-1319.

Lee, E., and De Camilli, P. (2002). Dynamin at actin tails. Proc Natl Acad Sci U S A *99*, 161-166.

Lee, M.S., Jun, D.H., Hwang, C.I., Park, S.S., Kang, J.J., Park, H.S., Kim, J., Kim, J.H., Seo, J.S., and Park, W.Y. (2006). Selection of neural differentiation-specific genes by comparing profiles of random differentiation. Stem Cells *24*, 1946-1955.

Lin, C., and Katanaev, V.L. (2013). Kermit interacts with Galphao, Vang, and motor proteins in Drosophila planar cell polarity. PLoS One *8*, e76885.

Lin, C., Koval, A., Tishchenko, S., Gabdulkhakov, A., Tin, U., Solis, G.P., and Katanaev, V.L. (2014). Double suppression of the Galpha protein activity by RGS proteins. Mol Cell *53*, 663-671.

Luchtenborg, A.M., Solis, G.P., Egger-Adam, D., Koval, A., Lin, C., Blanchard, M.G., Kellenberger, S., and Katanaev, V.L. (2014). Heterotrimeric Go protein links Wnt-Frizzled signaling with ankyrins to regulate the neuronal microtubule cytoskeleton. Development *141*, 3399-3409.

Majoul, I., Straub, M., Hell, S.W., Duden, R., and Soling, H.D. (2001). KDEL-cargo regulates interactions between proteins involved in COPI vesicle traffic: measurements in living cells using FRET. Dev Cell *1*, 139-153.

Maltese, W.A., Wilson, A.L., and Erdman, R.A. (1996). Prenylation-dependent interaction of Rab proteins with GDP dissociation inhibitors. Biochem Soc Trans *24*, 703-708.

Milligan, G., and Kostenis, E. (2006). Heterotrimeric G-proteins: a short history. Br J Pharmacol *147 Suppl 1*, S46-55.

Nakamura, N., Rabouille, C., Watson, R., Nilsson, T., Hui, N., Slusarewicz, P., Kreis, T.E., and Warren, G. (1995). Characterization of a cis-Golgi matrix protein, GM130. J Cell Biol *131*, 1715-1726.

Presley, J.F., Cole, N.B., Schroer, T.A., Hirschberg, K., Zaal, K.J., and Lippincott-Schwartz, J. (1997). ER-to-Golgi transport visualized in living cells. Nature *389*, 81-85.

Pulvirenti, T., Giannotta, M., Capestrano, M., Capitani, M., Pisanu, A., Polishchuk, R.S., San Pietro, E., Beznoussenko, G.V., Mironov, A.A., Turacchio, G.*, et al.* (2008). A traffic-activated Golgi-based signalling circuit coordinates the secretory pathway. Nat Cell Biol *10*, 912-922.

Purvanov, V., Koval, A., and Katanaev, V.L. (2010). A direct and functional interaction between Go and Rab5 during G protein-coupled receptor signaling. Sci Signal *3*, ra65.

Romero, N., Dumur, C.I., Martinez, H., Garcia, I.A., Monetta, P., Slavin, I., Sampieri, L., Koritschoner, N., Mironov, A.A., De Matteis, M.A.*, et al.* (2013). Rab1b overexpression modifies Golgi size and gene expression in HeLa cells and modulates the thyrotrophin response in thyroid cells in culture. Mol Biol Cell *24*, 617-632.

Shao, W., Wu, J., Chen, J., Lee, D.M., Tishkina, A., and Harris, T.J. (2010). A modifier screen for Bazooka/PAR-3 interacting genes in the Drosophila embryo epithelium. PLoS One *5*, e9938.

Solis, G.P., Schrock, Y., Hulsbusch, N., Wiechers, M., Plattner, H., and Stuermer, C.A. (2012). Reggies/flotillins regulate E-cadherin-mediated cell contact formation by affecting EGFR trafficking. Mol Biol Cell *23*, 1812-1825.

Sternweis, P.C., and Robishaw, J.D. (1984). Isolation of two proteins with high affinity for guanine nucleotides from membranes of bovine brain. J Biol Chem *259*, 13806-13813.

Strittmatter, S.M., Fishman, M.C., and Zhu, X.P. (1994). Activated mutants of the alpha subunit of G(o) promote an increased number of neurites per cell. J Neurosci *14*, 2327-2338.

Subach, O.M., Cranfill, P.J., Davidson, M.W., and Verkhusha, V.V. (2011). An enhanced monomeric blue fluorescent protein with the high chemical stability of the chromophore. PLoS One *6*, e28674.

Thaler, C., Koushik, S.V., Blank, P.S., and Vogel, S.S. (2005). Quantitative multiphoton spectral imaging and its use for measuring resonance energy transfer. Biophys J *89*, 2736-2749.

Townsley, F.M., Wilson, D.W., and Pelham, H.R. (1993). Mutational analysis of the human KDEL receptor: distinct structural requirements for Golgi retention, ligand binding and retrograde transport. EMBO J *12*, 2821-2829.

Wolfgang, W.J., Quan, F., Goldsmith, P., Unson, C., Spiegel, A., and Forte, M. (1990). Immunolocalization of G protein alpha-subunits in the Drosophila CNS. J Neurosci *10*, 1014-1024.

Yang, C., Slepnev, V.I., and Goud, B. (1994). Rab proteins form in vivo complexes with two isoforms of the GDP-dissociation inhibitor protein (GDI). J Biol Chem *269*, 31891-31899.

FIGURE LEGENDS

Figure 1

Bioinformatics analysis of the Gαo interactome

(A and B) Enrichment map of over-represented GO terms clustered in functional modules (A) built from Gαo partners. Zoom-in of the "Protein transport" module from (A) with the term "Vesicle-mediated transport" shown in green (B).

(C) Gαo partners of the term "Vesicle-mediated transport" grouped by function. Color-codes for nodes and edges indicate subcellular localization and screening method, respectively.

(D-G) *Drosophila* S2 cells expressing dGαo-GFP or GFP were allowed to spread for 30 (top) or 120min (bottom) to form protrusions. Rhodamine-phalloidin and anti-α-tubulin stained F-actin and microtubules, respectively (D). Quantification of parameters related to protrusion formation (E-G). Data represent mean ± SEM. ns, not significant; ***$p \leq 0.001$. Scale bars, 5μm.

See also Figure S1, Movie S1, and Tables S1 and S2.

Figure 2

Evolutionary conserved localization of Gαo at Golgi

(A-C) Golgi localization of Gαo-GFP determined in mouse N2a cells (A) by co-localization with Golgi markers GM130 and MannII-BFP. Human BE(2)C cells (B) showed endogenous Gαo co-localizing with GM130 at Golgi. In *Drosophila* S2 cells (C), dGαo-GFP labeled Golgi stacks marked by GalT-mRFP and GMAP-210. Color-channels are listed vertically top-to-bottom and selected areas are magnified with the channels displayed horizontally in the same order left-to-right. Scale bars, 10μm (A,B) and 5μm (C).

(D) Immunostaining of endogenous dGαo in *Drosophila* pupal wings expressing the *cis*-Golgi marker Arf79F-GFP at 22h APF. A selected region is magnified; dGαo/Arf79F-positive clusters indicated by arrowheads. Scale bar, 50μm.

(E-L) Development of protrusions in N2a (E-H) and S2 cells (I-L) induced by Gαo in the absence or presence of BFA. Quantification of parameters linked to neurite formation (F-H, J-L). Scale bar, 50μm (E) and 10μm (I).

(M and N) Gαo speeds up trafficking to PM as measured with the $VSVG^{ts045}$-GFP assay in N2a cells (M). Surface biotinylation determined PM levels of $VSVG^{ts045}$-GFP at different time points at 32°C. Biotinylated and input samples were tested with Abs against GFP and Gαo. Quantification (N).

(O-R) Reverse dimerization assay in N2a (O and P) and BE(2)C (Q and R) cells. D/D solubilizer induces reduction of the full-length GFP-FM4-hGH, and appearance and decrease of a furin-cleaved product (O and Q). Cell extracts were additionally tested with Abs against GFP, Gαo, α-tubulin (α-tub) and/or GST. Vertical line indicates that the two sides of the same membrane are shown with different exposition times for better visualization (O). Arrowheads point to relevant bands (O and Q). Quantification of the effect of Gαo overexpression (P), and its downregulation and re-expression (R).

Data represent mean ± SEM. ns, not significant; *$p \leq 0.01$; **$p \leq 0.005$; ***$p \leq 0.001$.

See also Figures S1 and S2, and Movies S2 and S3.

Figure 3

Functional interaction of Gαo with key small GTPases

(A-C) In N2a cells, a Golgi-only form of Gαo (goGαo-GFP) mostly absent from the PM as seen by co-expression of Gαo-mRFP (A, scale bar, 10μm) speeds up trafficking to PM as efficiently WT Gαo does (B and C, reverse dimerization assay with GST-fusions of Gαo and goGαo performed as in Figure 2). Vertical lines indicate different exposition times for each membrane part for better visualization (B).

(D) Pull-downs from N2a cells transfected with Gαo-GST and GFP-fusions of the small GTPases Rab1a, Rab3a and Arf1.

(E) Co-localization of Gαo-mRFP with GFP-tagged Rab1a, Rab3a and Arf1 in N2a cells. Boxed areas are magnified (right). Scale bar, 10μm.

(F-I) Neurite formation in N2a cells co-expressing Gαo-GFP with GFP-fusions of WT or DN forms of Rab1a, Rab3a and Arf1 (C). Quantification of neurite associated parameters (D-F). Scale bar, 20μm.

Data represent mean ± SEM. ns, not significant; *p≤0.01; **p≤0.005; ***p≤0.001.

See also Figures S2-S4 and Table S2.

Figure 4

Gαo interacts with small GTPases in *Drosophila*

(A-D) Protrusions in S2 cells co-expressing dGαo-GFP with GFP-fusions of WT or DN forms of dRab1, dRab3 and dArf79F (A). Quantification of protrusion linked parameters (B-D). Scale bar, 5μm.

(E and F) In *Drosophila* wings, the mwh phenotype induced by dGαo overexpression (red ovals) is boosted by dRab1 and dRab3 but not dArf79F (E). Quantification (F).

(G and H) The NMJ phenotypes induced by k/d of dGαo in *Drosophila* larvae are suppressed by dRab1 and dRab3 overexpression (G). Synaptic boutons are visualized by CD8-GFP-Sh and anti-HRP staining. Boxed regions are zoomed-in (right). Quantification of synaptic bouton numbers (F). Scale bar, 50μm.

Data represent mean ± SEM. Numbers in columns represent sample sizes. ns, not significant; *p≤0.01; **p≤0.005; ***p≤0.001.

See also Figures S4 and S5, and Movies S1, S4 and S5.

Figure 5

Gαo activates Rab1 and Rab3

(A and B) Gαo directly interacts with Rab1a, Rab3a and Arf1. Recombinant His_6-tagged Gαo is pulled-down by GST-fusions of the small GTPases but not GST (A). GDP- (top) and GTPγS-loaded (bottom) conformations of Rab1 and Rab3a bound more efficiently GTPγS-loaded Gαo. Proteins were detected by anti-His-tag and Ponceau S. Quantification (B).

(C-E) Golgi enlargement in N2a cells by co-expression of Gαo and GFP-Rab1a (C). Immunostainings against Gαo (squares at right bottom corners of GFP-Rab1a panels) and GM130 confirmed co-expression and marked Golgi, respectively. Golgi expansion induced by a CA mutant of Rab1a (GFP-Rab1aCA; D). Selected regions are magnified to the right. Quantification of Golgi area (E).

(F-H) Gαo enhanced the Golgi accumulation of FAPP1-PH-GFP in N2a cells (F). Gαo co-expression confirmed as in (C). Mean fluorescence intensity ratios of FAPP1-PH-GFP at the Golgi *vs*. total cell (G). Expression levels seen with Abs against GFP, Gαo and α-tubulin (H).

(I and J) Gαo activates Rab3a but not Arf1 in N2a cells. Recombinant GST-Rim2 and GST-CCA3 were used to pull-down activated GFP-Rab3a and Arf1-GFP, respectively (I). Abs against GFP and Gαo used for detection. Quantification of Rab3a and Arf1 pulled-down (J).

(K and L) Pull-downs from N2a cells transfected with Gαo-GST and GFP-fusions of Rab1a, Rab3a, and αGDI. Abs against GFP and Gαo were used for detection (K). Quantification of Rab1a and Rab3a pulled-down in the presence or absence of αGDI (L).

(M) Representative Western blots for the Gαo-Rab1a/Rab3a-αGDI complex formation *in vitro*. Purified GST-αGDI and His_6-tagged Rab1a or Rab3a were preassembled and immobilized on glutathione beads (in duplicate) to assess the interaction with His_6-Gαo. GST-αGDI alone was used as control.

(N) Co-localization of Gαo-mRFP with KDELR-GFP (top) and $KDELR^{D/N}$ (bottom) in N2a cells. Boxed regions are magnified. Scale bar, 10μm.

(O) Pull-down assay from N2a cells transfected with Gαo-GST and KDELR-GFP or $KDELR^{D/N}$-GFP. Abs against GFP and Gαo used for detection.

Data represent mean ± SEM. ns, not significant; *p≤0.01; **p≤0.005; ***p≤0.001. Scale bars, 10μm.

See also Figure S5 and S6.

Figure 6

Evolutionary conserved interaction of Gαo and KDELR

(A) Golgi co-localization of dGαo-GFP with dKDELR-mRFP (top) and dKDELR$^{D/N}$-mRFP (bottom) in S2 cells stained against GMAP-210. Selected areas magnified to the right. Scale bar, 5μm.

(B and C) dGαo interacts *in vivo* with dKDELR seen by the enhancement of the mwh phenotype in *Drosophila* wings (red ovals; B). Quantification of mwh numbers (C).

(D) Quantification of the GTP-Eu loading in saponin-permeabilized HeLa cells mock-transfected (Control) or co-expressing Gαo with GFP-fusions of the Golgi marker GalT, KDELR, or KDELR$^{D/N}$.

(E-G) Stimulation of KDELR activates Gαo in N2a cells (E). ssBFP^{KDEL} but not control ssBFP stimulates endogenous KDELR. Activated Gαo is detected by Abs against Gαo-GTP. Marked regions are zoomed-in. Mean fluorescence intensity ratios of active *vs*. total Gαo calculated at the PM and Golgi (F), and of total Gαo-GFP at the Golgi *vs*. PM (G). Scale bar, 10μm.

(H) In N2a cells, Gαo-BFP strongly co-localizes with mRFP-Gβ1 and GFP-Gγ3 at PM but not at Golgi. Marked region is magnified. Scale bar, 10μm.

(I) Pull-downs from N2a cells transfected with Gαo-GST (left) or GST-Gβ1 (right) and different combinations of KDELR-GFP, GFP-Gβ1, GFP-Gγ3 and Gαo-GFP. Abs against GFP and GST used for detection.

(J-M) Neurite outgrowth in N2a cells co-expressing Gαo-GFP with KDELR- or KDELR$^{D/N}$-GFP (J). Quantification of neurite linked parameters (K-M). Scale bar, 20μm.

(N-Q) Development of protrusions in S2 cells co-expressing dGαo-GFP with dKDELR- or dKDELR$^{D/N}$-mRFP (N). Quantification of protrusion related parameters (O-Q). Scale bar, 5µm.

Data represent mean ± SEM. Numbers in columns represent sample sizes. ns, not significant; **p≤0.005; ***p≤0.001.

See also Figure S4, S6 and S7.

Figure 7

Gαo links KDELR signaling to Rab GTPases

(A and B) Pull-downs from N2a cells transfected with Gαo-GST and combinations of GFP-αGDI, KDELR-GFP and ssBFP^{KDEL}. Abs against GFP and Gαo used for detection (A). Quantification of αGDI pulled-down (B).

(C and D) Effect of the co-expression of ssBFP^{KDEL} on Gαo-GST pull-down of KDELR-GFP in N2a cells. Abs against GFP and Gαo used for detection (C). Quantification of KDELR pulled-down (D).

(E-H) Pull-downs from N2a cells co-expressing Gαo-GST and combinations of ssBFP^{KDEL}, GFP-Rab1a WT or DN (E), and GFP-Rab3a WT or DN (G). Abs against GFP and Gαo used for detection (E and G). Quantification of Rab1a (F) and Rab3a (H) pulled-down by Gαo.

(I and J) Gαo downregulation affects Golgi accumulation of FAPP1-PH-GFP in BE(2)C cells (I). Stimulation of endogenous KDELR by ssBFP^{KDEL} but not ssBFP (squares at right bottom corners) increased Golgi recruitment of FAPP1-PH-GFP in control (shControl) cells, but not in Gαo-depleted (shGαo-A) cells. Re-expression of Gαo (not shown) rescued this phenotype. Mean fluorescence intensity ratios of FAPP1-PH-GFP at the Golgi *vs*. total cell (J). Scale bar, 10µm.

(K) Model of Gαo cooperative functions at the PM and Golgi apparatus required for protrusion outgrowth.

Data represent mean ± SEM. ns, not significant; *p≤0.01; **p≤0.005; ***p≤0.001.

SUPPLEMENTAL INFORMATION

Figure S1

Partners, expression and localization of Gαo, Related to Figures 1 and 2

(A) Enrichment Map of over-represented Gene Ontology (GO) terms clustered in functional modules built from the human orthologues of the interacting partners of *Drosophila* Gαo. Each node represents a set of genes associated with a particular GO annotation. The size of nodes indicates the relative number of genes, and its color intensity represents highly over-represented terms (low *p*-values). Thickness of edges shows the degree of overlap between the set of genes within nodes.

(B) RT-PCR analysis showed the expression of the Gα-subunits of the Gi/o subfamily in N2a cells. Amplification of actin was used as control.

(C and D) Comparison between non-tagged (Gαo), GFP-fused Gαo (Gαo-GFP, right) and its Golgi-only form (goGαo-GFP) in the induction of neurite outgrowth in N2a cells (A). A control GFP showed a very limited formation of neurites (Control). Quantification of transfected cells displaying neurites (D). Scale bar, 20 μm.

(E) N2a cells were transfected with a GFP-fusion of the *trans*-Golgi marker β-1,4-galactosyltransferase (GalT-GFP) and the non-tagged human Gαo. Immunostaining against Gαo revealed its co-localization with GalT-GFP at the Golgi region. Color-channels are listed vertically top-to-bottom and a selected area is magnified with the channels displayed horizontally in the same order left-to-right. Scale bars, 10 μm.

(F) Image of a mouse cortical neuron at 7 DIV immunostained against endogenous Gαo and the *cis*-Golgi marker GM130. Boxed area is enlarged as in panel (E). Scale bar, 10μm.

(G) N2a cells were transfected with a GFP-fusion of *Drosophila* Gαo (dGαo-GFP) and immunostained against GM130. dGαo-GFP co-localized at the Golgi with GM130. A selected is zoomed-in as in (E). Scale bars, 10 μm.

(H) Immunostaining of endogenous dGαo in *Drosophila* pupal wings co-expressing an RNAi against dGαo and the *cis*-Golgi marker Arf79F-GFP at 22 hr APF. The specificity of the Ab

against dGαo is indicated by the almost total lack of signal by the downregulation of dGαo. Scale bar, 50μm.

(I) N2a cells expressing a GFP-fusion of Gαo (Gαo-GFP) were treatment with 1 μg/ml Brefeldin A for 18 hr (bottom) or with methanol as control (1 μl/ml, top) and then immunostained against the *cis*-Golgi marker GM130. Brefeldin A induced disassemble of the Golgi apparatus and the loss of Gαo-GFP from the perinuclear region without any noticeable effect on its plasma membrane localization. Boxed areas are enlarged as in panel (E). Scale bar, 10 μm.

(J and K) Western blot of N2a cells expressing the non-tagged Gαo treated with 1 μg/ml Brefeldin A for 18 hr (B) and of S2 cells expressing a GFP-fusion of the *Drosophila* Gαo (dGαo-GFP) treated with 20 μg/ml Brefeldin A for 2.5 hr (C). Controls represent cells treated with the corresponding volumes of methanol. Samples were tested with Abs against Gαo, GFP and α-tubulin (α-tub) as loading control, and no apparent variations in Gαo protein levels were observed.

Data represent mean ± SEM. ns, not significant; ***$p \leq 0.001$.

Figure S2

Gαo pull-downs, Related to Figure 3

(A-B) Characterization of the shRNA permanently transfected BE(2)C cell lines. Specific immunostaining (A) and Western blot (B) showed the almost complete depletion of Gαo in the lines shGαo-A and shGαo-B, but not in the parental and shControl lines. Phallodin was used to label F-actin as control staining (A) and an Ab against α-tubulin (α-tub) used as loading control (B). Scale bar, 50 μm.

(C) Western blot of pull-downs from N2a cells transfected with Gαo-GST and its Golgi-only form goGαo-GST. The goGαo-GST construct was able to efficiently interact with GFP-fusions of the small GTPases Rab1a, Rab3a and Arf1 as well as KDELR. Abs against GFP, GST and Gαo were used for detection.

(D) The correct expression of the GST-fusion constructs of Gαo (Gαo-GST, top) and KDELR (KDELR-GST, bottom) were confirmed by immunostaining against GST in N2a cells co-expressing the Golgi marker GalT-GFP. Scale bar, 10 μm.

(E-H) Western blots of the pull-downs from N2a cells co-transfected with Gαo-GST and GFP-fusions of the partners specified in each panel. The KDELR-GST construct served as control. Abs against GFP and GST were used for detection.

Figure S3

Co-localization of Gαo with small GTPases, Related to Figure 3

(A-C) Confocal images of N2a cells co-transfected with an mRFP-fusion of Gαo (Gαo-mRFP) and GFP-constructs of small GTPases from the Arf (A) and Rab (B) families as indicated in each panel as well as dynamin-1 (Dyn1-GFP; C) and -2 (Dyn2-GFP; C), and clathrin light chain (GFP-clathrin; C). Selected areas are zoomed-in to the right as in Figure S1E. Scale bars, 10 μm.

(D-F) The sole expression of GFP-fusions of Rab1a (left), Rab3a (middle) or Arf1 (right) in N2a cells did not increase neurite outgrowth nor total length of spontaneously formed neurites. Quantification of transfected cells displaying neurites (E) and neurite total length (F) compared to GFP control. Scale bar, 20 μm.

(G and H) Western blot of N2a cells co-expressing Gαo-GFP with GFP-fusions of wild-type (WT) or DN mutant constructs of Rab1a, Rab3a and Arf1 (G). Abs against GFP and α-tubulin (α-tub) were used. Note the reduced Gαo protein level detected by the co-expression of Arf1DN. Quantification of Gαo-GFP levels (H).

(I) Western blot of N2a cells co-transfected with the non-tagged Gαo and GFP-fusions of the dominant negative (DN) mutants of Rab1a, Rab3a and Arf1. Reduced Gαo protein level were observed by the co-expression of Arf1DN. Abs against Gαo, GFP and α-tubulin (α-tub) as loading control were used.

Figure S4

Co-localization of *Drosophila* Gαo with small GTPases, Related to Figures 3, 4 and 6

(A and B) Confocal images of N2a cells expressing the DN mutant of Arf1 (Arf1DN-GFP) showed disassemble of the Golgi apparatus indicated by the immunostaining against the *cis*-Golgi marker GM130 (A). Gαo-mRFP was co-expressed together with the mutants GFP-Rab1aDN (top), GFP-Rab3aDN (middle) and Arf1DN-GFP (bottom) in N2a cells (B). Marked regions are zoomed-in to the right as in Figure S1E. Scale bars, 10 μm.

(C and D) Confocal images of S2 cells co-transfected with a GFP-fusion of the *Drosophila* Gαo (dGαo-GFP) and the mRFP-construct of dRab1 (mRFP-dRab1) showed their co-localization at tubulated Golgi-stacks visualized by the *cis*-Golgi marker GMAP-210 (top, C). The sole expression mRFP-dRab1 did not produce this phenotype (bottom, C). dGαo-GFP co-localized at the Golgi with mRFP-dRab3 (top, D) and dArf79F-mRFP (bottom, D). Scale bars, 5 μm

(E and F) S2 cells co-expressing GFP (for visualization) and mRFP-fusions of dRab1, dRab3, dArf79F and dKDELR did not form protrusions after 30 (top) or 120 min (bottom) seeding (E). Quantification of transfected cells forming protrusions after 120 min seeding (F). Scale bar, 10 μm

(G and H) Western blot of N2a cells co-transfected with dGαo-GFP and mRFP-constructs of the wild-type and mutant forms of dRab1, dRab3, dArf79F, and dKDELR (G). Quantification of dGαo-GFP protein levels (H). Abs against GFP and α-tubulin (α-tub) as loading control were used.

Data represent mean ± SEM. ns, not significant; *$p \leq 0.01$.

Figure S5

Gαo functional interaction with small GTPases at the Golgi, Related to Figures 4 and 5

.

(A) Confocal images of S2 cells co-expressing dGαo-GFP and the mRFP-dRab1DN (top), mRFP-dRab3DN (middle) and dArf79FDN-mRFP (bottom) were immunostained against GMAP-210. Note the almost complete disassemble of Golgi-stacks by the mutant of dArf79F. Scale bar, 5 μm.

(B) Immunostaining against the *cis*-Golgi marker GM130 in N2a cells expressing the constitutive active (CA) Q205L mutant of Gαo (GαoCA-GFP, top) or the dominant negative (DN) mutant of Rab1a (GFP-Rab1aDN, bottom) showed no apparent effect on Golgi morphology. Selected areas are zoomed-in to the right as in Figure S1E. Scale bar, 10 μm.

(C) An enlargement of the Golgi apparatus is observed in N2a cells co-expressing the non-tagged Gαo and a GFP-fusion of Rab1b (GFP-Rab1b). Immunostainings against Gαo (squares at right bottom corners of GFP-Rab1b panels) and GM130 confirmed co-expression and marked the Golgi, respectively. Marked regions are magnified to the right as in Figure S1E. Scale bar, 10 μm.

(D-F) The expression of the BFP-fusion of Gαo (Gαo-BFP) enhanced the accumulation of the GFP-construct of Rim2 (GFP-Rim2) at the GM130-positive Golgi region in N2a cells (D). Gαo-BFP co-expression is shown in the square at the right bottom corner of the corresponding GFP-Rim2 panel (bottom, D). Boxed areas are magnified (right, as in Figure S1E). Mean fluorescence intensity ratios of GFP-Rim2 at the Golgi *vs*. total cell (E). Western blot for the expression of GFP-Rim2 using Abs against GFP, Gαo and α-tubulin (α-tub) as loading control (F). No evident variation in the levels of GFP-Rim2 was observed by Gαo co-expression. Data represent mean ± SEM. ***$p \leq 0.001$. Scale bar, 10 μm.

(G) Western blots of the pull-down from N2a cells co-transfected with Gαo-GST and a GFP-fusion of α-GDI. The KDELR-GST construct served as control. Abs against GFP and GST were used for detection

(H) A Western blot of an *in vitro* binding assay confirmed the interaction of recombinant His_6-tagged Gαo and baculovirus-purified Rab1a and Rab3a. An Ab against His-tag was used for detection, and the Ponceau S staining were used to visualize Rab1a and Rab3a.

(I and J) A BODIPY-GTP uptake assay indicates that GTPγS-loaded Gαo does not possess GEF activity towards baculovirus-purified Rab1a (I) and Rab3a (J). BODIPY-GTP uptake in presence of EDTA (I and J) was used to control the maximal rate of nucleotide loading of Rab1a and Rab3a.

Figure S6

Gαo does not translocate form the PM to the Golgi upon activation, Related to Figures 5 and 6

(A and B) Western blots for the expression of GFP-fusions of Gαo at its C-terminus (Gαo-GFP) or inserted downstream of the glycine residue at position 92 ($G\alpha o^{Gly92}$-GFP). Note the lower expression levels of $G\alpha o^{Gly92}$-GFP (arrowheads) compared to Gαo-GFP (A) and to the endogenous Gαi3 in non-transfected N2a cells (B). Abs against GFP, Gαo/i3 and α-tubulin (α-tub) as loading control were used.

(C) The $G\alpha o^{Gly92}$-GFP construct (right) showed a similar subcellular localization than Gαo-GFP (left) at the perinuclear Golgi region and the plasma membrane. Scale bar, 10 μm.

(D-I) N2a cells were co-transfected with Gαo-GFP (top) or $G\alpha o^{Gly92}$-GFP (bottom) and the muscarinic acetylcholine receptor 2 (M2R, D and E) or the cannabinoid receptor type-1 (CB_1R, F and G). Cells were recorded every second for 2 min before stimulation (arrowheads) with 100 μM Acetylcholine (Ach, D and E) or 10 μM HU-210 (F and G) during 3 min. Cells expressing only the GFP-fusions of Gαo were stimulated with 5 μM Mastoparan-7 (H and I) and recorded as above. Mean fluorescence intensities of selected Golgi regions were measured from 10 different cells (colored lines) and an empty region was used as background (black line). Low expression level of $G\alpha o^{Gly92}$-GFP correlates with low fluorescence intensities (E, G and I) compared to Gαo-GFP signals (D, F and H).

(J) Confocal image of a *Drosophila* pupal wing at 30 hr after puparium formation (APF) showed the correct expression of the *Drosophila* KDELR transgene (dKDELR-mRFP). Scale bar, 50 μm.

(K) Western blot of the Gαo immunoprecipitation (IP) using the Ab against active Gαo (Gαo-GTP). N2a cell extracts expressing non-tagged Gαo were pre-incubated with GDP or GTPγS

previous to the IP. The Ab against total Gαo used for detection revealed the specificity of the Gαo-GTP Ab towards GTPγS-loaded Gαo (arrowhead).

(L) N2a cells expressing the wild-type (top) or the constitutive active Q205L mutant (bottom) of a GFP-fusion of Gαo (Gαo-GFP) were immunostained using the Gαo-GTP Ab. Confocal images recorded using equal settings confirmed the specificity of the Gαo-GTP Ab for the detection of Gαo on its active conformation. Scale bar, 10 μm.

(M-O) N2a cells were co-transfected with Gαo-GFP and a secretable BFP construct containing the KDEL retention signal (ssBFP^{kdel}) or a control ssBFP, and cell extracts (M) and culture media (N) were analyzed by Western blot. An Ab against GFP was used for detection, and the anti-α-tubulin (α-tub) Ab and Ponceau S staining were used as loading controls. The ssBFP^{kdel} construct was detected in cell extracts (M) but not in the media (N), whereas the control ssBFP was almost completely secreted. No apparent variation in Gαo-GFP expression levels were observed in extracts (M). Confocal images of N2a cells expressing cytosolic BFP (left), control ssBFP (middle) or ssBFP^{kdel} (right) showed the retention of the latter in a compartment resembling the endoplasmic reticulum (O). A selected area is zoomed-in (right). Scale bar, 10 μm.

Figure S7

KDELR activates Gαo at the Golgi, Related to Figures 3 and 6

(A and B) Overexpression of KDELR increased Gαo activity at the Golgi region in N2a cells (A). Active Gαo-GFP was detected by immunostaining against GTP-loaded Gαo (Gαo-GTP). Marked regions are magnified (right, as in Figure S1E). Mean fluorescence intensity ratios of active *vs*. total Gαo calculated at the PM and Golgi (B).

(C) Overexpression of Gαo-GFP (above) or Gαo-mRFP (below) did not induce the co-accumulation of endogenous Gβ1 (above) or GFP-Gβ1 (below) at the Golgi apparatus, indicating that Golgi membranes contain mostly monomeric Gαo in N2a cells. Selected areas are magnified to the right as in Figure S1E.

(D and E) Western blot of N2a cells co-expressing Gαo-GFP with KDELR- or KDELR$^{D/N}$-GFP. Anti-GFP and α-tubulin (α-tub) Abs were used (D). Quantification of Gαo-GFP levels (E).

(F) Confocal image of N2a cells expressing the R1WTSH-GFP construct were immunostained against the *cis*-Golgi marker GM130. Note the almost exclusive Golgi localization of R1WTSH-GFP. A boxed area is magnified to the right as in figure S1E.

Data represent mean ± SEM. ns, not significant; ***$p \leq 0.001$. Scale bars, 10 μm.

STAR METHODS

CONTACT FOR REAGENT AND RESOURCE SHARING

Further information and requests for resources and reagents should be directed to and will be fulfilled by Lead Contact, Vladimir L. Katanaev (vladimir.katanaev@unil.ch).

EXPERIMENTAL MODEL AND SUBJECT DETAILS

***Drosophila* Stocks**

The following *Drosophila* lines were used: *MS1096-Gal4, UAS-Gαo* (Katanaev et al., 2005), *OK371-Gal4; CD8-GFP-Sh* (Luchtenborg et al., 2014); *MS1096-Gal4* (8860), *pnr-Gal4* (25758), *hs-hid* (24638), *UAS-Rab1* (24104) and *UAS-Rab3* (9763) – from Bloomington *Drosophila* Stock Center (BDSC); *UAS-Arf79F-GFP* was kindly provided by Tony J. C. Harris (University of Toronto); *UAS-RNAi-Gαo* (110552 and 19124) as well as the other *UAS-RNAi* lines – from Vienna *Drosophila* Resource Center (VDRC); *lines* containing *P-element insertional mutations* – from the Szeged *Drosophila* Stock Centre. *UAS-KDELR-mRFP* line was generated through site-specific germ-line transformation of *φ*X-22A line with attP-landing site on the chromosome arm 2L (24481, BDSC). All crosses were performed at 25°C on the standard cornmeal medium.

Cell lines and culture conditions

Male mouse neuroblastoma Neuro-2a (N2a) and female human epithelial HeLa cells were maintained in MEM (Thermo Fisher Scientific), supplemented with 10% FCS, 2 mM L-glutamine, 1 mM pyruvate, and 1% penicillin-streptomycin at 37°C and 5% CO_2.

Male human neuroblastoma BE(2)C cells (ATCC CRL-2268) were generously provided by Karim Abid (University Hospital of Lausanne). Cells were grown in DMEM/F-12 (Thermo Fisher Scientific), supplemented with 10% FCS, 2.5 mM L-glutamine, 1200 mg/L sodium bicarbonate, and 1% penicillin-streptomycin at 37°C and 5% CO_2.

Male *Drosophila* Schneider-2 (S2) cells were maintained in Schneider's Drosophila Medium (Lonza) supplemented with 10% FCS and 1% penicillin-streptomycin at 28°C.

Female *Spodoptera frugiperda* (Sf9) cells were maintained in TNM-FH (Sigma-Aldrich) supplemented with 10% FCS and 1% penicillin-streptomycin at 28°C either as shaken suspension (60 rpm).

Poly-L-lysine-coated coverslips containing primary mouse cortical neurons obtained from E16 female and male embryos (C57BL/6J mice) grown in Neurobasal medium (Thermo Fisher Scientific) containing 2%

B27 supplement, 1 mM L-glutamine and 1% penicillin-streptomycin were kindly provided by Omar Alijevic (University of Lausanne).

All vector transfections were carried out with X-tremeGENE 9 or HP (Roche). Briefly, DNA plasmids were mixed to equal mass rations and incubated for 5 min at room temperature. Then, the transfection reagent was diluted in Opti-MEM (Thermo Fisher Scientific) to a ratio of 5 µl reagent/100 µl medium, vortexed and added to a plasmid mix of 1.5 µg, vortexed and incubated for 20 min at room temperature, and finally added dropwise on cells grown in 12-well plates to 80-90% confluence. Transfection were lineally scale up when needed.

METHOD DETAILS

Screens

Two-hybrid screening

A saturating yeast two-hybrid screening was performed by Hybrigenics (Hybrigenics-Services). As the prey, a random-primed *Drosophila* adult head cDNA library constructed into pP6 plasmid and 54 and 95 million clones (5- and 9.5-fold the complexity of the library) were screened for Gαo and for Gαo[Q205L], respectively, using a mating approach with Y187 (matα) and L40ΔGal4 (mata) yeast strains. His+ colonies were selected on a medium lacking tryptophan, leucine, and histidine for the Gαo WT and mutant (n = 225 and 171, respectively). Positive prey fragments were amplified by PCR and sequenced at their 5′ and 3′ junctions. The resulting sequences were used to identify the corresponding interacting proteins in the FlyBase database using a fully automated procedure. A confidence score (predicted biological score) was attributed to each interaction (Table S1). Many Gαo interaction partners were identified in multiple independent hits, and half of these interactions showed the highest confidence scores. The other half had a lower or non-computable confidence score, and was represented by only one or two hits, suggesting a lower probability of these interactions.

Affinity purification screening

Unlike the yeast-two hybrid screen which identifies proteins directly interacting with the bait, the affinity purification screen has the advantage of identification of multiprotein complexes binding the bait. Thus, *Escherichia coli* Rosetta-gami 2(DE3) (Novagen) was transformed with His_6-Gαo, His_6-Gαo[Q205L] or His_6-Gαi as control (Kopein and Katanaev, 2009), grown at 37°C to an OD_{600}=0.5 before induction with 1 mM IPTG and additional growth overnight at 28°C, followed by harvesting by centrifugation and storage at -20°C. All subsequent procedures were performed at 4°C. Cell pellets were resuspended in PBS supplemented with 1 mM EGTA, 5 mM β-mercaptoethanol, and 1 mM PMSF, and lysed by a cell disruptor at 0.8 psi (Constant Systems). Debris was removed by centrifugation at 18,000xg for 30 min at 4°C. The

supernatant was applied to Ni-NTA agarose beads (QIAGEN) pre-equilibrated in the same buffer and purification of the His_6-Gαo proteins was performed using the ÄKTAprime plus protein purification system (GE Healthcare). The Ni-NTA beads were washed three times with 10 resin volumes of washing buffer (PBS supplemented with 1 mM EGTA, 5 mM β-mercaptoethanol, 0.1 mM PMSF, and 30 mM imidazole). Proteins were eluted with 200 mM imidazole in the washing buffer. The buffer of purified proteins was exchange to 50 mM HEPES, pH 7.5, 150 mM KCl, 10 mM NaCl, and 1 mM DTT using Amicon 10kDa Centrifugal Filter Units (Millipore), and proteins were coupled to CNBr-activated Sepharose 4 Fast Flow beads (GE Healthcare). This coupling does not decrease the guanine nucleotide-binding properties of Gαo (Kopein and Katanaev, 2009). CNBr-immobilized Gαo (50% slurry, 100 µl) was preloaded with 100 µM GDP or GTPγS in 50 mM HEPES, pH 8.0, 100 mM KCl, 25 mM MgCl2, and 1 mM DTT for 30 min at 25°C. A 20-fold volume excess of *Drosophila* head extracts was added to the slurry and incubated for 4 hr at 4°C under rotation. Matrixes were centrifuged (200xg for 1 min at 4°C), supernatant discarded, and beads were washed two times with 10 bed volumes of the binding buffer (50 mM HEPES, pH 7.5, 150 mM KCl, 10 mM NaCl, 2 mM EGTA, protease inhibitor cocktail (Roche), 0.5% Nonidet P-40, and 0.1% Tween20) at 4°C. Bound proteins were eluted by 8 M urea, separated by SDS-PAGE, and numerous bands seen to be specifically retained on the Gαo-matrixes were subjected to proteomic analysis at the Proteomics Facility University of Konstanz, Germany.

For the generation of *Drosophila* head extracts, adult flies were anesthetized by CO_2 and frozen using liquid nitrogen. Heads were separated from the bodies using the Mini-Sieve set (Bel-Art Products) and smashed on ice in a glass-rod homogenizer (Sartorius) in a hypotonic buffer (10 mM HEPES, pH 7.5, 2 mM EGTA, and protease inhibitor cocktail). After adjusting the ionic strength by adding KCl to 100 mM and HEPES to 50 mM, the debris was removed by a 15 s spin at 200xg and 4°C. The supernatant was centrifuged at 20,000xg for 60 min at 4°C. The pellet was solubilized by rotation for 4 hr at 4°C in 50 mM HEPES, pH 7.5, 150 mM KCl, 10 mM NaCl, 2 mM EGTA, 0.5% NP-40, 0.1% Tween 20, and protease inhibitor cocktail to a concentration of 1.5 mg/ml. Extracts were cleared by a final centrifugation at 20,000xg for 30 min at 4°C. The resulting supernatant was immediately used in pulldown experiments.

Genetic screening on essential genes

To take advantage of *Drosophila* genetics in order to find physiologically relevant Gαo partners, we overexpressed Gαo in developing *Drosophila* wing. Such overexpression leads to a defect in wing spreading due to perturbation in the late stages of wing maturation. We recombined the *MS1096-Gal4* line driving expression within the wing with the *UAS-Gαo* transgene on the first chromosome for the ease of screening. The resulting *MS1096-Gal4, UAS-Gαo* line had the following phenotypes: 1) 78% of heterozygous female flies had folded wings; 2) 93% of hemizygous male flies had folded wings; 3) the

hemizygous male viability was decreased; 4) the size of hemizygous male flies was severely decreased as compared to the females and normal male flies; 5) asymmetric cell divisions in the sensory organ lineage were often defective, resulting in aberrant sensory bristles of the wing margin; 6) planar cell polarity defects were seen in the wing blade, mainly as production of multiple wing hairs. In this suppressor-enhancer screen, we used the wing spreading and the male viability defects as the main read-out phenotypes; in some cases, the planar cell polarity phenotypes of the resulting wings were also analyzed (Table S1). The *MS1096-Gal4, UAS-Gαo* line was crossed to a collection of the *P-element insertional* mutant lines, carrying aberrations in ca. 50% of the second chromosome essential genes which is ca. 25% of the total vital genes of the *Drosophila* genome (Szeged *Drosophila* Stock Centre). At least twenty individuals from each cross were collected and analyzed. Genes, mutations of which suppressed or enhanced Gαo gain-of-function read-out phenotypes, were considered as hits. Statistical differences in the penetrance of these phenotypes from the control group (*MS1096-Gal4, UAS-Gαo* line) were used to evaluate the confidence scores.

Loss-of-function genetic screening

In contrast to Gαo mutants which are early embryonic lethal (Fremion et al., 1999) its tissue-specific knockdown by *UAS-RNAi* transgenes gives viable phenotype. The effectiveness of these constructs was previously confirmed (Luchtenborg et al., 2014). Based on that, we designed genetic loss-of-function suppressor-enhancer screen using RNAi-mediated downregulation of the targeted genes. Thus, we created *MS1096-Gal4; +; UAS-RNAi-Gαo* and *+; UAS-RNAi-Gαo; pnr-Gal4* lines, driving expression of the *UAS-RNAi* transgenes in the wing and notum tissues, respectively. Combination of the two different systems using same approach allows screening for Gαo partners implicated in different tissue developmental programs, thus potentially uncovering more genetic interactions. For the ease of screening, created lines also contained an *hs-hid* transgene on the Y chromosome to obtain virgin females in large numbers: 3rd instar larvae were exposed to a heat-shock at 37°C for 1 hr to kill only males carrying this transgene. This suppressor-enhancer screen was carried out using a cohort of transgenic RNAi lines targeting ca. 10% of protein-coding genes of *Drosophila* genome according to the latest Flybase (FB2017_03) release. The RNAi lines were successively crossed to the lines described above. Minimum twenty flies of both sexes (amount of the analyzed individuals varied largely depending on the viability of the progeny) from each cross were analyzed: phenotypes were identified, their strength judged in a semi-quantitative manner. Since Gαo downregulation itself produced no or just very mild phenotypes in these screen-systems, we considered as hits the genes which loss-of-function phenotypes (if any) was suppressed or enhanced by co-downregulation of Gαo. The false-positive and false-negative rates for the VDRC RNAi library are estimated to be 7 and 29.4%, respectively. All results and supporting information of the screenings can be found in Table S1.

Noteworthy, each of these screening approaches has its own advantages and shortcomings, essentially targeting different subspaces of the interactome (Beltrao et al., 2012) and resulting in a limited overlap of the interaction partners identified in the different screens (Table S1). In a complementary manner, the interaction partners from the different screens build up a near-complete Gαo interactome.

Bioinformatics analysis

Gene Ontology (GO) terms enrichment analysis was done by DAVID (https://david.ncifcrf.gov/) using the whole *Drosophila* genome as background. Over-represented GO terms from the "biological process" domain were used to generate a Functional Enrichment Map. For that we applied an Enrichment Map plugin (http://www.baderlab.org/Software/EnrichmentMap) which uses Cytoscape (http://www.cytoscape.org/) as a software platform to visualize the outcome as a network. Tune parameters were: P-value cut-off of ≤ 0.001, Q-value cut-off of ≤ 0.05 (equals Benjamini correction values), overlap coefficient cut-off of ≤ 0.6. Resulting network was clustered using MCL clustering algorithm and then annotated by ClusterMaker (http://www.rbvi.ucsf.edu/cytoscape/cluster/clusterMaker.shtml) and WordCloud (http://baderlab.org/Software/WordCloudPlugin) plugins, respectively. Annotations of the final functional modules were manually edited. The same bioinformatics analysis was applied to generate the Enrichment Map of human orthologues. For orthology prediction, we used an in-house-made PERL scripts which extract and unify the data from the 10 major orthology databases (Bilousov et al., 2014). The programs created in-house are available at the laboratory's web-page (https://www.unil.ch/dpt/home/menuinst/recherche/groupe-katanaev/files.html). To identify the genes involved in different aspects of vesicle-mediated transport we selected genes associated with the respective term as the backbone, and supplemented this list by adding manually the genes having related GO annotations, and also genes whose human orthologues are known to be involved in vesicle-mediated trafficking. All results of the bioinformatics analysis can be found in Table S2.

Permanently-transfected BE(2) cells

Permanent Gαo depletion in BE(2)C cells was obtained by shRNA interference with annealed primers (Table S3) expressed in the pRetroSuper vector (Oligoengine) as previously described (Solis et al., 2012). Thus, annealed primers were cloned using the BamHI and HindIII sites of the pRetroSuper vector, and the empty vector was used as control. For generation of stable-transfected cell lines, shRNA vectors were transfected into BE(2)C cells, and after 48 hr cells were cultured under selection in 5 μg/ml puromycin (InvivoGen). Cell lines were grown in medium supplemented with 2 μg/ml puromycin to maintain selection pressure.

Plasmids and molecular cloning

Wild-type (WT) and Q205L mutant of human Gαo in pcDNA3.1+ (Thermo Fisher Scientific) were obtained from Missouri S&T cDNA Resource Center and used as template to generate C-terminal GFP, mRFP and BFP fusions. Specifically, Gαo cDNAs were PCR-amplified (primers listed in Table S3) and cloned into the EcoRI and ApaI sites of pEGFP-N1 (Clontech), pmRFP-N1 (Claudia Stuermer, University of Konstanz) and pEBFP2-N1 (Addgene, 54595). For the generation of the Golgi-only construct of Gαo (goGαo-GFP), the cDNA fragment containing the amino acids 30 to 354 of the rat Gαo (Kopein and Katanaev, 2009) was PCR-amplified and cloned in frame into the R1WTSH-GFP vector (Claudia Stuermer, University of Konstanz) in the BamHI/AgeI sites laying between R1WTSH and GFP. The R1WTSH sequence encodes for the N-terminal 30 amino acids of reggie-1/flotillin-2, and showed an almost exclusive Golgi localization in N2a cells (Figure S7F) due to myristoylated and palmitoylated residues within this region. Deletion of the N-terminal 29 amino acids of Gαo (highly conserved among Gαi/o members) was chosen because a corresponding Gαi1 construct showed that this region is necessary for membrane binding but dispensable for pivotal biochemical properties, such as GPCR binding and GPCR-mediated activation. To generate the Gαo-GST constructs, the GST cDNA was PCR-amplified from pGEX-4T-1 (GE Healthcare) and used to replace the AgeI/NotI GFP sequence from Gαo-GFP and goGαo-GFP. The *Drosophila* Gαo cDNA (Kopein and Katanaev, 2009) was PCR-amplified and cloned into pEGFP-N1 by EcoRI and BamHI to generate a C-terminal GFP-fusion. The dGαo-GFP sequence was then digested with EcoRI and NotI, and subcloned into the pAc5.1/V5-HisA plasmid (Thermo Fisher Scientific) for its expression in *Drosophila* cells. The His_6-tagged Gαo was previously reported (Lin et al., 2014), and the $Gαo^{Gly92}$-GFP construct was kindly provided by Narasimhan Gautam (Akgoz et al., 2004). The BamHI/XhoI insert containing the Rab1a cDNA was cut from the pMyc-Rab1a plasmid (Dupre et al., 2006) and ligated into the BglII and SalI sites of pEGFP-C1 (Clontech) and into pGEX-4T-1 by the same restriction sites to generate the GFP-Rab1a and the bacterial GST-Rab1a constructs, respectively. The Rab3a sequence was PCR-amplified from the GFP-Rab3a plasmid provided by Robert D. Burgoyne (University of Liverpool), digested with BamHI and XhoI, and inserted into the same sites of the pGEX-4T-1 plasmid to produce the GST-Rab3a bacterial construct. For baculovirus expression, the BamHI/NotI coding inserts of Rab1a and Rab3a cut from the GST plasmids were ligated into the same sites of the pFastBac-NT vector with a N-terminal His_6-tag (Thermo Fisher Scientific). The Arf1-GFP plasmid (Chun et al., 2008) was used to create the GST-Arf1 plasmid for bacterial expression by PCR amplification, digestion with BamHI and XhoI, and insertion into the matching sites of pGEX-4T-1. The S25N and Q70L mutants of Rab1a, the T36N mutant of Rab3a and the T31N mutant of Arf1 were obtained by point mutagenesis. The Rab1b cDNA was amplified from the plasmid pSV-Rab1b provided by Angelika Barnekow (University Muenster), cut with BamHI and KpnI, and inserted into pEGFP-C1 by BglII and KpnI. The plasmids pJAF-Arf2, pJAF-Arf3 and pJAF-Arf4 obtained

from Gregory J. Pazour (University of Massachusetts Medical School) were used to generate GFP-fusions of Arf2, Arf3 and Arf4, respectively, by cutting the Arf cDNAs with KpnI and ligating into the same site of pEGFP-N1. The GST-αGDI plasmid was kindly provided by Jean Gruenberg (University of Geneva) and Marino Zerial (Max Planck Institute of Molecular Cell Biology and Genetics), and the GFP-αGDI construct was generated by ligating the KpnI/XmaI fragment from the original GST-αGDI into the same sites of pEGFP-C1. The GalT-GFP, -mRFP and -BFP constructs were created by replacing the AgeI/NotI mTurquoise2 sequence of the GalT-mTurquoise2 plasmid (Goedhart et al., 2012) by the corresponding GFP, mRFP and BFP cDNAs cut from pEGFP-N1, pmRFP-N1 and pEBFP2-N1, respectively. The resulting GalT-mRFP sequence was digested using AfeI and NotI, and inserted into pAc5.1/V5-HisA by EcoRV and NotI for expression in *Drosophila* cells. The AgeI/BsrGI GFP insert from the pEGFP-C1 was used to replace the corresponding mRFP sequence from the mRFP-Clathrin plasmid (Claudia Stuermer, University of Konstanz). The KDELR-CFP was generously provided by Angel Velasco (University of Seville) and the KDELR-GFP and -GST constructs were created by replacing the AgeI/NotI CFP sequence by the corresponding GFP or GST inserts cut from pEGFP-N1 and Gαo-GST, respectively. The KDELR D193N mutant was generated by point mutagenesis. The secretable GFP construct (ssGFP) containing the prion protein secretion signal upstream of GFP in the pEGFP-C1 plasmid (provided by Edward Málaga-Trillo, Universidad Peruana Cayetano Heredia) was used to generate the ssBFP construct by exchanging the AgeI/BsrGI GFP sequence with the matching BFP insert from pEBFP2-N1. A C-terminal KDEL retention sequence was introduced into the ssBFP to generate the ssBFP^{KDEL} plasmid by point mutagenesis. The pEF-T7-Rim2-RBD plasmid obtained from Mitsunori Fukuda (Tohoku University) was used to generate the bacterial GST-Rim2 construct by cutting with the BamHI and NotI enzymes, and ligating into pGEX-4T-1 by the same sites. The GST-Rim2 vector was then digested with BamHI and EcoRI, and the insert containing the Rim2-RBD sequence was subcloned into the BglII and EcoRI sites of pEGFP-C1 to create the GFP-Rim2 plasmid. The GFP-Gβ1 construct was created by replacing the AgeI/BsrGI mCerulean sequence of the mCerulean-Gβ1 plasmid (Thaler et al., 2005) with the corresponding GFP cDNA cut from pEGFP-C1. For the GST-Gβ1, the GST sequence was PCR-amplified from the pGEX-4T-1 plasmid, and used to replace the AgeI/XhoI mCerulean cDNA from the original plasmid. The Gγ3 cDNA was digested from the pHA-Gγ3 plasmid (Missouri S&T cDNA Resource Center) using HindIII and XhoI, and ligated into pEGFP-C3 (Clontech) by HindIII and SalI to generate a GFP-Gγ3 construct. The *Drosophila* cDNAs for Rab1 (FI01544), Rab3 (LP05860), Arf79F (LD24904) and KDELR (LD06574) were obtained from the Drosophila Genomics Resource Center (DGRC). The mRFP-dRab1 was generated by PCR amplification, digestion with EcoRI and BamHI, and ligation into the pmRFP-C1 cut with the same enzymes. The resulting plasmid was subsequently digested with AgeI and BamHI, and subcloned into the same sites of pAc5.1/V5-HisA to generate the mRFP-dRab1 construct for expression in *Drosophila* cells. To create the

mRFP-dRab3 construct, the dRab3 was amplified by PCR, the product was digested with EcoRI and KpnI, and inserted into the pmRFP-C1 vector linearized with the same enzymes. The mRFP-dRab3 sequence was then cut with the NheI and ApaI enzymes, and ligated into the pAc5.1/V5-HisA plasmid digested with XbaI and ApaI. The cDNAs for dArf79F and dKDELR were PCR-amplified, digested with KpnI and BamHI, and separately ligated into pmRFP-N1 by the same sites. The dArf79F-mRFP and dKDELR-mRFP sequences were then cut using the KpnI and NotI enzymes, and subcloned into the corresponding sites of pAc5.1/V5-HisA for *Drosophila* expression. The dRab1 S25N, dRab3 T35N, dArf79F T31N and dKDELR D193N mutants were created by point mutagenesis using the oligonucleotides for their mammalian counterparts. To generate the UAS-dKDELR-mRFP plasmid, the dKDELR-mRFP sequence was cut from the plasmid described above by BglII and NotI enzymes and subcloned into corresponding sites of the pUASTattB vector (FBmc0003002; http://flybase.org/). This was used for site-specific germ-line transformation of *Drosophila* embryos and generation of a transgenic fly line. The following plasmids were kindly provided as indicated: the ts045 mutant of the VSVG-GFP by Jennifer Lippincott-Schwartz (National Institutes of Health), the GFP-FM4-hGH by Andrew Peden (The University of Sheffield), the GFP-Rab4a by Marci A. Scidmore (Cornell University), the GFP-Rab5a by Peter van der Sluijs (University Medical Center Utrecht), the FAPP1-PH-GFP construct by Tamas Balla (National Institutes of Health), the GST-GGA3 plasmid by Jean-Luc Parent (Université de Sherbrooke), the cannabinoid receptor type-1 by Mary E. Abood (Temple University), and the Dyn2-GFP by Claudia Stuermer (University of Konstanz). The muscarinic acetylcholine receptor 2 plasmid was from the Missouri S&T cDNA Resource Center. The following vectors were additionally obtained from Addgene: GFP-Rab7a (Choudhury et al., 2002), GFP-Rab11a (Choudhury et al., 2002), Arf5-GFP (Chun et al., 2008), Arf6-CFP (Beemiller et al., 2006), Dyn1-GFP (Lee and De Camilli, 2002), and BFP-MannII (Subach et al., 2011).

Immunofluorescence and microscopy

For immunostaining, N2a and BE(2)C were transfected for 6 hr, trypsinized and seeded on poly-L-lysine-coated coverslips for additional 18 hr before fixation. S2 cells were transfected for 24 hr, washed and resuspendend in complete media, and seeded on poly-L-lysine-coated coverslips for 30 or 120 min before fixation. All cells were fixed for 20 min with 4% paraformaldehyde in PBS, permeabilized for 1 min using ice-cold PBS supplemented with 0.1% Triton X-100, blocked for 30 min with PBS supplemented with 1% BSA, incubated with primary in blocking buffer for 2 hr cells at room temperature, washed and subsequently incubated with fluorescent secondary antibodies in blocking buffer for 2 hr cells at room temperature. All fluorescent-labelled secondary antibodies were from Jackson ImmunoResearch. Coverslips were finally mounted with Vectashield (Vector Labs) for microscopy analysis. Cells were recorded with a Plan-Apochromat 63x/1.4 oil and a Plan-Apochromat 20x/0.8 objectives on a LSM780

Quasar Confocal Microscope and further processed using the ZEN blue software (all Zeiss). When fluorescence quantification was required (see below), all images were recorded using the same confocal settings, and fluorescence mean intensities were determined using ImageJ (National Institutes of Health).

Neurite outgrowth assay

The Neurite outgrowth assay was as previously described (Luchtenborg et al., 2014). Briefly, N2a cells were co-transfected for 18 hr with the plasmids indicated in the corresponding figures. Then, cells were trypsinized and seeded on poly-L-lysine-coated coverslips for additional 24 hr to allow neurite formation. For Brefeldin A (BFA; Sigma-Aldrich) treatment, transfected N2a cells were allowed to adhere on coverslips for 6 hr and incubated for additional 18 hr with 1 μg/ml of BFA or 1μg/ml methanol as control in complete MEM. Cells were finally PFA-fixed, stained with rhodamine-phalloidin (Molecular Probes) and DAPI (Sigma-Aldrich), and mounted for microscopy analysis. Samples were recorded with a Plan-Neofluar 10x/0.3 objective on an Axio Imager.M1 microscope equipped with an AxioCam HRc camera, and analyzed using the AxioVision software (all from Zeiss) and ImageJ. The number of transfected cells displaying neurites, neurites per cell and total neurite length were scored from 10-20 randomly taken images (≥100 cells per condition), and statistical analysis were determined using one-way ANOVA or Student's *t*-test.

Protrusion formation assay in S2 cells

S2 cells were transfected for 24 hr with the plasmids indicated in the corresponding figures. Cells were washed, resuspended in fresh media and seeded on poly-L-lysine-coated coverslips for 30 or 120 min at 28°C to allow formation of protrusions. For BFA treatment, transfected S2 cells were resuspended in fresh media supplemented with 20 μg/ml of BFA (or methanol as control) and incubated for 30 min prior to the seeding on poly-L-lysine-coated coverslips for additional 120 min all at 28°C. Cells were finally PFA-fixed, and directly stained with rhodamine-phalloidin or permeabilized, immunostained and mounted for microscopy analysis. Samples were recorded with a Plan-Neofluar 20x/0.50 objective on an Axio Imager.M1 microscope equipped with an AxioCam HRc camera and analyzed using AxioVision software and ImageJ. The amount of transfected cells displaying protrusions, the number of structures per cell and the length of the longest protrusion were scored from 15-20 randomly taken images (≥100 cells per condition), and one-way ANOVA or Student's *t*-test was used for statistical analysis.

Biochemical analyses

N2a, BE(2)C and S2 cells were lysed with ice-cold Lysis buffer (20 mM Tris-HCl, pH 7.5, 100 mM NaCl, 5 mM $MgCl_2$, 2 mM EDTA, 1% Triton X-100 and 10% glycerin) supplemented with a protease inhibitor cocktail. Extracts were cleared by centrifugation at 15,000xg and 4°C, boiled at 95°C for 5 min and finally

analyzed by SDS-PAGE and Western blots (WBs). Alternatively, transfected N2a and S2 cells were treated with BFA as described above (Neurite outgrowth assay and Protrusion formation assay in S2 cells), and directly lysed and prepared for SDS-PAGE and WBs. All HRP-labelled secondary antibodies were from Jackson ImmunoResearch. Quantification of blots was done using ImageJ from at least 3 independent experiments and statistical analysis was carried out using one-way ANOVA or Student's *t*-test.

GST-based pull-down

N2a cells were harvested after 24 hr post-transfection with GST-lysis buffer (1% Triton X-100 and 10% glycerol in PBS) supplemented with a protease inhibitor cocktail. Cleared cell extracts were incubated with 30 µl of Glutathione Sepharose 4B beads (GE Healthcare) overnight at 4°C. Beads were repeatedly washed with GST-lysis buffer, prepared for SDS-PAGE and finally analyzed by Western blot using anti-Gαo, anti-GFP and anti-GST Abs. When required, Student's *t*-test was used for statistical analysis of at least 4 independent experiments.

Pull-down of GTP-loaded Rab3a and Arf1

For the pull-down of active GTP-loaded Rab3a and Arf1, the GST-fusion constructs of Rim2 and GGA3 were expressed in *Escherichia coli* BL21-CodonPlus (DE3)-RIPL (Stratagene) and isolated from bacteria extracts using glutathione Sepharose 4B beads (GE Healthcare) in GST-lysis buffer. After several wash steps, loaded beads were stored in GST-lysis buffer at a 50% slurry and 4°C.

N2a cells were co-transfected for 24 hr with Gαo and the GFP-fusion constructs of Arf1 or Rab3a, and the empty pcDNA3.1+ plasmid was used as control. Cell lysates were obtained using the GST-lysis buffer described above (GST-based pull-down) and cleared extracts were incubated under rotation with 20 µl of the corresponding GST-loaded beads for 1 hr at 4°C. Beads were repeatedly washed, and bound proteins were eluted with 40 mM reduced glutathione (Sigma-Aldrich) in TBS buffer (20 mM Tris-HCl, pH 8.0, and 150 mM NaCl). Samples were prepared for SDS–PAGE, and WBs carried out using anti-GFP and anti-Gαo Abs. Student's *t*-test was used for statistical analysis of 4 independent experiments.

***In vitro* binding assay**

Recombinant His_6-tagged Gαo and the GST-fusions of Arf1, Rab1a, Rab3a and αGDI were expressed in *Escherichia coli* Rosetta-gami (Novagen) and purified with the corresponding tag-specific affinity beads Ni-NTA agarose (QIAGEN) and glutathione Sepharose 4B beads. Protein purity was assessed by SDS-PAGE and Coomassie blue staining, and GTP-binding activities were controlled as previously described (Lin et al., 2014).

For the *in vitro* binding assay, His_6-Gαo was preloaded with 1 mM GDP or GTPγS in TBS buffer supplemented with 1 mM DTT and 5 mM $MgCl_2$ for 2 hr at 22°C. The excess of nucleotides was removed by a 10,000x buffer exchange using Amicon 10kDa Centrifugal Filter Units (Millipore). Samples were cleared by centrifugation at 15,000xg for 5 min, and protein concentrations were normalized. Simultaneously, the GST-tagged small GTPases or pure GST were incubated with 1 mM GDP or GTPγS in TBS supplemented with 5 mM EDTA for 1 hr at 22°C. Proteins were subsequently bound to glutathione Sepharose 4B beads at 50 nmol per ml of resin, and washed with binding buffer (TBS containing 1% Triton X-100, 1% glycerol and 0.2 mM DTT). After the last wash, 20 µl of beads were mixed with GDP- or GTPγS-loaded His_6-Gαo to a final concentration of 1 µM and incubated under rotation for 1 hr at 22°C. Beads were thoroughly washed and bound proteins were eluted with binding buffer supplemented with 10 mM reduced glutathione. Eluates were prepared for SDS-PAGE and WB analysis was done using an antibody against the RGS-His epitope. A ponceau S solution (Sigma-Aldrich) was used to detect GST proteins on nitrocellulose membranes prior to the WB. Statistical analysis of 3 independent experiments was done using Student's *t*-test.

Baculovirus protein expression and analysis

Human Rab1a and Rab3a were produced in Sf9 cells using Bac-to-Bac baculovirus expression system (Thermo Fisher Scientific). The baculovirus stock obtained after 5 days post initial transfection of *E.coli*-derived bacmid was amplified as follows: it was diluted 1:10 in the fresh Sf9 culture with ca. $0.5x10^7$ cells/ml and left for 4 days on the shaker. The cell debris was removed by centrifugation for 5 min at 1,000xg to produce cleared supernatant. This cycle has been repeated until the total volume of the baculovirus supernatant was enough to inoculate preparative amounts of the culture. For the expression, 150 ml of Sf9 cells at $5x10^6$ cells/ml were infected with freshly produced viral stock and shaken for 2 days at 60 rpm. The cells were harvested, washed and the membrane-bound Rabs were purified. Briefly, cells were lysed by a cell disruptor at 0.8 psi (Constant Systems), cell debris was removed by 5 min centrifugation at 1,000xg and 4°C, and cell membranes were harvested by ultracentrifugation at 100,000xg for 1 hr and 4°C. Membrane associated (geranylated) Rabs were solubilized from the membrane pellets in TBS buffer containing 1% CHAPS and purified using Ni-NTA agarose beads (QIAGEN).

Purified His_6-Rabs were bound to GST-αGDI (see *in vitro* binding assay) by a detergent gradual dilution. Briefly, 1 mg of GST-αGDI were mixed with 2-3 mg of Rab proteins in TBS buffer containing 1% CHAPS, 1 mM GDP and 5 mM $MgCl_2$. Subsequently, the mixture was diluted on ice by adding TBS buffer in order to reduce CHAPS concentration by 0.1% every 30 min. When the concentration of CHAPS was reduced to 0.3%, the mixture was incubated overnight on ice, any precipitate was removed by 10 min centrifugation at 4,000xg and 4°C, and the complex was isolated by sequential tandem purification using first glutathione

Sepharose 4B and second Ni-NTA beads. The formation and purity of the His_6-Rab/GST-αGDI complexes were confirmed by SDS-PAGE followed by Coomassie staining.

A His_6-Gαo *in vitro* binding assay using glutathione Sepharose 4B beads was performed essentially as described above (*In vitro* binding assay) with following modifications: the Gαo binding to the Rab/αGDI complexes was performed in His_6-tag elution buffer (TBS supplemented with 0.1% CHAPS and 300 mM imidazole, pH 7.6). Final concentration of the complex was 100 µg/ml for Rab1a and 50 µg/ml for Rab3a, and Gαo was supplemented at 500 µg/ml. Samples were finally analyzed by SDS-PAGE and WB against GST and RGS-His epitope.

Binding of Gαo to Rabs immobilized on the CNBr sepharose (GE Healthcare) was analyzed essentially as described in (Lin et al., 2014). Briefly, the coupling buffer for CNBr beads was 20 mM HEPES, pH 7.4, 150 mM NaCl, 1% CHAPS. Subsequently, immobilized proteins were prepared by mixing a total of 100 µg of His_6-Rab1a, His_6-Rab3a or purified GST (as control) with 30 µl of the beads. Binding was performed in a total volume of 100 µl and His_6-Gαo was added to a final concentration of 1 mg/ml. Samples were repeatedly washed and beads directly boiled for SDS-PAGE and Western blot analysis.

The Rab1a and Rab3a kinetic assays using fluorescent BODIPY-GTP (Molecular Probes) were performed as described previously (Lin et al., 2014) with the following modifications: Rab proteins were diluted at 3 µM in assay buffer (TBS, 0.5% CHAPS, 5 mM MgCl2, 0.1% BSA) and mixed in 96-well plates with GTPγS-loaded His_6-Gαo or MBP as control at a final concentration of 10 µM. Following 10 min incubation, the reaction was started by addition of BODIPY-GTP to the final concentration of 0.6 µM, and recorded using a time-lapse fluorescence measurement in a VICTOR3 plate reader (Perkin Elmer). To control whether absence of Gαo on Rab proteins is not due to already maximal rate of nucleotide incorporation at given conditions, we additionally performed the same assay in presence of 10 mM EDTA, which is known to strip off Mg^{2+} from Rab-GDP and drastically enhance the nucleotide uptake. For baseline, 10 µM GTPγS-loaded Gαo was measured in the same experiment in the absence of Rabs. Preloading of Gαo with GTPγS was produced by incubation of 100 µM His_6-Gαo with 1 mM GTPγS in TBS supplemented with 10 mM $MgCl_2$ for 2 hr at RT, and the removal of excess GTPγS by a 10,000-fold buffer exchange to TBS using Amicon 10kDa Centrifugal Filter Units (Millipore).

VSVG transport assay

N2a cells were co-transfected with $VSVG^{ts045}$-GFP and Gαo or empty pcDNA3.1+ as control for 18 hr at 40°C to allow the expression and accumulation of the VSVG mutant in the ER. Then, cells were quickly cooled down at 32°C with serum-free MEM supplemented with 20 mM Hepes, pH 7.4 and 50 µM cyclohexamide to block *de novo* synthesis of $VSVG^{ts045}$-GFP, and kept at 32°C for additional 30 and 60

min. Biotinylation of cell surface proteins was carried out as previously described (Solis et al., 2012). Briefly, cells were incubated on ice with 0.5 mg/ml sulfo-NHS-SS-biotin (Pierce) in PBS for 30 min and free sulfo-NHS-SS-biotin was quenched by two 5 min washes with ice-cold 50 mM NH_4Cl in PBS. Cell extracts were done with Lysis buffer as described above (Biochemical analyses) and biotinylated proteins were collected from cleared extracts with 20 µl of NeutrAvidin beads (Pierce) overnight under rotation at 4°C. Samples were finally analyzed by Western blot using Abs against GFP and Gαo. One-way ANOVA was used for statistical analysis of 3 independent experiments.

Reverse dimerization assay

The reverse dimerization assays was carried out as previous described (Gordon et al., 2010). Briefly, N2a or BE(2)C cells were co-transfected with GFP-FM4-hGH and Gαo, Gαo-GST, goGαo-GST, or empty pcDNA3.1+ for 18 hr, and additionally incubated for 30 min at normal culture conditions with MEM or DMEM/F-12 supplemented with 20 mM Hepes, pH 7.4 and 50 µM cyclohexamide to block *de novo* synthesis of GFP-FM4-hGH. Then, the D/D solubilizer (Clontech) was added to the cells at a final concentration of 1 µM to allow GFP-FM4-hGH secretion. The assay was stopped by adding ice-cold PBS at the time points indicated in the corresponding figures, cells were washed 3 times with ice-cold PBS, lysed as described above (Biochemical analyses) and prepared for SDS-PAGE and WB using Abs against GFP, Gαo, GST and α-tubulin. Statistical analysis of at least 3 independent experiments was done using one-way ANOVA or Student's *t*-test.

Quantification of Golgi area

To determine the area covered by the Golgi apparatus in N2a cells, an immunostaing against GM130 was carried out as described above (Immunofluorescence and microscopy) using a Cy3-conjugated secondary antibody. Briefly, N2a cells were co-transfected with the constructs indicated in the corresponding figure, and the empty pEGFP-N1 and pcDNA3.1+ plasmids were used as control and/or to normalize DNA quantities for transfection. The co-expression of the non-tagged Gαo was confirmed by immunostaining using an antibody against Gαo/i3 and a Cy5-coupled secondary antibody. The area covered by the GM130 staining was measured from confocal images using the AxioVision software (>100 cells per condition), and statistical analysis was carried out using one-way ANOVA.

Golgi accumulation of FAPP1-PH-GFP and GFP-Rim2

Confocal images of N2a cells co-transfected with FAPP1-PH-GFP and Gαo or control pcDNA3.1+, or BE(2)C cells co-transfected with FAPP1-PH-GFP and BFP, $ssBFP^{KDEL}$, or $ssBFP^{KDEL}$ plus Gαo-GST were used to determine FAPP1-PH-GFP accumulation at the Golgi. To avoid interferences due to different expression levels of the construct among single cells, GFP-fluorescence was measured at the Golgi region

indicated by the GM130 immunostaining (not shown in the final images) as well as at the total cell area, and the ratio values were used to determine the relative accumulation of the construct at the Golgi apparatus. The co-expression of Gαo was confirmed by immunostaining using an antibody against Gαo/i3 and a Cy5-coupled secondary antibody. Similarly, confocal images of N2a cells co-expressing GFP-Rim2 and Gαo-BFP or control GalT-BFP were analyzed as above. Student's *t*-test was used for statistical analysis of ≥50 cells per condition.

Europium-labeled GTP assay

HeLa cells seeded on 96-well plates until 60-70% confluence were transfected with the 12 µg/ml of total plasmid DNA of the constructs indicated in the corresponding figure. After 24 hr, the medium was removed, the cell layer was quickly rinsed 2 times with 100 µl per well of Europium-labeled GTP (GTP-Eu) buffer (50 mM HEPES, pH 7.5, 150 mM NaCl, and 1 mM MgCl2), and cellular membranes were permeabilized with GTP-Eu buffer containing 0.5% saponin for 10 min at RT and shaking. Then, permeabilized cells were incubated with 100 µM control (DTSEKDAS) or KDEL-containing (DTSEKDEL) peptides in DMSO, the reaction was started by adding 5 µl of 50 nM GTP-Eu (Perkin Elmer), and was allowed to proceed for 15 min with shaking. Cells were than scraped and transferred to 96-well AcroWell filter plates (Sigma-Aldrich). Wells were washed once with TBS supplemented with 100 µM $MgCl_2$ and measured in a VICTOR3 plate reader (Perkin Elmer) using a built-in protocol for Europium label (Koval and Katanaev, 2011). The activation of the Gαo was measured as a ratio (in %) between the fluorescence of wells stimulated by KDEL-containing peptide (n=7) and basal fluorescence in control wells (n=5) with n=4-9 independent repeats for each condition. Statistical significance was determined by Student's *t*-test.

Activation of Gαo by KDELR

The ability of the antibody against active Gαo to detect GTP-loaded Gαo was determined by an immunoprecipitation assay. N2a cells expressing Gαo were harvested using the Assay-lysis buffer (20 mM Tris-HCl, pH 7.4, 150 mM NaCl, 1 mM EDTA, 10 mM $MgCl_2$ and 1% Triton X-100) supplemented with protease inhibitors, the cleared lysate was split in two equal parts and incubated for 90 min at 30°C in the presence of 1 mM GDP or 100 µM GTPγS. Then, the antibody and protein A/G beads were added to each sample and rotated for 30 min at 4°C. Beads were washed with Assay-lysis buffer and finally prepared for SDS-PAGE and WB analysis. The specificity of the anti-active Gαo antibody was parallely tested by immunostaining performed as described above (Immunofluorescence and microscopy) and using a Cy3-coupled secondary antibody. Stained N2a cells expressing the Gαo-GFP WT or Q205L mutant we recorded using the same confocal settings to assess fluorescence intensity.

To characterize the ssBFP and ssBFP^{KDEL} constructs, N2a cells were separately co-transfected with Gαo-GFP and one of the constructs for 6 h, the transfection media was exchanged by fresh complete media, and cells were incubated by additional 18 hr at normal culture conditions. Then, media were collected and cell extracts prepared using Lysis buffer as described above (Biochemical analyses). Cleared media and cell extracts were prepared for SDS-PAGE, and WB analysis was done against GFP and α-tubulin. A ponceau S solution was used as loading control for culture media. The retention at the ER of the ssBFP^{KDEL} construct was determined by confocal microscopy in transfected N2a cells.

Then, N2a cells co-expressing Gαo-GFP and ssBFP^{KDEL} or control ssBFP were immunostained using an antibody against GTP-loaded Gαo and a Cy3-conjugated secondary antibody to determine the levels of Gαo activation. The fluorescence mean intensities derived from the Cy3 and GFP fluorophores were measured from confocal images at the PM and perinuclear regions marked by Gαo-GFP, and their ratio values at each compartment were used to determine the GTP-loading of Gαo over total level of the protein. A similar analysis was done in N2a cells co-transfected with Gαo-GFP and KDELR-GST or control pcDNA3.1+ plasmids. At least 50 cells per condition were analyzed and Student's *t*-test was used for statistical analysis.

RT-PCR

Total RNA was extracted from N2a cells using the NucleoSpin RNA kit (Macherey-Nagel). The cDNA synthesis was done by the HIV Reverse Transcriptase (Thermo Fisher Scientific), and the resulting product was used as template for the PCRs with the ThermoPol DNA Taq polymerase (New England Biolabs). Briefly, 1 µg of total RNA were mixed with 2 µl of 50 µM oligo(dT) primer to a 12 µl final volume, incubated 3 min at 85°C, and then placed on ice. Then, 2 µl of the 10X Reaction buffer, 1 µl dNTPs (10 mM each), and 1 µl of the HIV Reverse Transcriptase (freshly diluted to a 1 U/µl in 1X Reaction buffer) were added to a final volume of 20 µl. The reverse transcription reaction was achieved incubating at 43°C for 1 hr and then at 92°C for 10 min to inactivate the HIV Reverse Transcriptase. Finally, 1 µl of the resulting cDNA was used to run each PCR, adding 5 µl of 10X ThermoPol Reaction Buffer, 1 µl of dNTPs, 1 µl of Forward and Reverse primers (20 µM), 0.25 µl of the *Taq* DNA Polymerase to a final concentration of 50 µl. The PCR cycle was as follows: Initial denaturation at 95°C and 30 secs, 30 cycles of 95°C for 30 secs, 55°C for 30 sec, and 68°C for 1 min. Amplification of β-actin was used as control. All primers (listed in Table S3) were designed using the Primer3Plus web-interface (http://www.bioinformatics.nl/cgi-bin/primer3plus/primer3plus.cgi).

Live imaging

N2a cells were transfected for 6 hr with the plasmids indicated in the corresponding movie, trypsinized and seeded on poly-L-lysine-coated coverslips, and further kept under normal culture conditions overnight.

Then, coverslips were washed with a Hank's Balanced Salt Solution (Gibco) supplemented with 10 mM Hepes (pH 7.4), mounted on a Chamlide CMB magnetic chamber (Live cell instrument), and kept at 37°C until recording. Cells expressing Gαo-GFP or GalT-GFP were recorded at one image per second for 3 min. Cells expressing Gαo-GFP or $G\alpha o^{Gly92}$-GFP were recorded at one image per second for 2 min prior to the stimulation with 100 μM Acetylcholine (Sigma-Aldrich), 10 μM HU-210 (Cayman Chemical) or 5 μM Mastoparan-7 (Sigma-Aldrich) for additional 3 min. Recordings were done in a VisiScope Cell Explorer System (Visitron Systems) equipped with a Plan-Apochromat 63x/1.4 oil objective on an Axio Observer.A1 microscope (Zeiss), a CoolSNAP HQ2 CCD camera (Photometrics), a VisiChrome Polychromator with a Xenon-lamp 75 Watts, and the MetaFluor Fluorescence Imaging software (Molecular Devices). For analysis, movies were generated from stacks using the "Invert LUT" function of the ImageJ software, and the fluorescence mean intensity of an area at the center of the Golgi region was measured from stacks in 10 cells per condition.

Transfected S2 cells expressing dGαo-GFP alone or together with mRFP-dRab1 WT or DN were washed with complete media, mounted on poly-L-lysine-coated coverslips placed into a Chamlide CMB magnetic chamber, and allowed to spread and form protrusions for 30 min at 28°C before recording. Images were then recorded every 5 sec for 15 min as described above and edition was done with ImageJ.

Analysis of *Drosophila* tissues

Adult wings were collected in 70% ethanol, subsequently replaced by isopropanol, and then mounted in GMM for the light microscopy analysis (Katanaev et al., 2005). Multiple wing hair (mwh) events were counted in the B1 region of the wing blade. Samples were recorded in a Plan-Neofluar 20x/0.50 objective on an Axio Imager.M1 microscope equipped with an AxioCam HRc camera and analyzed using ImageJ. Statistical analysis was determined using Student's *t*-test.

For immunostaining of pupal wings, white prepupae were staged at 25°C, pupae were collected at 22 or 30 hr after puparium formation (APF), cleaned from viscera, and then fixed with a 4% paraformaldehyde solution in PBS for 20 min. After fixation, pupal wings were decuticlized and permeabilized first with 0.5% NP-40 in PBS for 30 min, and then with 0.2% Tween-20 in PBS for 10 min. Samples were then immunostained and mounted with Vectashield for microscopy analysis.

Drosophila NMJs were obtained as in (Luchtenborg et al., 2014). Shortly, 3rd instar larvae were collected in cold PBS, dissected and then fixed for 20 min with 4% paraformaldehyde in PBS. After permeabilization in PBS supplemented with 0.05% Triton X-100 and 5% goat serum for 1 hr, samples were immunostained and mounted with Vectashield for fluorescence microscopy. Statistical analysis was determined using Student's *t*-test.

Pupal wings and NMJs were recorded with a Plan-Apochromat 63x/1.4 oil and a Plan-Apochromat 20x/0.8 objectives, respectively, on a LSM780 Quasar Confocal Microscope and further processed using the ZEN blue software.

QUANTIFICATION AND STATISTICAL ANALYSIS

While mentioned, n represents the number of flies used in the experiment. Data are represented as mean ± SEM. Statistics analysis was performed using Prism v5.03. Student's *t*-test was used in Figures 1F, 1G, 2F-H, 2J-L, 2R, 3C, 4F, 4H, 5B, 5G, 5J, 5L, 6C, 6D, 6F, 6G, 7B, 7D, 7F, 7H, 7J, S1D, S4H, S5E, and S7B. ANOVA was used in Figures 1E, 2N, 2P, 3G-I, 4B-D, 5E, 6K-M, 6O-Q, S3E, S3F, S3H, S4F, and S7E. In all figures, *$p \leq 0.01$; **$p \leq 0.005$; ***$p \leq 0.001$.

DATA AND SOFTWARE AVAILABILITY

For orthology prediction (see Bioinformatics analysis), we used an in-house-made PERL scripts which extract and unify the data from the 10 major orthology databases. The programs created in-house are available at the laboratory's web-page (https://www.unil.ch/dpt/home/menuinst/recherche/groupe-katanaev/files.html).

Movie S1

Protrusion dynamics of *Drosophila* S2 cells expressing dGαo-GFP, Related to Figures 1 and 4

S2a cells expressing dGαo-GFP were allowed to form protrusions for 30 min and then recorded at one image per 5 seconds for 15 min as described in Supplemental Experimental Procedures. The Movie (24 frames per second) shows a representative cell displaying highly dynamic protrusions with some structures getting fully extended and retracted, and other more stable protrusions that form very motile side branches.

Movies S2 and S3

Static Golgi localization of Gαo-GFP in N2a cells, Related to Figure 2

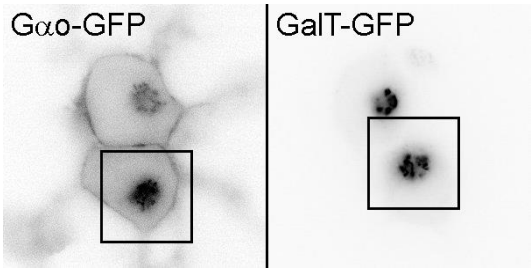

N2a cells expressing Gαo-GFP (Movie S2) or the *trans*-Golgi marker β-1,4-galactosyltransferase (GalT-GFP; Movie S3) were recorded at one image per second for 3 min as described in Supplemental Experimental Procedures. Movies (36 frames per second) show a selected Golgi regions marked in the image shown above at 36 frames per second. Gαo-GFP showed a rather static Golgi localization compared to a more motile behavior of GalT-GFP.

Movies S4 and S5

Protrusion dynamics in *Drosophila* S2 cells expressing dGαo-GFP is affected by dRab1, Related to Figure 4

S2 cells co-transfected with dGαo-GFP and dRab1 wild-type or dominant negative (DN) mutant were prepared and recorded as in Movie S1. A representative S2 cell co-expressing the

dRab1DN mutant showed a reduced formation of protrusions which appear less dynamic (Movie S4). A dramatic increase in plasma membrane (PM) motility was induced by the co-expression of dRab1 wild-type: large PM regions extended broad protrusions that quickly developed into long filopodia-like structures (Movie S5).

Table S1

Gαo interacting partners, Related to Figure 1

Excel sheets containing the Gαo interacting partners separated by screen method: yeast-two hybrid (Y2H), pull-downs (Proteomic), the suppressor-enhancer screens of mutants in the 2nd chromosome (Mutant) or RNAi-based knockdowns (RNAi), and published data (Literature). Confidence scores are provided when feasible at the corresponding columns. Additional gen information can be found at http://flybase.org/ and https://www.ncbi.nlm.nih.gov/gene/ using the FBgn and Entrez IDs, respectively. *Drosophila* lines, phenotypes and type of interaction (suppression or enhancement) are also described at the respective columns. Human orthologues are additionally provided as gene symbols.

Table S2

Bioinformatics, Related to Figures 1 and 3

(Excel sheet A) Over-represented Gene Ontology (GO) terms assigned to the genes listed in Table S1. Enrichment analysis was done on a DAVID bioinformatics platform using the whole *Drosophila* genome as background with a set *p*-value cut-off ≤ 0.05 (adjusted by the Benjamini correction procedure). Genes listed as Entrez IDs associated with a particular GO term are provided in the corresponding column.

(Excel sheet B) *Drosophila* partners of Gαo and their mammalian counterparts involved in vesicle-mediated trafficking grouped according to their reported functions. Main subcellular localizations (related to functions) are also specified.

Table S3

Sequences of the oligonucleotide used in this work, related to the STAR Methods.

CellPress

KEY RESOURCES TABLE

REAGENT or RESOURCE	SOURCE	IDENTIFIER
Antibodies		
Anti-Gαo	Santa Cruz Biotechnology	Cat# sc-13532
Anti-Gαo	Merck	Cat# 371726
Anti-GTP-loaded-Gαo	NewEast Biosciences	Cat# 26901
Anti-Gαo *Drosophila*	(Luchtenborg et al., 2014)	N/A
Anti-GM130	BD Biosciences	Cat# 610823
Anti-RGS-His	Qiagen	Cat# 34650
Anti-GFP	Roche	Cat# 11814460001
Anti-GFP	GeneTex	Cat# GTX113617
Anti-α-Tubulin	Sigma-Aldrich	Cat# T6199
Anti-GST	Developmental Studies Hybridoma Bank	Cat# P1A12
Anti-Dlg	Developmental Studies Hybridoma Bank	Cat# 4F3 anti-discs large
Anti-Gβ1	Proteintech	Cat# 10247-2-AP
Anti-GMAP-210	Pascal Thérond (Université Nice Sophia Antipolis)	N/A
Anti-GST, HRP-conjugated	GE Healthcare	Cat# RPN1236
Anti-HRP, Cy3-conjugated	Jackson ImmunoResearch	Cat# 123-165-021
Bacterial and Virus Strains		
One Shot TOP10	Thermo Fisher Scientific	Cat# C404010
Rosetta-gami 2(DE3)	Novagen	Cat# 71351
BL21-CodonPlus (DE3)-RIPL	Agilent Technologies	Cat# 230280
MAX Efficiency DH10Bac	Thermo Fisher Scientific	Cat# 10361012
Baculovirus for the expression of His_6-Rab1a	This paper	N/A
Baculovirus for the expression of His_6-Rab3a	This paper	N/A
Biological Samples		
Chemicals, Peptides, and Recombinant Proteins		
GTPγS	Sigma-Aldrich	Cat# G8634
GDP	Sigma-Aldrich	Cat# G7127
Brefeldin A	Sigma-Aldrich	Cat# B7651
DAPI	Sigma-Aldrich	Cat# 32670
Brefeldin A	Sigma-Aldrich	Cat# B7651
L-Glutathione reduced	Sigma-Aldrich	Cat# G4251
Acetylcholine	Sigma-Aldrich	Cat# A2661
Mastoparan-7	Sigma-Aldrich	Cat# M212
HU-210	Cayman Chemical	Cat# 90083
BODIPY FL GTPγS	Molecular probes	Cat# G22183
GTP-Eu	PerkinElmer	Cat# 13804910
D/D solubilizer	Clontech	Cat# 635054
Puromycin	InvivoGen	Cat# ant-pr-1
VECTASHIELD Mounting Medium	Vector Laboratories	Cat# H-1400

EZ-Link Sulfo-NHS-SS-Biotin	Thermo Fisher Scientific	Cat# 21331
NeutrAvidin Agarose	Thermo Fisher Scientific	Cat# 29201
DTSEKDEL	Peptide Chemistry Facility (University of Lausanne)	N/A
DTSEKDAS	Peptide Chemistry Facility (University of Lausanne)	N/A
Critical Commercial Assays		
Yeast two-hybrid screening	Hybrigenics-Services	https://www.hybrigenics-services.com/
Proteomic analysis	Proteomics Facility University of Konstanz	https://www.proteomics-facility.uni-konstanz.de/
Deposited Data		
Experimental Models: Cell Lines		
Mouse neuroblastoma Neuro-2a	ATCC	Cat# CCL-131
Human epithelial HeLa	ATCC	Cat# CCL-2
Human neuroblastoma BE(2)C	Karim Abid (University Hospital of Lausanne)	N/A
Drosophila Schneider-2	Thermo Fisher Scientific	Cat# R69007
Spodoptera frugiperda Sf9	ATCC	Cat# CRL-1711
Primary mouse cortical neurons	Omar Alijevic (University of Lausanne)	N/A
Experimental Models: Organisms/Strains		
D. melanogaster: lines containing P-element insertional mutations	Szeged Drosophila Stock Centre	Table S1
D. melanogaster: a cohort of transgenic RNAi lines	Vienna Drosophila Resource Center	Table S1
D. melanogaster: MS1096-Gal4: w[1118] P{w[+mW.hs]=GawB}Bx[MS1096]	Bloomington Drosophila Stock Center	BDSC: 8860; FlyBase: FBti0002374
D. melanogaster: pnr-Gal4: P{w[+mC]=UAS-Dcr-2.D}1, w[1118]; P{w[+mW.hs]=GawB}pnr[MD237]/TM3, Ser[1]	Bloomington Drosophila Stock Center	BDSC: 25758; FlyBase: FBti0004011
D. melanogaster: hs-hid: w[1118]/Dp(2;Y)G, P{w[+mC]=hs-hid}Y	Bloomington Drosophila Stock Center	BDSC: 24638; FlyBase: FBti0017539
D. melanogaster: MS1096-Gal4,UAS-Gαo	(Katanaev et al., 2005)	N/A
D. melanogaster: UAS-RNAi-Gαo: P{KK109018}VIE-260B;	Vienna Drosophila Resource Center	VDRC: 110552; FlyBase: FBtp0067090

D. melanogaster: UAS-RNAi-Gαo: w[1118]; P{GD8640}v19124	Vienna Drosophila Resource Center	VDRC: 19124; FlyBase: FBtp0035456
D. melanogaster: OK371-Gal4; CD8-GFP-Sh: w[1118]; P{w[+mW.hs]=GawB}VGlut[OK371]; P{Mhc.CD8-GFP-Sh}	(Luchtenborg et al., 2014)	N/A
D. melanogaster: UAS-Rab1: y[1] w[*]; P{w[+mC]=UAST-YFP.Rab1}Mes2[01]	Bloomington Drosophila Stock Center	BDSC: 24104; FlyBase: FBtp0039147
D. melanogaster: UAS-Rab3: y[1] w[*]; P{w[+mC]=UASp-YFP.Rab3}eIF4EHP[05b]/TM3, Sb[1]	Bloomington Drosophila Stock Center	BDSC: 9763; FlyBase: FBtp0039153
D. melanogaster: UAS-Arf79F: w[*]; P{w[+mC]=UAS-Arf79F.GFP}attP2	Tony J. C. Harris (University of Toronto)	BDSC: 65850; FlyBase: FBtp0071683
D. melanogaster: φX-22A: y[1] M{vas-int.Dm}ZH-2A w[*]; M{3xP3-RFP.attP'}ZH-22A	Bloomington Drosophila Stock Center	BDSC: 24481; FlyBase: FBti0099696
D. melanogaster: UAS-KDELR-mRFP	This paper	N/A
Oligonucleotides		
Oligonucleotide primers for RT-PCR are listed in Table S3	This paper	N/A
Oligonucleotide primers for shRNA-based downregulation of Gαo are listed in in Table S3	This paper	N/A
Oligonucleotide primers for cloning and sub-cloning are listed in in Table S3	This paper	N/A
Recombinant DNA		
pRetroSuper	Oligoengine	Cat# VEC-pRT-0002
pcDNA3.1+	Thermo Fisher Scientific	Cat# V79020
pFastBac NT	Thermo Fisher Scientific	Cat# 12562029
pAc5.1/V5-HisA	Thermo Fisher Scientific	Cat# V411020
pEGFP-C1	Clontech	N/A
pEGFP-C3	Clontech	N/A
pEGFP-N1	Clontech	N/A
pEBFP2-N1	Gift from Michael Davidson	Addgene Cat# 54595
pGEX-4T-1	GE Healthcare	Cat# 28-9545-49
pUASTattB	(Lin et al., 2014)	N/A
pcDNA3.1+ Gαo *Drosophila*	(Kopein and Katanaev, 2009)	N/A
pHis6-Gαo *Drosophila*	(Kopein and Katanaev, 2009)	N/A
pHis6-Gαo Q205L *Drosophila*	(Kopein and Katanaev, 2009)	N/A
pHis6-Gαi	(Kopein and Katanaev, 2009)	N/A

pHis6-Gαo Rat	(Kopein and Katanaev, 2009)	N/A
pHis6-Gαo Human	(Lin et al., 2014)	N/A
pcDNA3.1+ Gαo	cDNA Resource Center	Cat# GNA0OA0000
pcDNA3.1+ Gαo Q205L	cDNA Resource Center	Cat# GNA0OA00C0
pcDNA3.1+ Muscarinic acetylcholine receptor 2	cDNA Resource Center	Cat# MAR0200000
pcDNA3.1+ HA-Gγ3	cDNA Resource Center	Cat# GNG030HN00
pMyc-Rab1a	(Dupre et al., 2006)	Addgene Cat# 46776
pArf1-GFP	(Chun et al., 2008)	Addgene Cat# 39554
pGalT-mTurquoise2	(Goedhart et al., 2012)	Addgene Cat# 36205
pBFP-MannII	(Subach et al., 2011)	Addgene Cat# 55309
pmCerulean-Gβ1	(Thaler et al., 2005)	Addgene Cat# 27810
pGFP-Rab7a	(Choudhury et al., 2002)	Addgene Cat# 12605
pGFP-Rab11a	(Choudhury et al., 2002)	Addgene Cat# 12674
pArf5-GFP	(Chun et al., 2008)	Addgene Cat# 39557
pArf6-CFP	(Beemiller et al., 2006)	Addgene Cat# 11382
pDyn1-GFP	(Lee and De Camilli, 2002)	Addgene Cat# 22163
pmRFP-N1	Claudia Stuermer (University of Konstanz)	N/A
pR1WTSH-GFP	Claudia Stuermer (University of Konstanz)	N/A
pDyn2-GFP	Claudia Stuermer (University of Konstanz)	N/A
pmRFP-Clathrin	Claudia Stuermer (University of Konstanz)	N/A
pR1WTSH-GFP	Claudia Stuermer (University of Konstanz)	N/A
pFlc-1 Rab1 *Drosophila*	*Drosophila* Genomics Resource Center	Cat# FI01544
pOT2 Rab3 *Drosophila*	*Drosophila* Genomics Resource Center	Cat# LP05860
pOT2 Arf79F *Drosophila*	Drosophila Genomics Resource Center	Cat# LD24904
pBS SK(-) KDELR *Drosophila*	Drosophila Genomics Resource Center	Cat# LD06574
pcDNA3.1+ $G\alpha o^{Gly92}$-GFP	Narasimhan Gautam (Washington University School of Medicine)	N/A
pSV-Rab1b	Angelika Barnekow (University Muenster)	N/A
pGFP-Rab3a	Robert D. Burgoyne (University of Liverpool)	N/A
pJAF-Arf2	Gregory J. Pazour (University of Massachusetts Medical School)	N/A
pJAF-Arf3	Gregory J. Pazour (University of Massachusetts Medical School)	N/A
pJAF-Arf4	Gregory J. Pazour (University of Massachusetts Medical School)	N/A
pGST-αGDI	Jean Gruenberg (University of Geneva)	N/A

pKDELR-ECFP	Angel Velasco (University of Seville)	N/A
pssGFP	Edward Málaga-Trillo (Universidad Peruana Cayetano Heredia)	N/A
pEF-T7-Rim2-RBD	Mitsunori Fukuda (Tohoku University)	N/A
pVSVG-GFP^{ts045}	Jennifer Lippincott-Schwartz (National Institutes of Health)	N/A
pGFP-FM4-hGH	Andrew Peden (The University of Sheffield)	N/A
pGFP-Rab4a	Marci A. Scidmore (Cornell University)	N/A
pGFP-Rab5a	Peter van der Sluijs (University Medical Center Utrecht)	N/A
pFAPP1-PH-GFP	Tamas Balla (National Institutes of Health)	N/A
pGST-GGA3	Jean-Luc Parent (Université de Sherbrooke)	N/A
pcDNA3 cannabinoid receptor type-1	Mary E. Abood (Temple University)	N/A
Software and Algorithms		
Prism v5.03	Graphpad	https://www.graphpad.com/
DAVID	DAVID Bioinformatic Team	https://david.ncifcrf.gov/
EnrichmentMap	Gary Bader (University of Toronto)	http://apps.cytoscape.org/apps/enrichmentmap
Cytoscape	The Cytoscape Consortium	http://www.cytoscape.org/download.php
ClusterMaker	Resource for Biocomputing, Visualization, and Informatics (RBVI)	http://apps.cytoscape.org/apps/clustermaker
WordCloud	Gary Bader (University of Toronto)	http://apps.cytoscape.org/apps/wordcloud
Primer3Plus web-interface	Andreas Untergasser and Harm Nijveen (National Institutes of Health)	http://www.bioinformatics.nl/cgi-bin/primer3plus/primer3plus.cgi
Bioinformatics scripts	(Bilousov et al., 2014)	http://www.unil.ch/dpt/home/menuinst/recherche/groupe-katanaev/files.html

Other		
Ni-NTA Agarose	Qiagen	Cat# 30230
CNBr-activated Sepharose 4 Fast Flow	GE Healthcare	Cat# 17098101
Glutathione Sepharose 4B	GE Healthcare	Cat# 17075601
Chamlide CMB magnetic chamber	Live cell instrument	Cat# CM-B15-1PB

Figure 1

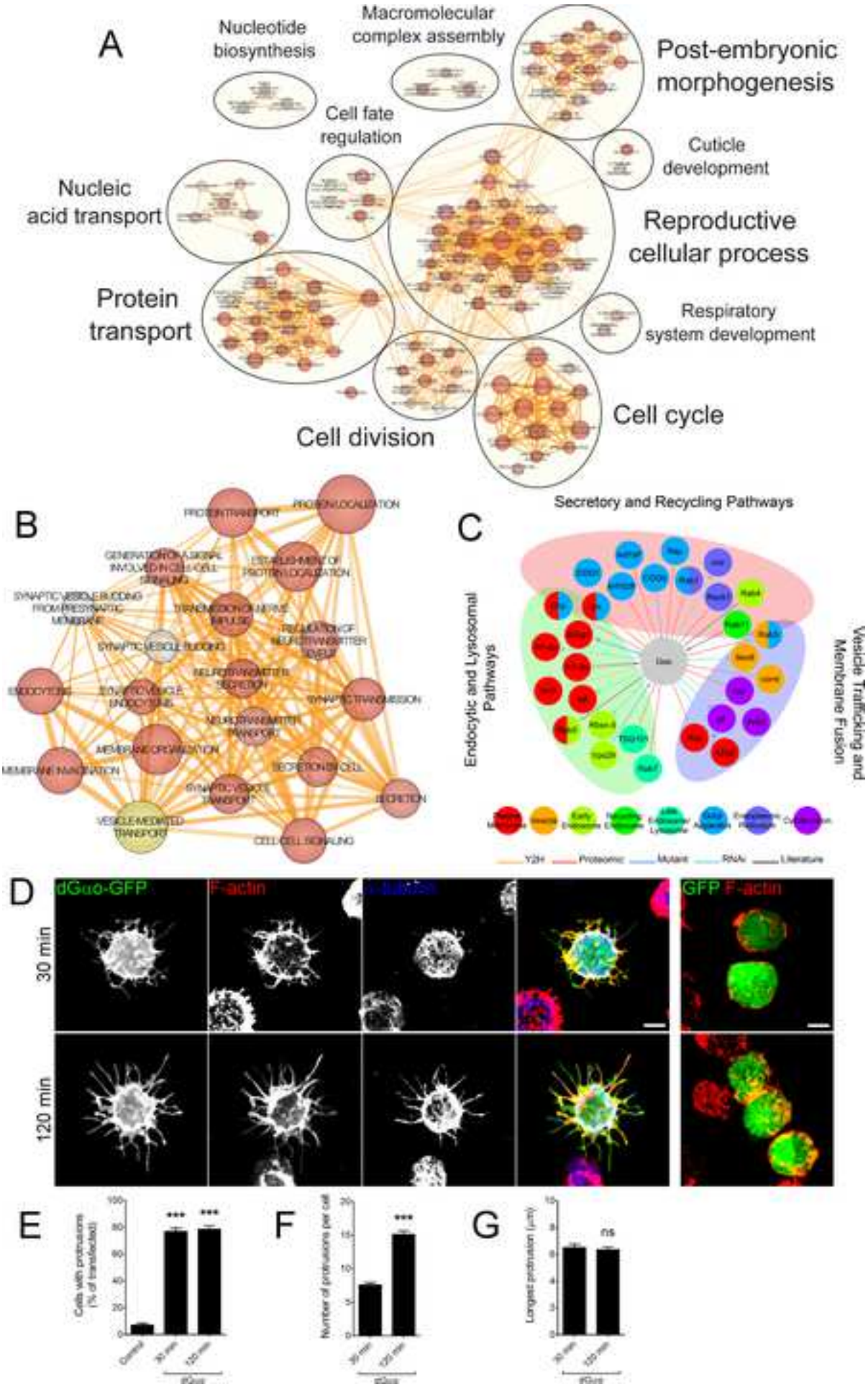
A
Nucleotide biosynthesis
Macromolecular complex assembly
Post-embryonic morphogenesis
Cell fate regulation
Cuticle development
Nucleic acid transport
Reproductive cellular process
Protein transport
Respiratory system development
Cell cycle
Cell division
B
C
Secretory and Recycling Pathways
Endocytic and Lysosomal Pathways
Vesicle Trafficking and Membrane Fusion
Y2H
Proteomic
Mutant
RNAi
Literature
D
dGαo-GFP
F-actin
GFP F-actin
30 min
120 min
E
F
G
Cells with protrusions (% of transfected)
Number of protrusions per cell
Longest protrusion (μm)
***
***
***
ns
Control
30 min
120 min
dGαo

Figure 2

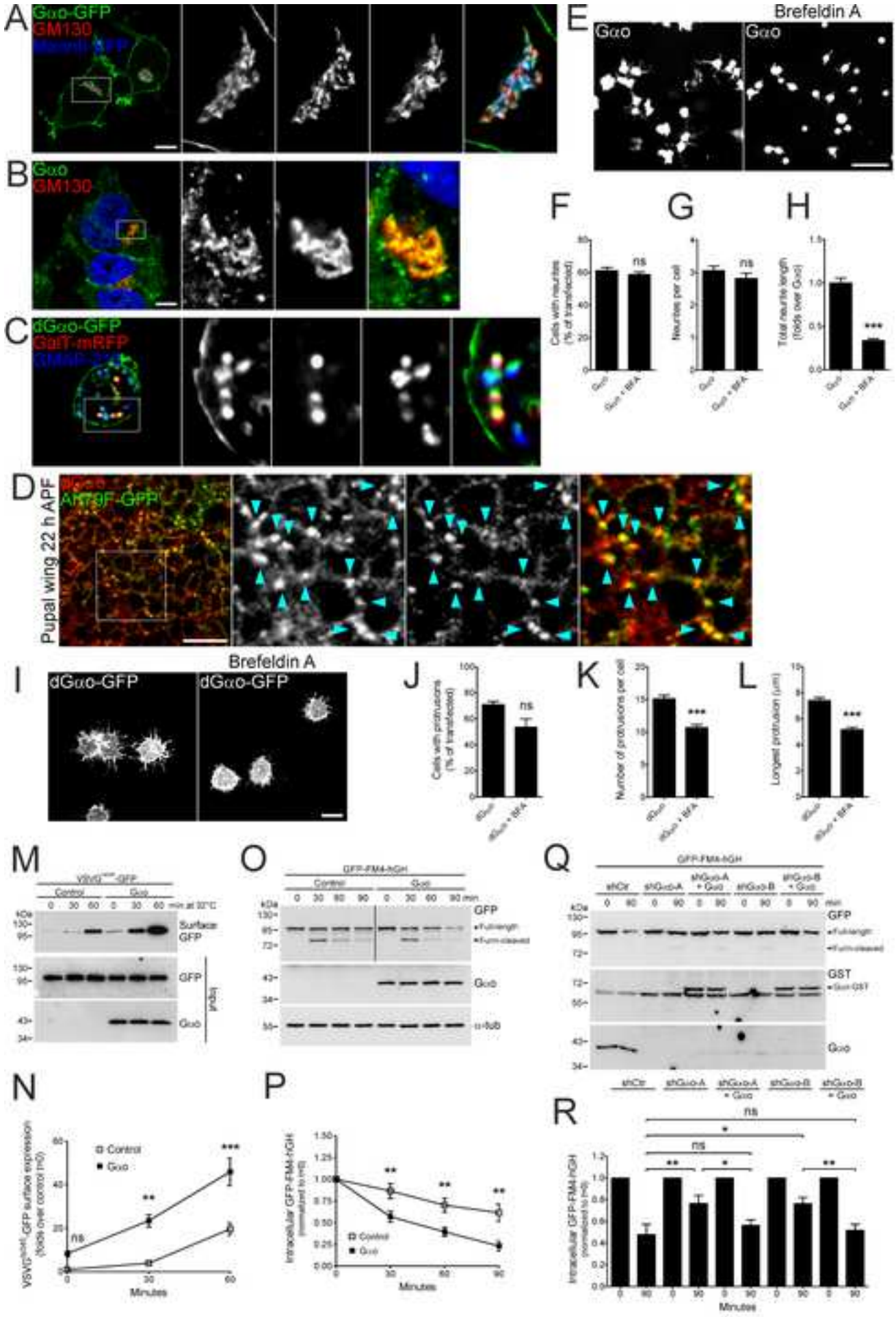
A
Gαo-GFP
GM130
B
Gαo
GM130
C
dGαo-GFP
GalT-mRFP
D
Pupal wing 22 h APF
dGαo
Arf79F-GFP
E
Brefeldin A
Gαo
Gαo
F
Cells with neurites (% of transfected)
ns
G
Neurites per cell
ns
H
Total neurite length (folds over Gαo)
***
I
Brefeldin A
dGαo-GFP
dGαo-GFP
J
Cells with protrusions (% of transfected)
ns
K
Number of protrusions per cell
***
L
Longest protrusion (µm)
***
M
Control
Gαo
Surface GFP
GFP
Input
Gαo
O
GFP-FM4-hGH
Control
Gαo
GFP
Full-length
Furin-cleaved
Gαo
α-tub
Q
GFP-FM4-hGH
shCtr
shGαo-A
shGαo-A + Gαo
shGαo-B
shGαo-B + Gαo
GFP
Full-length
Furin-cleaved
GST
Gαo-GST
Gαo
N
Control
Gαo
ns
**
***
Minutes
P
Control
Gαo
**
**
**
Minutes
R
ns
*
ns
**
*
**
Minutes

Figure 3

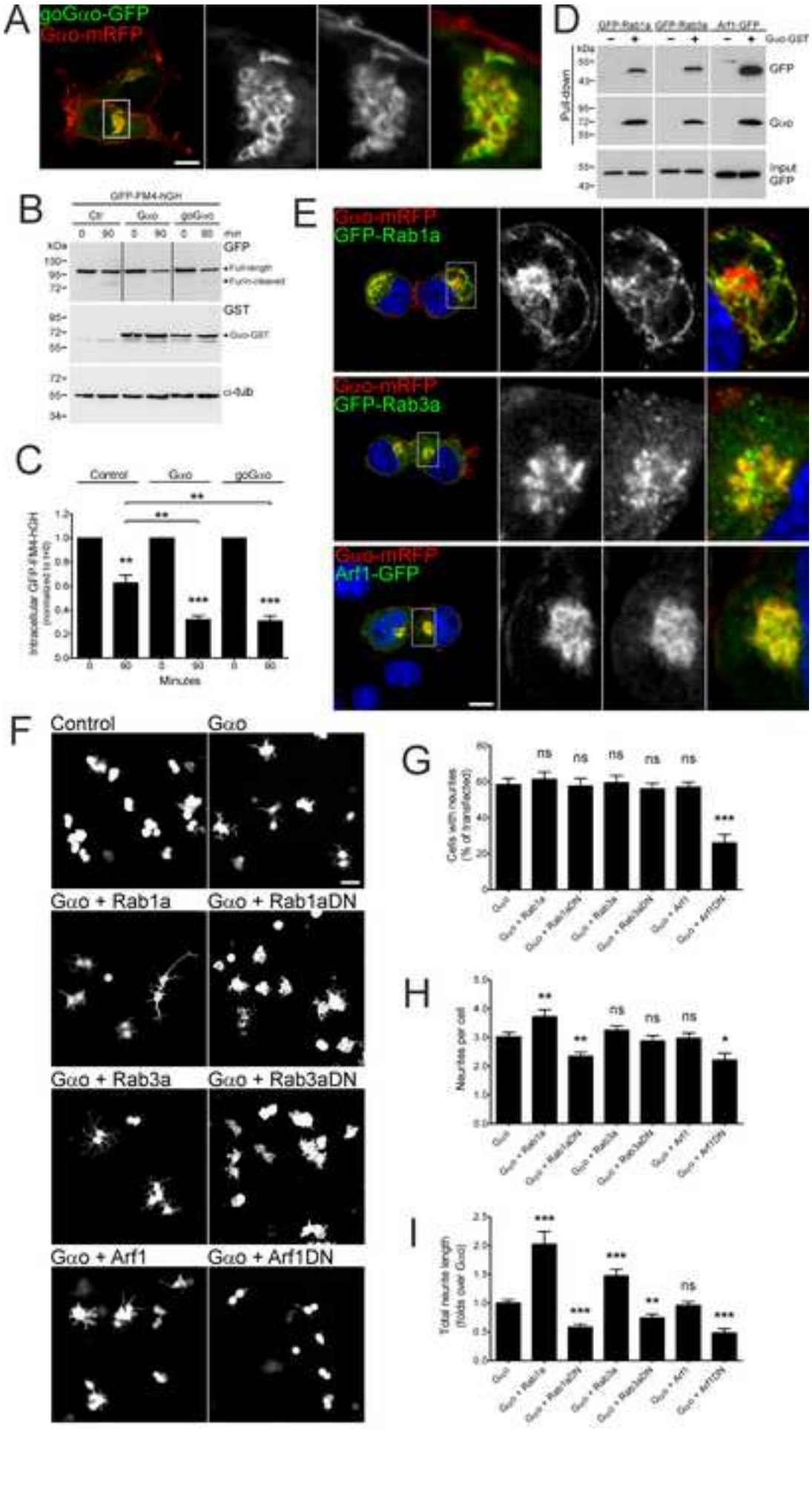
A
goGαo-GFP
Gαo-mRFP
D
GFP-Rab1a
GFP-Rab3a
Arf1-GFP
Gαo-GST
Pull-down
GFP
Gαo
Input GFP
B
GFP-PM4-hGH
Ctr
Gαo
goGαo
min
GFP
Full-length
Furin-cleaved
GST
Gαo-GST
ci-tub
C
Control
Gαo
goGαo
Intracellular GFP-PM4-hGH (normalized to t=0)
Minutes
E
Gαo-mRFP
GFP-Rab1a
GFP-Rab3a
Arf1-GFP
F
Control
Gαo
Gαo + Rab1a
Gαo + Rab1aDN
Gαo + Rab3a
Gαo + Rab3aDN
Gαo + Arf1
Gαo + Arf1DN
G
Cells with neurites (% of transfected)
H
Neurites per cell
I
Total neurite length (folds over Gαo)
Gαo
Gαo + Rab1a
Gαo + Rab1aDN
Gαo + Rab3a
Gαo + Rab3aDN
Gαo + Arf1
Gαo + Arf1DN

Figure 4

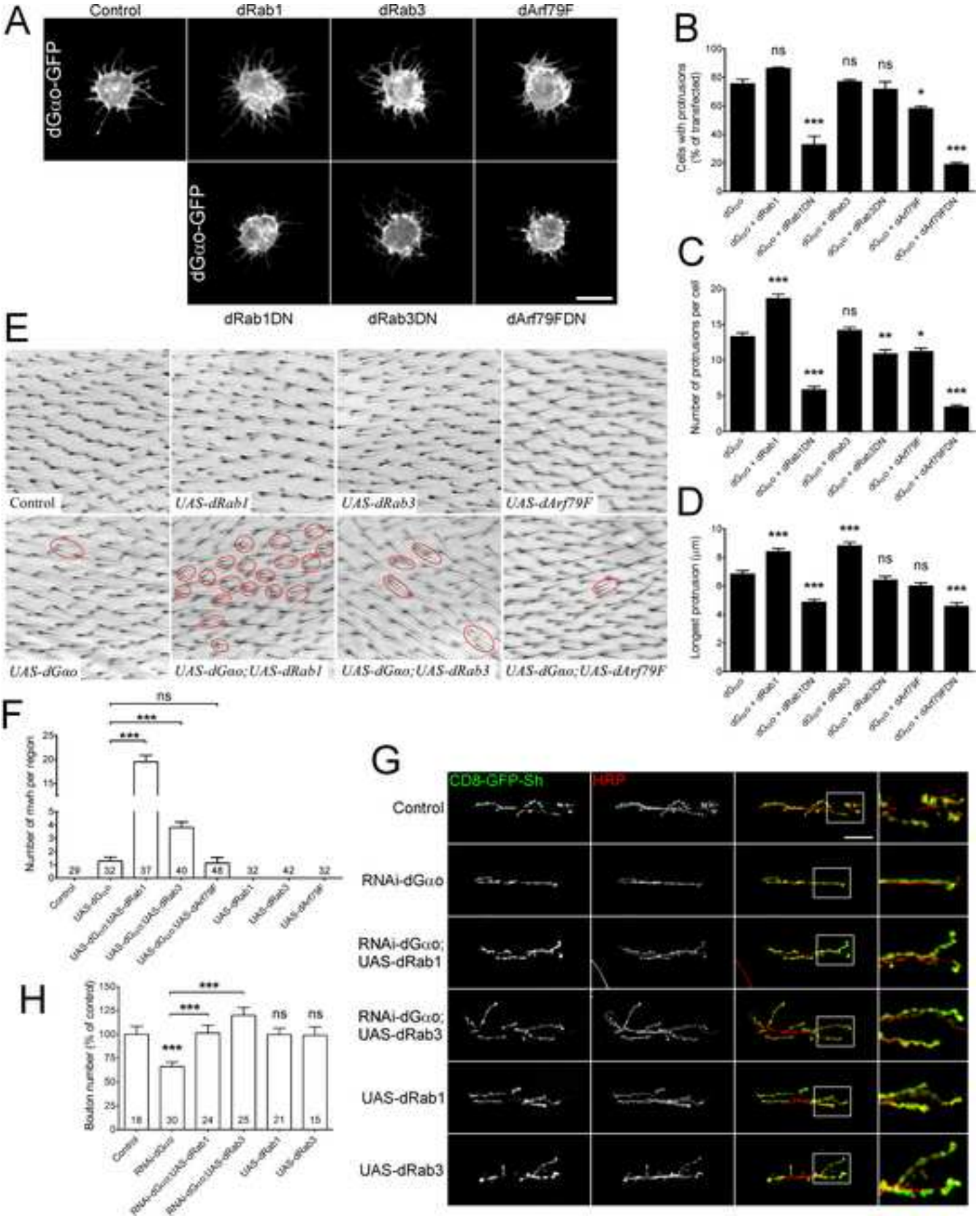
A
Control
dRab1
dRab3
dArf79F
dGαo-GFP
dGαo-GFP
dRab1DN
dRab3DN
dArf79FDN
B
Cells with protrusions (% of transfected)
ns
ns
ns
***
*
***
dGαo
dGαo + dRab1
dGαo + dRab1DN
dGαo + dRab3
dGαo + dRab3DN
dGαo + dArf79F
dGαo + dArf79FDN
C
Number of protrusions per cell
***
ns
***
**
*
***
D
Longest protrusion (μm)
***
***
***
ns
ns
***
E
Control
UAS-dRab1
UAS-dRab3
UAS-dArf79F
UAS-dGαo
UAS-dGαo;UAS-dRab1
UAS-dGαo;UAS-dRab3
UAS-dGαo;UAS-dArf79F
F
Number of mwh per region
ns
***
***
29
32
37
40
48
32
42
32
Control
UAS-dGαo
UAS-dGαo;UAS-dRab1
UAS-dGαo;UAS-dRab3
UAS-dGαo;UAS-dArf79F
UAS-dRab1
UAS-dRab3
UAS-dArf79F
G
CD8-GFP-Sh
HRP
Control
RNAi-dGαo
RNAi-dGαo; UAS-dRab1
RNAi-dGαo; UAS-dRab3
UAS-dRab1
UAS-dRab3
H
Bouton number (% of control)
***
***
***
ns
ns
18
30
24
25
21
15
Control
RNAi-dGαo
RNAi-dGαo;UAS-dRab1
RNAi-dGαo;UAS-dRab3
UAS-dRab1
UAS-dRab3

Figure 5

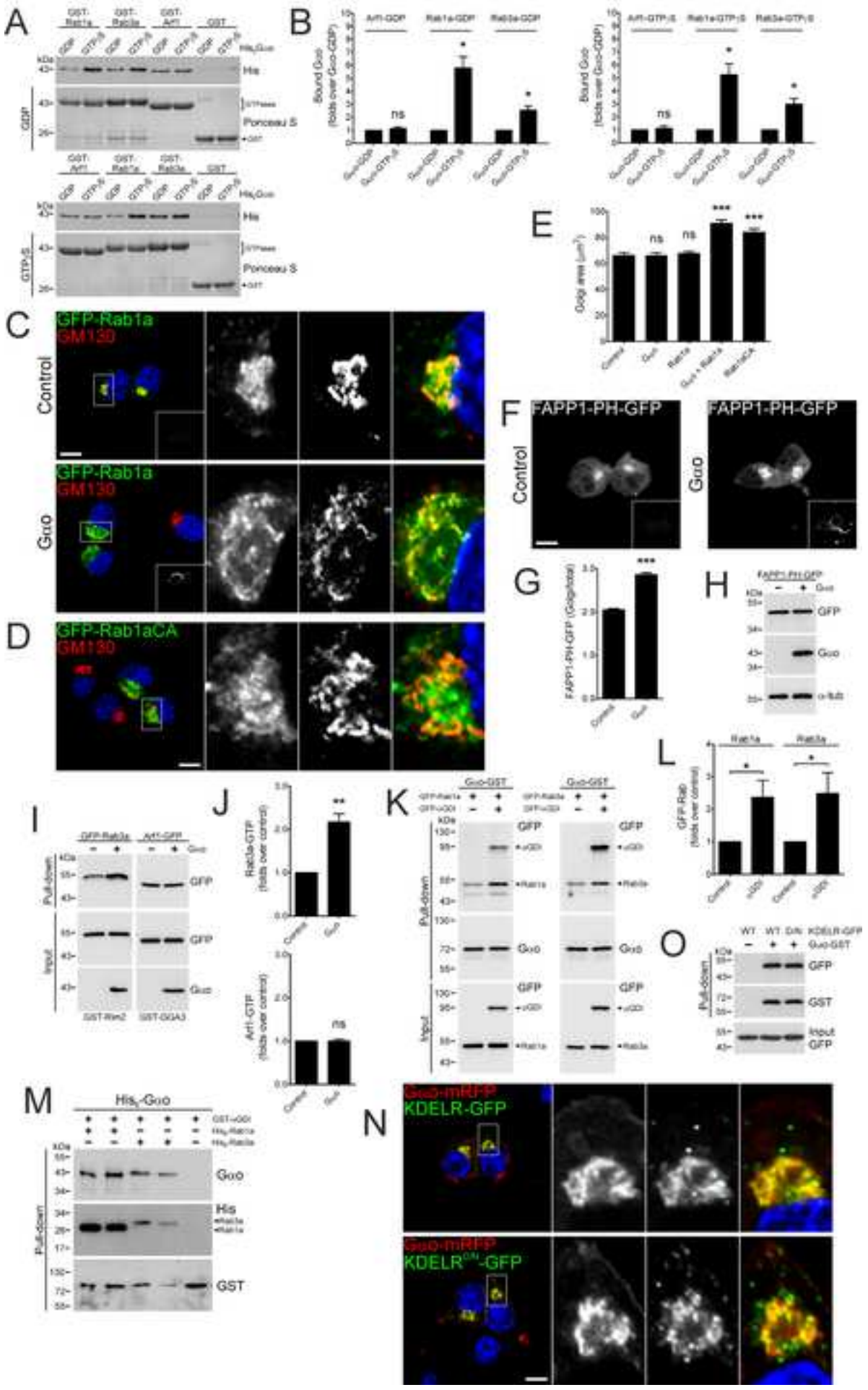
A
GST-Rab1a
GST-Rab3a
GST-Arf1
GST
GDP
GTP-γS
His
Ponceau S
B
Arf1-GDP
Rab1a-GDP
Rab3a-GDP
Arf1-GTP-γS
Rab1a-GTP-γS
Rab3a-GTP-γS
Bound Gαo (folds over Gαo-GDP)
ns
C
GFP-Rab1a
GM130
Control
Gαo
D
GFP-Rab1aCA
E
Golgi area (μm²)
Control
Gαo
Rab1a
Gαo + Rab1a
Rab1aCA
F
FAPP1-PH-GFP
Control
Gαo
G
FAPP1-PH-GFP (Golgi/total)
H
GFP
Gαo
α-Tub
I
GFP-Rab3a
Arf1-GFP
Pull-down
Input
GST-Rim2
GST-GGA3
J
Rab3a-GTP (folds over control)
Arf1-GTP (folds over control)
K
Gαo-GST
GFP-Rab1a
GFP-vGD1
Rab1a
L
GFP-Rab (folds over control)
Rab1a
Rab3a
M
His6-Gαo
GST-vGD1
His6-Rab1a
His6-Rab3a
Gαo
His
GST
N
Gαo-mRFP
KDELR-GFP
KDELR^DN-GFP
O
WT
WT
D/N
KDELR-GFP
Gαo-GST
GST
Input GFP

Figure 6

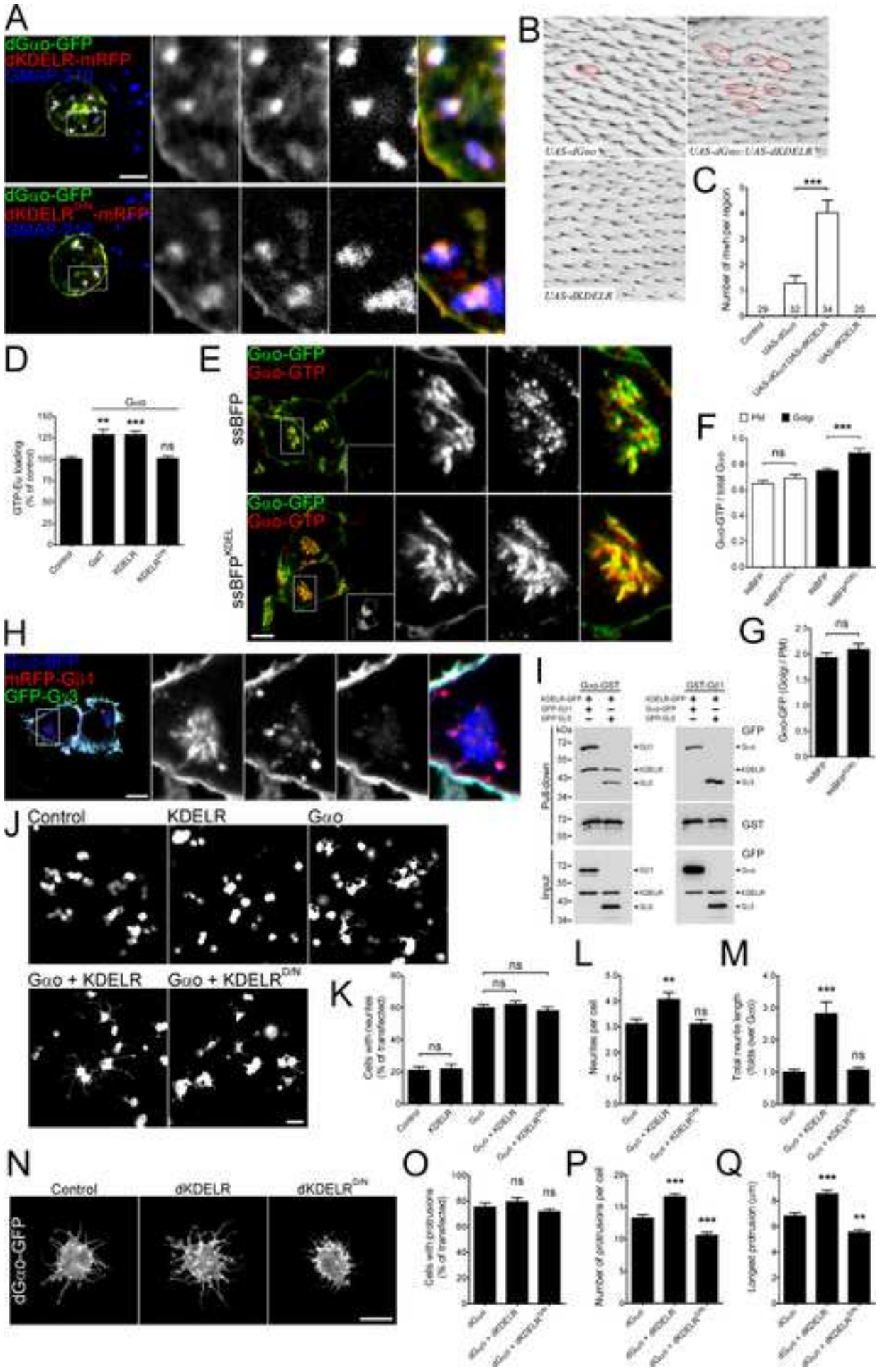
A
dGαo-GFP
dKDELR-mRFP
dKDELR^D/N-mRFP
B
UAS-dGαo
UAS-dGαo;UAS-dKDELR
UAS-dKDELR
C
Number of mesh per region
***
29
32
34
20
Control
UAS-dGαo
UAS-dGαo;UAS-dKDELR
UAS-dKDELR
D
Gαo
GTP-Eu loading (% of control)
**
***
ns
Control
GoLoco
KDELR
KDELR^D/N
E
Gαo-GFP
Gαo-GTP
ssBFP
ssBFP^KDEL
F
PM
Golgi
Gαo-GTP / total Gαo
ns
***
ssBFP
ssBFP^KDEL
G
Gαo-GFP (Golgi / PM)
ns
H
mRFP-Gβ1
GFP-Gγ3
I
Gαo-GST
GST-Gβ1
KDELR-GFP
GFP-Gβ1
Gαo-GFP
GFP-Gγ3
kDa
72
55
43
34
Pull-down
Input
GFP
GST
J
Control
KDELR
Gαo
Gαo + KDELR
Gαo + KDELR^D/N
K
Cells with neurites (% of transfected)
ns
ns
ns
Control
KDELR
Gαo
Gαo + KDELR
Gαo + KDELR^D/N
L
Neurites per cell
**
ns
M
Total neurite length (folds over Gαo)
***
ns
N
Control
dKDELR
dKDELR^D/N
dGαo-GFP
O
Cells with protrusions (% of transfected)
ns
ns
dGαo
dGαo + dKDELR
dGαo + dKDELR^D/N
P
Number of protrusions per cell
***
***
Q
Longest protrusion (µm)
***
**

Figure 7

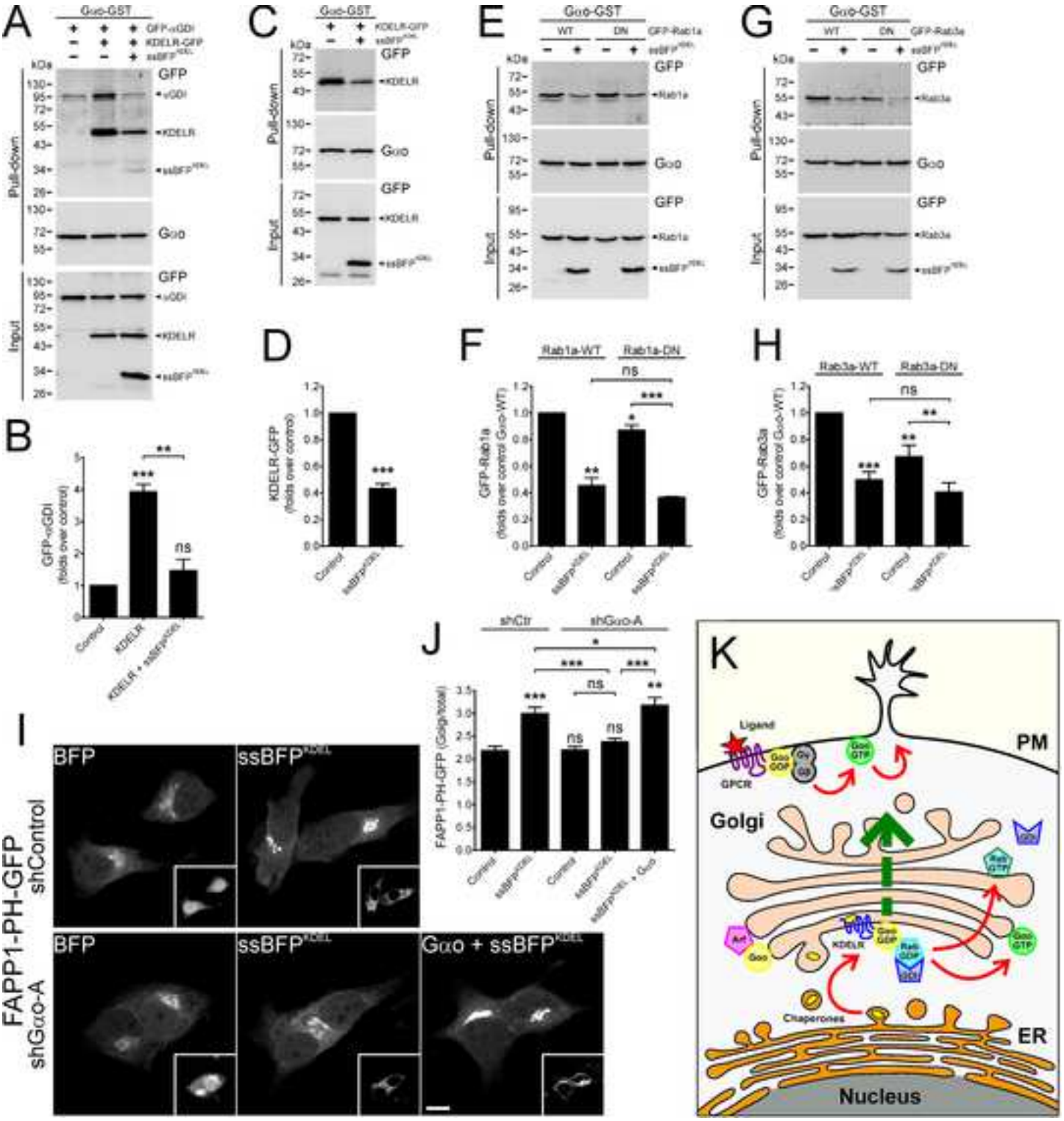
A
Gαo-GST
GFP-αGDI
KDELR-GFP
ssBFP^KDEL
Pull-down
Input
GFP
αGDI
KDELR
Gαo
B
GFP-αGDI (folds over control)
Control
KDELR
KDELR + ssBFP^KDEL
C
KDELR-GFP
D
KDELR-GFP (folds over control)
E
WT
DN
GFP-Rab1a
Rab1a
F
Rab1a-WT
Rab1a-DN
GFP-Rab1a (folds over control Gαo-WT)
G
GFP-Rab3a
Rab3a
H
Rab3a-WT
Rab3a-DN
GFP-Rab3a (folds over control Gαo-WT)
I
FAPP1-PH-GFP
shControl
shGαo-A
BFP
ssBFP^KDEL
Gαo + ssBFP^KDEL
J
shCtr
shGαo-A
FAPP1-PH-GFP (Golgi/total)
K
Ligand
GPCR
PM
Golgi
KDELR
Chaperones
ER
Nucleus

Supplemental Figure 1

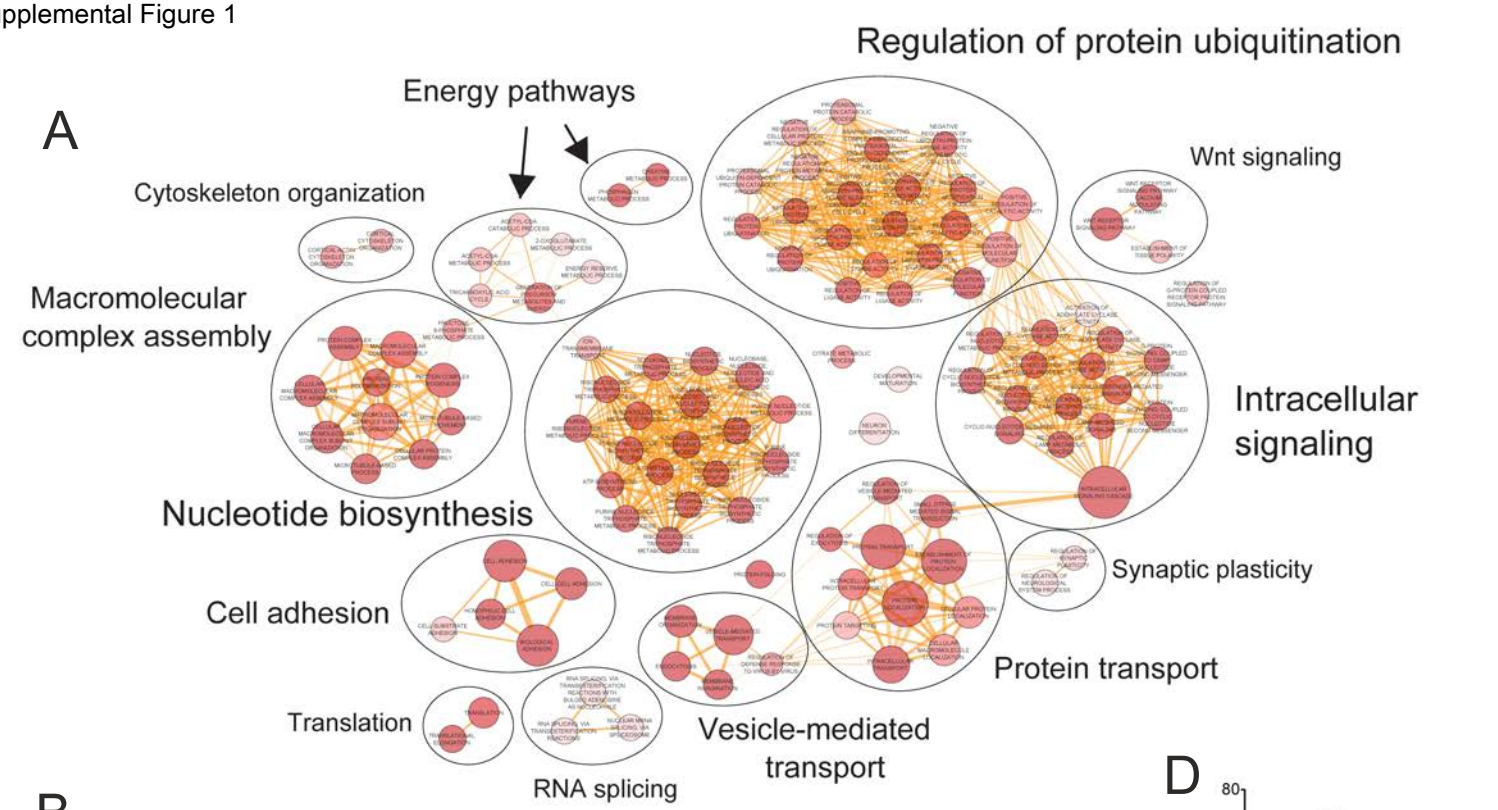

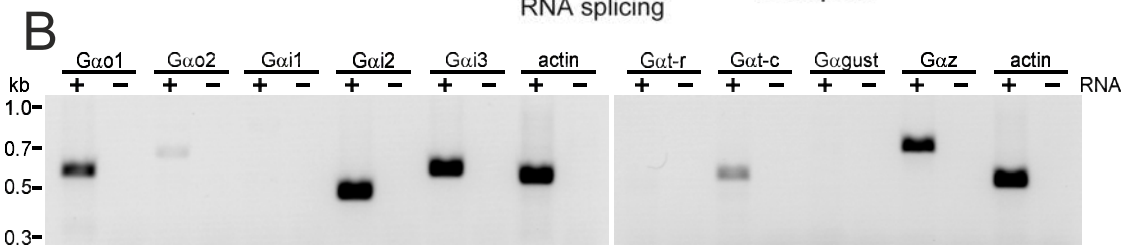

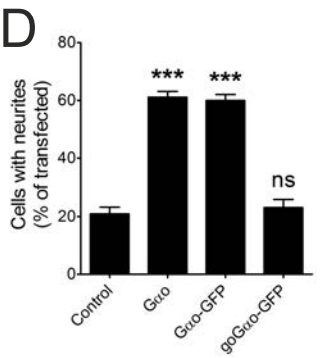

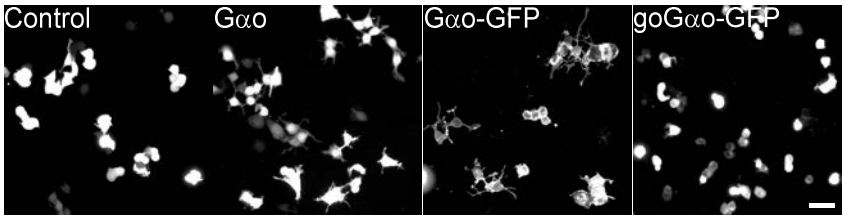

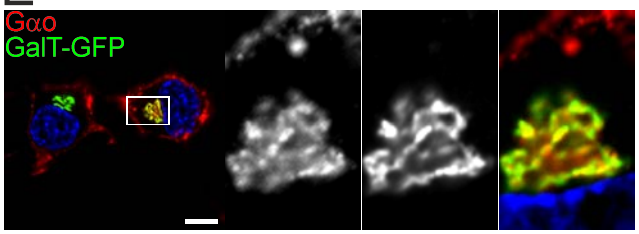

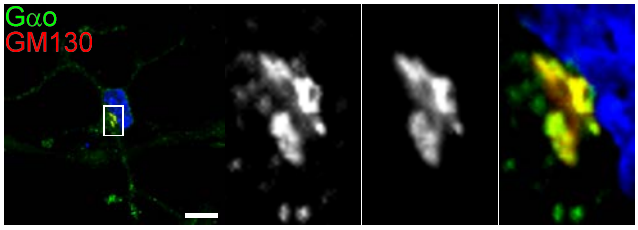

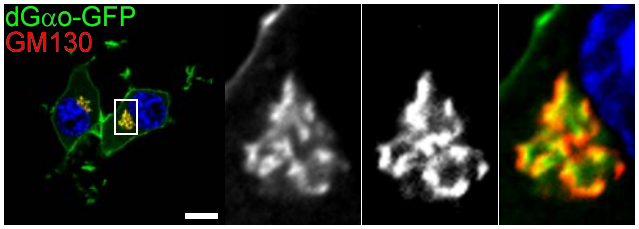

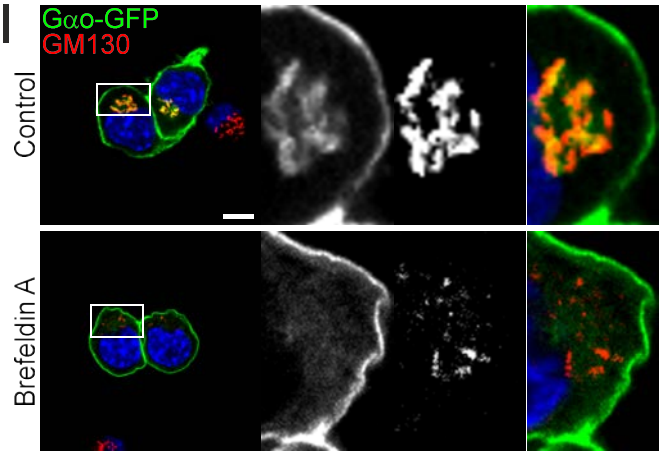

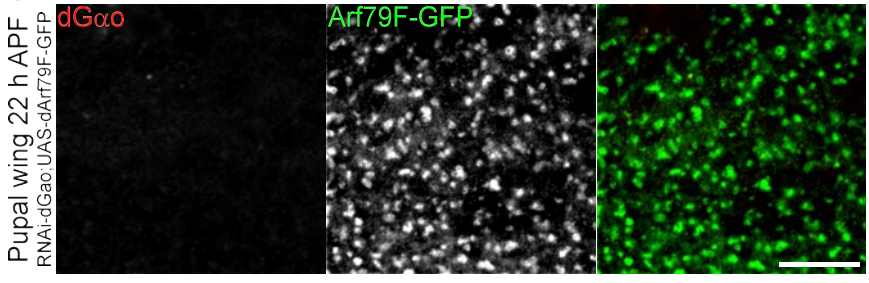

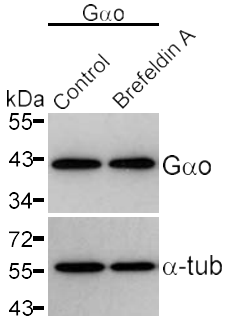

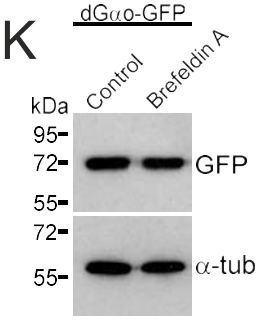

Figure S1_Solis et al.

Supplemental Figure 2

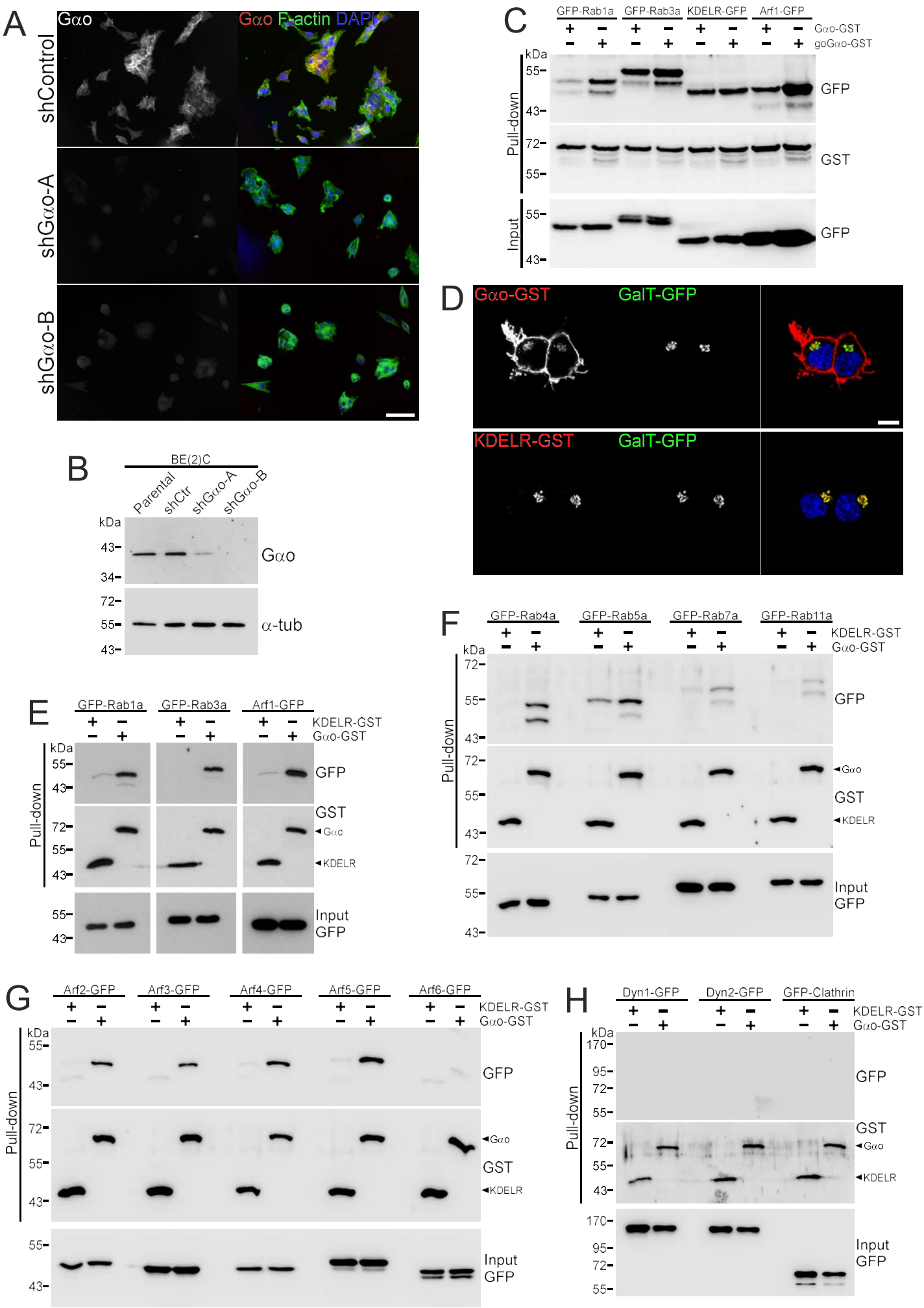

Figure S2_Solis et al.

Supplemental Figure 3

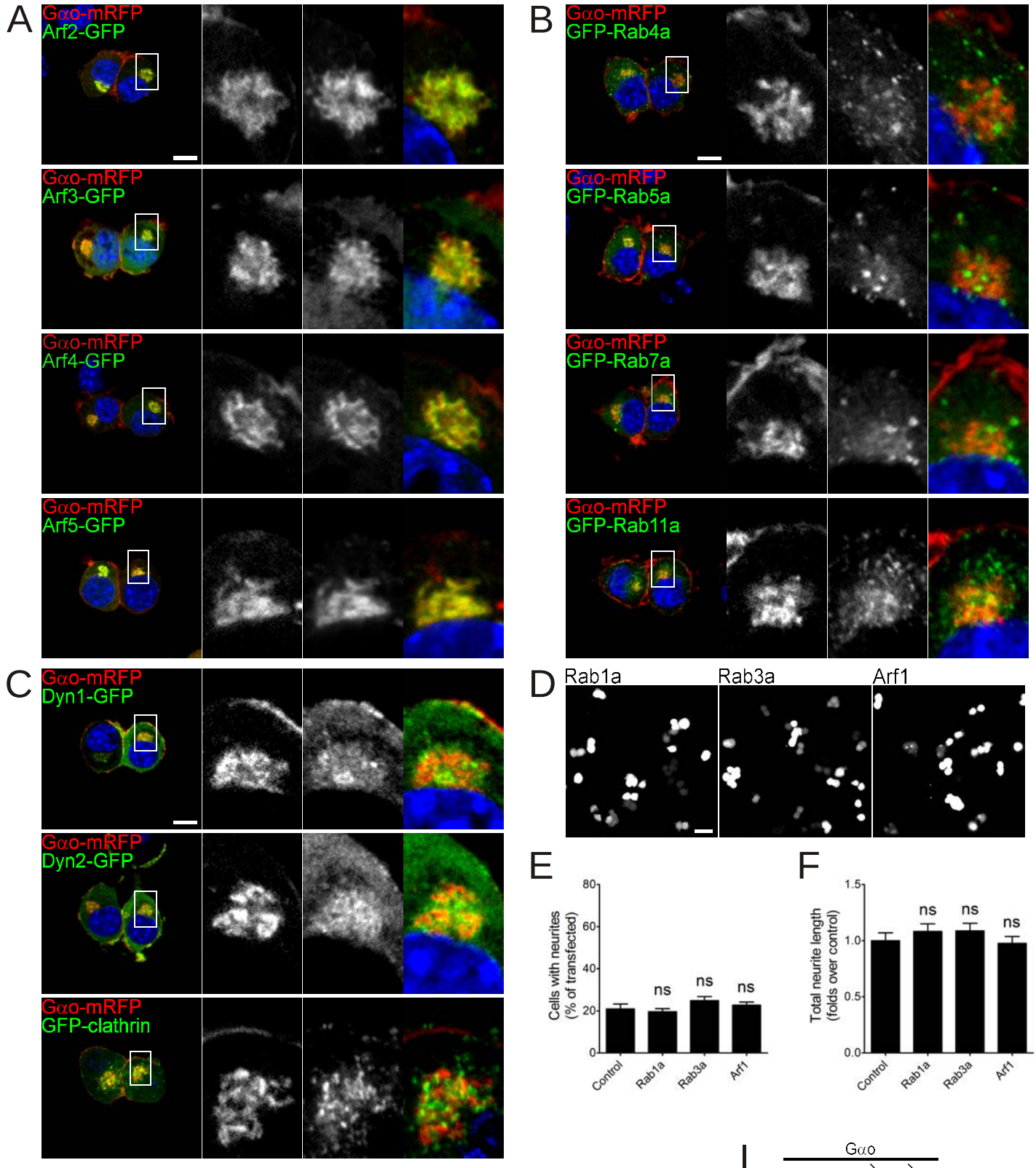

Figure S3_Solis et al.

Supplemental Figure 4

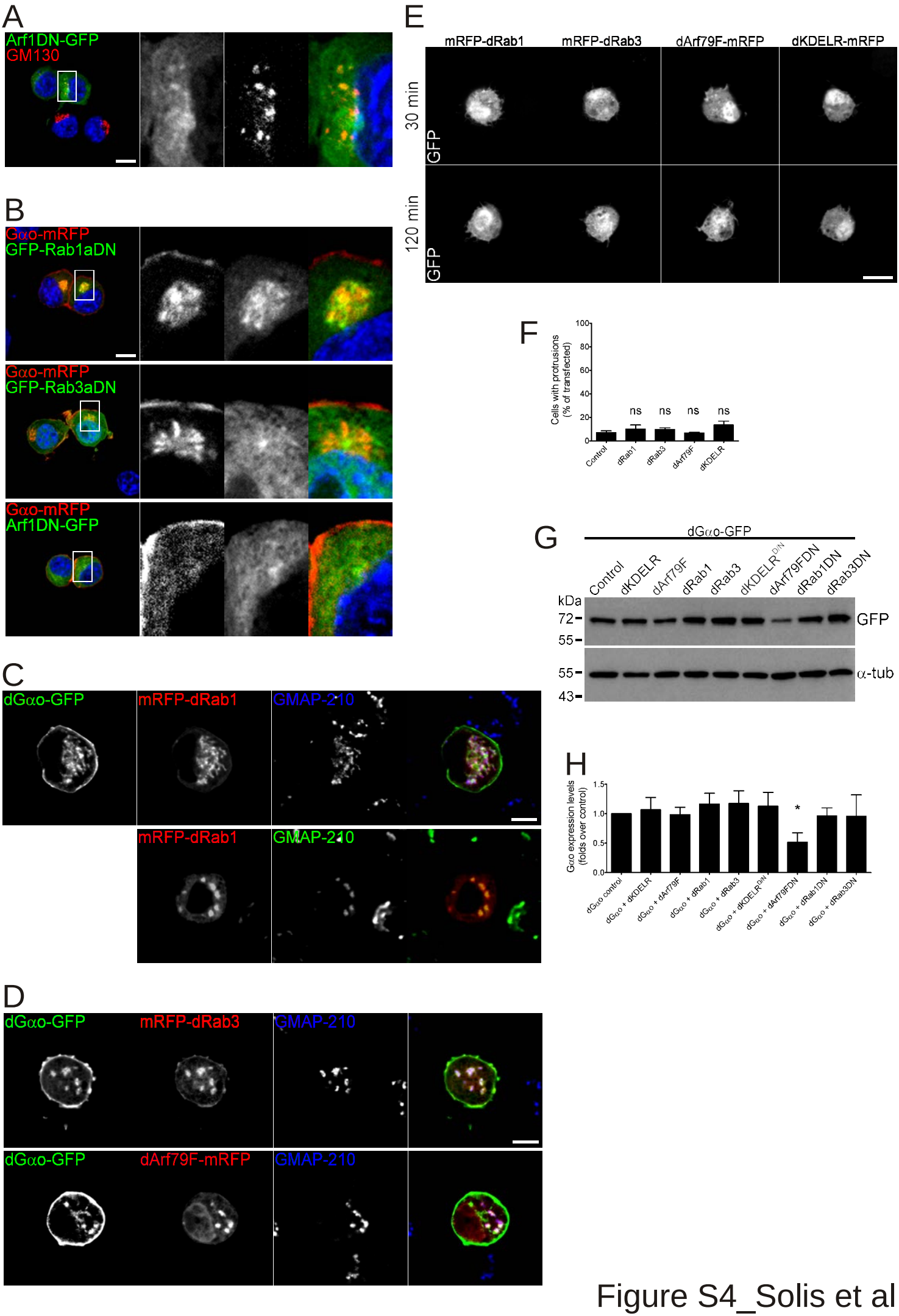

Figure S4_Solis et al.

Supplemental Figure 5

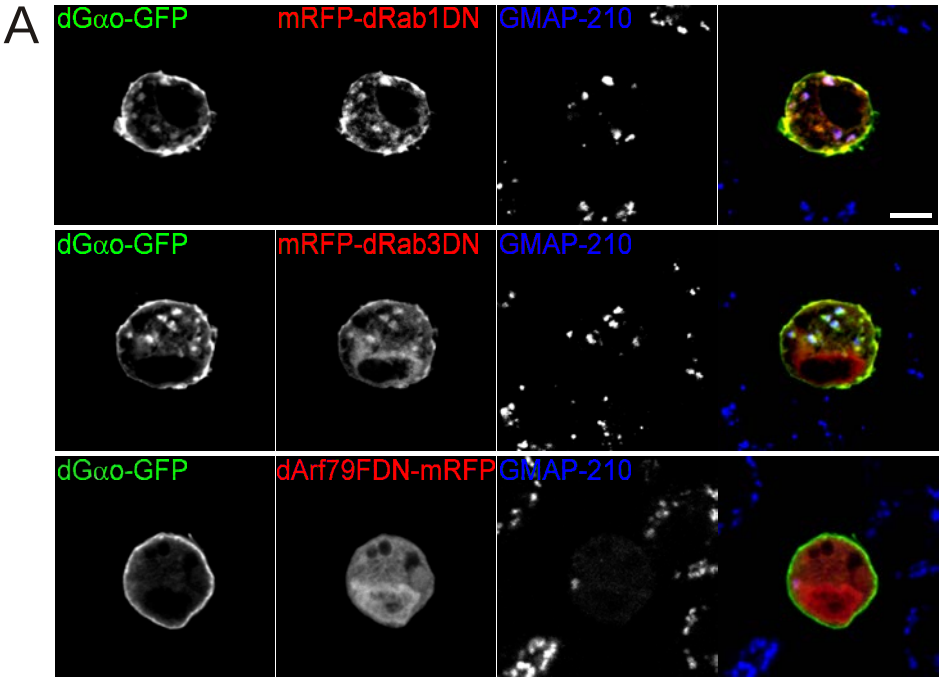

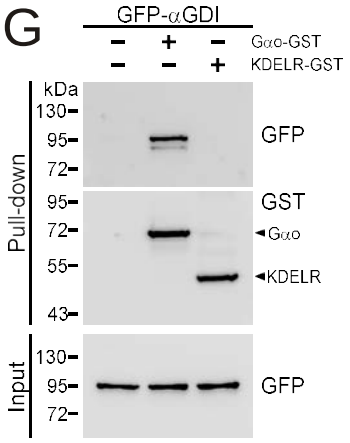

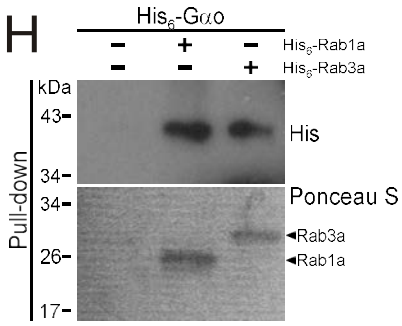

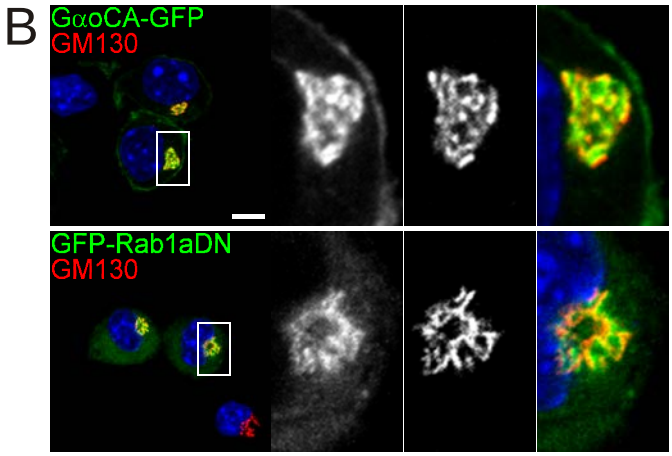

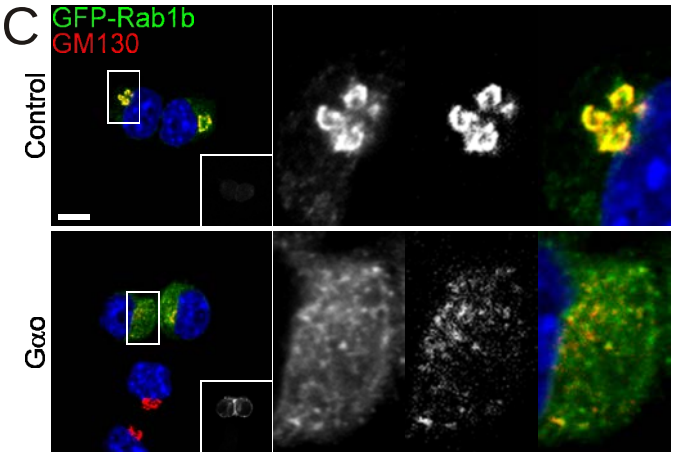

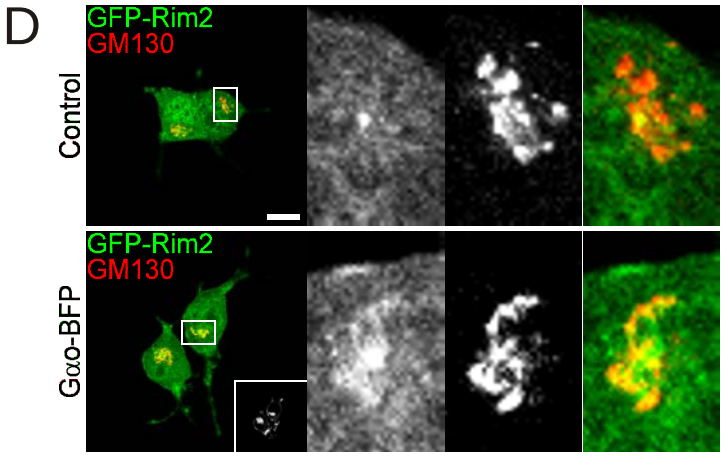

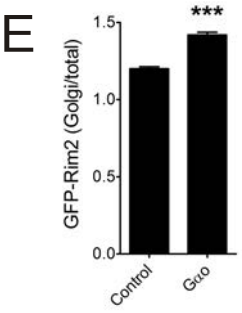

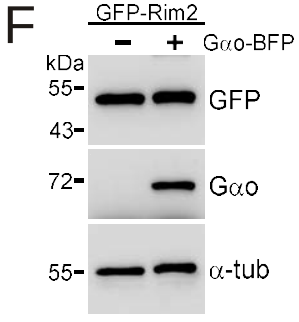

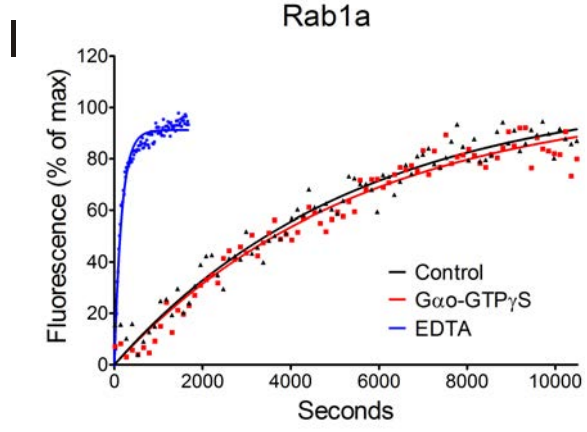

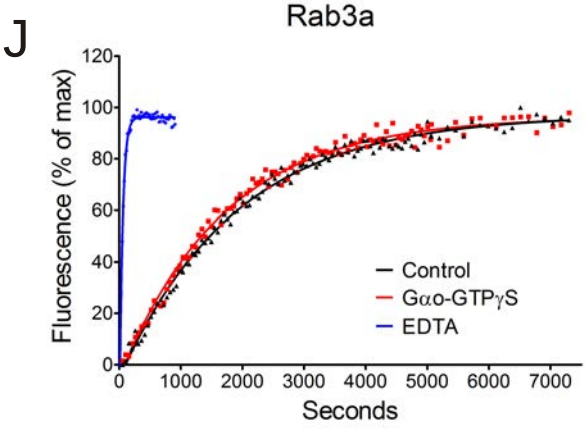

Figure S5_Solis et al.

Supplemental Figure 6

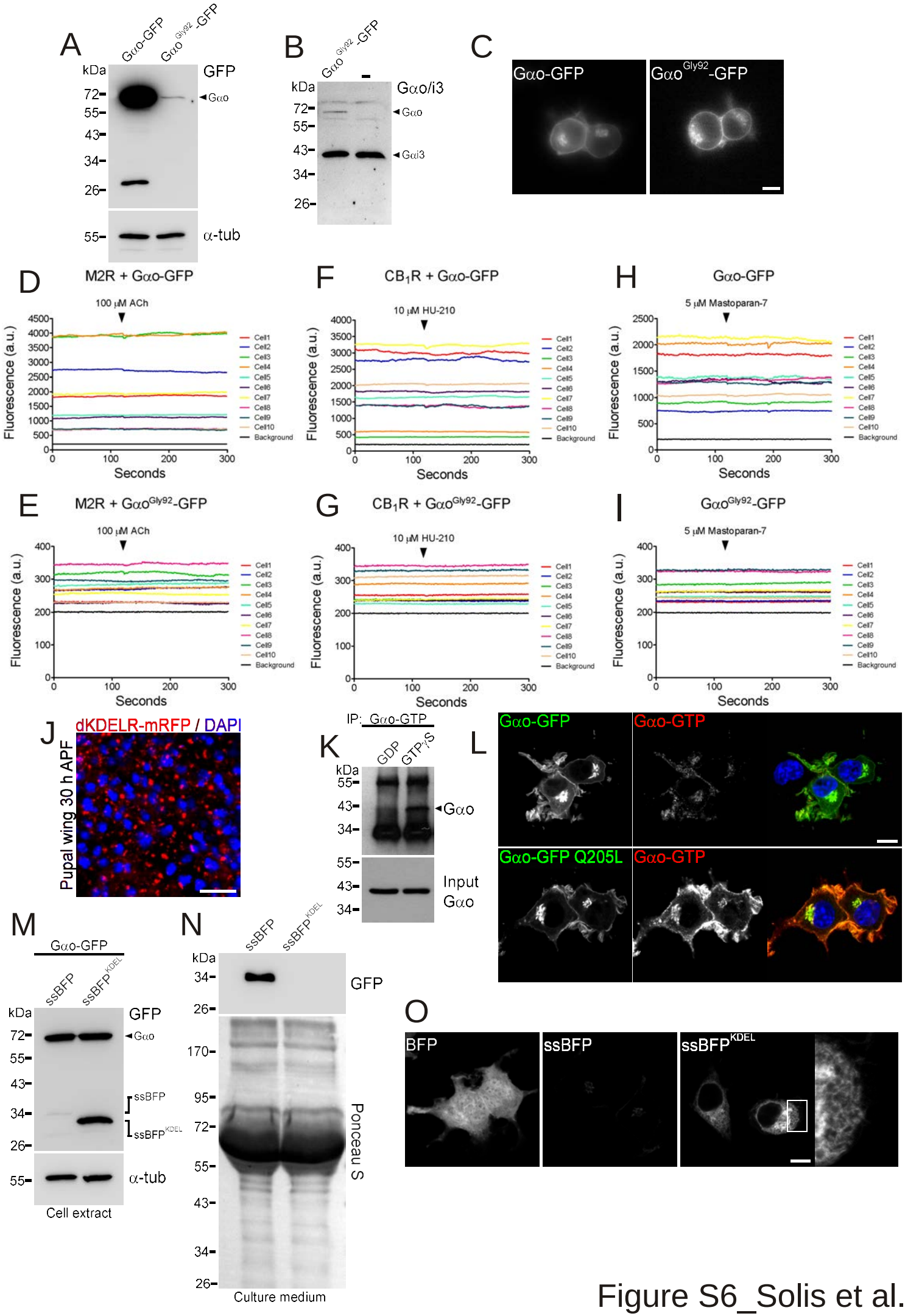

Figure S6_Solis et al.

Supplemental Figure 7

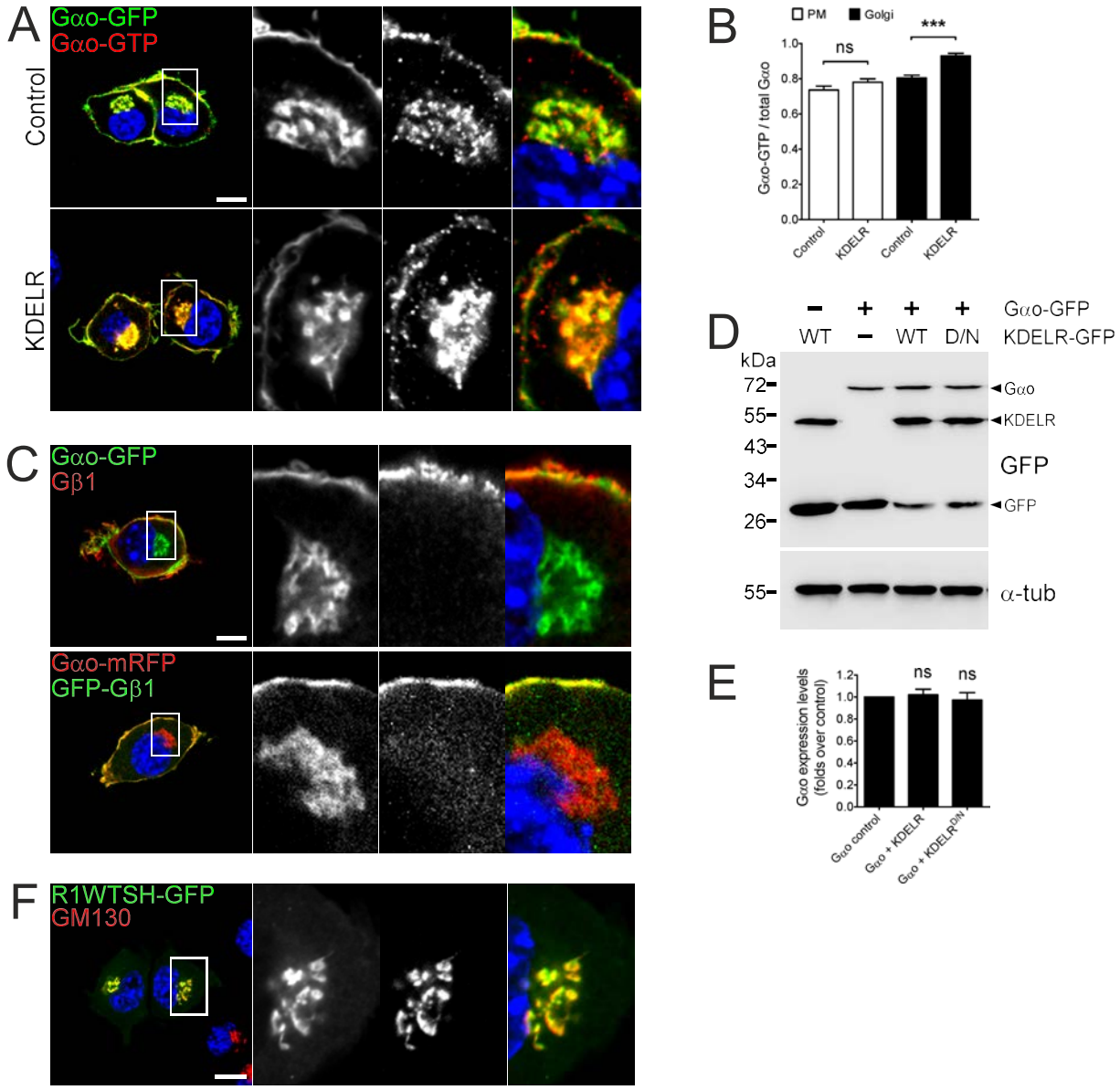

Figure S7_Solis et al.